Neurodegeneration and Reorganization in Spinal Cord Disorders

Dissertation

zur

Erlangung der naturwissenschaftlichen Doktorwürde

(Dr. sc. nat.)

vorgelegt der

Mathematisch-naturwissenschaftlichen Fakultät

der

Universität Zürich

von

Patrick Grabher

von

Sursee LU

Promotionskomitee

Prof. Dr. Markus Rudin (Vorsitz)

Prof. Dr. Armin Curt (Leitung der Dissertation)

Dr. Patrick Freund

Prof. Dr. Dominik Bach

Zürich, 2016

Table of Contents

Summary

The unique interplay of the brain, the spinal cord, composing the central nervous system (CNS), and the peripheral nervous system is crucial for the integration of sensory information and for the generation of appropriate motor output. If this interplay is interrupted by a lesion, it has dramatic consequences for the individual and causes impairment below and at the level of the injury. To get an estimate of the incidence of spinal cord disorders, between 8 and 83 individuals per million individuals will suffer from traumatic spinal cord injury (SCI) each year. In cervical spondylotic myelopathy (CSM) that causes cervical cord damage, the incidence has not been reported. However, it will increase in context of the aging population.

Next to the devastating consequences of spinal cord disorders in impairment of normal body function, neurodegeneration and reorganization is triggered that both may compete with each other. Non-invasive imaging techniques provide the opportunity to investigate these changes in the CNS. Most studies have focused on neurodegeneration using structural magnetic resonance imaging (MRI) which revealed atrophic changes (i.e. volume loss) predominantly in the sensorimotor system in chronic SCI. Advanced quantitative imaging techniques now enable the investigation of the underlying ultra-structure and are more specific to the pathophysiological processes (e.g. axonal degeneration, demyelination, iron accumulation).

Based on the literature, the aim of this thesis was therefore to investigate the temporal pattern and magnitude of neurodegeneration and reorganization in the CNS above the level of injury and to probe its capacity for neuroplasticity to enhance neurological and functional outcome during rehabilitation using standard and advanced imaging techniques in spinal cord disorders.

In the first study, we assessed the temporal and spatial trajectory of remote spinal and supraspinal atrophy and the underlying ultra-structure within the sensory system following acute traumatic SCI during one year follow-up. We demonstrated progressive atrophy in cervical cord and brain that was paralleled by reduction in myelin content and thus emphasizing that atrophy is related to changes in the underlying ultra-structure. The widespread degeneration and its extent in the sensory system resembled the one seen in the

motor system. Crucially, sensory outcomes at one year were related to the extent of progressive atrophy and integrity of the ultra-structure.

In the second study, we assessed more specifically neurodegeneration in brainstem pathways and nuclei in chronic SCI. The oldest motor command (e.g. rubrospinal system) and integrating systems (e.g. periaqueductal gray) of the brainstem are still understudied in humans, but play a crucial role in recovery of motor function in rodents and non-human primates. We observed atrophy in the major brainstem pathways and widespread myelin loss in areas of brainstem nuclei. This indicates the higher sensitivity of measures that are closer related to the underlying pathology. Interestingly, we found myelin loss within the periaqueductal gray that is involved in the endogenous pain inhibition system. Crucially, the magnitude of myelin loss in the periaqueductal gray was related to spinothalamic dysfunction. No alterations were found in the rubrospinal system and thus emphasize the diminished role in human motor function compared to rodents and non-human primates.

In our third study, we investigated the effects of neurorehabilitation on performance and neuroplasticity within the CNS. Recovery after SCI is supported by intensive neurorehabilitation programs that are pivotal to improve patients' independence and quality of life. Whether performance improvements relate to adaption of compensatory movement strategies or to the brain's capacity for neuroplasticity, remains unknown. For the first time, we could identify performance improvement-induced volume increases within the brain and brainstem due to virtual-reality augmented training of the lower extremities in SCI. We provide evidence that neurorehabilitation is effective to engage the CNS, that neuroplasticity can be induced next to areas of atrophy, and that the underlying mechanisms are either recovery from neurodegeneration or reorganization of healthy neuronal networks.

In the last study, we aimed to investigate the consequences of CSM to the macro- and microstructure above the level of compression. We identified spinal cord gray and white matter atrophy and alterations in the microstructure of the corticospinal tracts and posterior columns in patients with CSM. The identified changes resembled those seen in traumatic SCI. Crucially, spinal cord pathology related to posterior column dysfunction and impaired functional independence. Despite minor motor dysfunction, corticospinal integrity was altered and thus is promising to identify early and subclinical signs of cord pathology.

In summary, we were able to show progressive and widespread neurodegeneration in the spinal cord, brainstem, and brain remote to the level of injury using state-of-the-art computational neuroanatomy. The application of quantitative MRI readouts is clinically feasible and allows us to investigate pathological mechanisms with higher specificity in-vivo. Thus, quantitative imaging may improve clinical trial designs and provide targetable outcome measures for pharmacological and neuro-rehabilitative interventions that aim to attenuate neurodegenerative processes and promote recovery.

Zusammenfassung

Das einzigartige Zusammenspiel des Gehirns und Rückenmarks, welche das Zentralnervensystem (ZNS) ausmachen, und des peripheren Nervensystems ist wichtig für die Integration sensorischer Informationen und der Generierung optimaler Bewegungsabläufe. Wird dieses Zusammenspiel jedoch durch eine Läsion unterbrochen, hat dies schwerwiegende Konsequenzen für den Einzelnen und verursacht unter anderem Beeinträchtigungen auf der Höhe und unterhalb der Läsion. Jährlich erleiden zwischen 8 bis 83 Personen pro Million Menschen eine traumatische Rückenmarkverletzung. Die Inzidenz für zervikale spondylotische Myelopathien, welche das zervikale Rückenmark schädigen, ist unbekannt. Sie wird aber in Einbezug des Alterns der Bevölkerung ansteigen.

Neben den direkten Folgen einer Rückenmarkverletzung findet Neurodegeneration und Reorganisation im ZNS statt, welche gegebenenfalls miteinander konkurrieren können. Nicht-invasive bildgebende Verfahren bieten heute die Möglichkeit diese Veränderungen im ZNS zu untersuchen. Die meisten Studien haben mittels struktureller Magnetresonanztomographie (MRT) Atrophie (d.h. Volumenverlust) im sensomotorischen System nach einer chronischen Rückenmarkverletzung festgestellt. Moderne und quantitative bildgebende Verfahren bieten heutzutage die Möglichkeit an, Veränderungen in der Ultrastruktur zu untersuchen und sind somit spezifischer für pathophysiologische Prozesse (z.B. axonale Degeneration, Demyelinisierung, Anreicherung von Eisen).

Das Ziel dieser Doktorarbeit war es, basierend auf der aktuellen Literatur, das zeitliche Muster und Ausmass degenerativer Veränderungen und Reorganisation oberhalb der Läsion und den Effekt von Neuroplastizität bei der Wiederherstellung neurologischer und funktioneller Körperfunktionen im ZNS nach einer Rückenmarkverletzung mittels standardmässiger und fortgeschrittener bildgebender Verfahren zu untersuchen.

In der ersten Studie untersuchten wir die zeitliche und räumliche Trajektorie spinaler und supraspinaler Atrophie und die zugrundeliegende Ultrastruktur (d.h. Gehalt von Myelin) innerhalb des sensorischen Systems nach einer akuten traumatischen Rückenmarkverletzung im Verlauf des ersten Jahres. Wir konnten bei Patienten mit einer Rückenmarkverletzung fortschreitende Atrophie im zervikalen Rückenmark und im sensorischen System des Gehirns

feststellen, welche mit einer Reduktion von Myelin einherging. Diese weitläufigen Veränderungen gleichen denjenigen, die im motorischen System festgestellt wurden. Die sensorische Funktion ein Jahr nach der Verletzung wiederspiegelte sich im Ausmass der fortschreitenden Atrophie und der Integrität der Ultrastruktur.

In der zweiten Studie untersuchten wir die neurodegenerativen Veränderungen der Hirnstammbahnen und Hirnstammkerne bei Patienten mit einer chronischen Rückenmarkverletzung. Die ältesten motorischen (z.B. rubrospinales System) und integrierenden Steuerungssysteme (z.B. periaquäduktales Grau) des Hirnstamms und deren Rolle für die Erholung nach einer Rückenmarkverletzung sind im Menschen kaum untersucht, spielen aber eine wichtige Rolle in der Erholung bei Nagetieren und nicht-menschlichen Primaten. Wir stellten Atrophie in den grossen Hirnstammbahnen und einen weitläufigen Verlust von Myelin in den Hirnstammkernen fest. Dies zeigt die höhere Sensitivität für Messmethoden, die näher bei der zugrunde liegenden Pathologie sind. Interessanterweise haben wir eine Abnahme von Myelin im periaquäduktalem Grau entdeckt, welche ein Teil des endogenen Schmerzunterdrückungssystems ist. Das Ausmass des Myelinverlustes geht mit der Dysfunktion des spinothalamischen Traktes einher. Keine Veränderung wurde im rubrospinalen System entdeckt. Dies unterstreicht somit die eher marginale Rolle der Hirnstammbahnen bei der motorischen Funktion beim Menschen.

In der dritten Studie untersuchten wir den Effekt von Neurorehabilitation auf die Leistungsverbesserung und Neuroplastizität im ZNS. Die Genesung von Patienten nach einer Rückenmarkverletzung wird durch intensive Neurorehabilitation unterstützt und ist zentral für die Verbesserung der Eigenständigkeit und Lebensqualität. Ob Verbesserungen betreffend der Leistung auf die Entwicklung kompensatorischer Bewegungsmuster oder die Neuroplastizität des Gehirns zurückzuführen sind, ist unbekannt. In dieser Pilotstudie konnten wir zum ersten Mal die direkten Folgen des virtuell verstärken Gangtrainings im ZNS aufzeigen. Die Volumenveränderungen im Gehirn gingen mit der Verbesserung der Leistung, welche durch die Neurorehabilitation erreicht wurde, einher. Somit zeigen wir, dass Neurorehabilitation effektiv das ZNS stimulieren kann, dass Neuroplastizität auch in Gebieten mit Atrophie induziert wird, und dass dies auf der Erholung des neuronalen Gewebes nach degenerativen Veränderungen und/oder auf die Reorganisation von gesunden neuronalen Netzwerken zurückzuführen ist.

In der letzten Studie untersuchten wir die Folgen einer zervikalen spondylotischen Myelopathie auf die Makro- und Mikrostruktur des Rückenmarks oberhalb der Stenose. In dieser Studie stellten wir Atrophie in der grauen und weissen Substanz und Veränderungen in der Mikrostruktur der Kortikospinalbahnen und der Hinterstrangbahnen fest. Diese Veränderungen sind sehr ähnlich mit denen nach einer traumatischen Rückenmarkverletzung. Interessanterweise steht die Pathologie im Rückenmark mit der Dysfunktion der Hinterstrangbahnen und der funktionellen Eigenständigkeit in Bezug. Trotz der minimalen motorischen Funktionsstörung war die Integrität der Kortikospinalbahnen deutlich vermindert. Dies ist ein vielversprechendes Resultat, da es frühe pathologische Veränderungen zeigt, welche klinisch noch asymptomatisch sind.

Zusammenfassend wurde in dieser Dissertation gezeigt, dass eine fortschreitende und weitläufige Neurodegeneration im Rückenmark, Hirnstamm und Gehirn fernab der eigentlichen Verletzung stattfindet und mittels hochmoderner neuroanatomischer Methoden aufgezeigt werden kann. Die Anwendung von quantitativen MRT-basierten Messparametern ist im klinischen Alltag anwendbar und ermöglicht uns, pathologische Veränderungen in-vivo mit einer höheren Spezifität zu untersuchen. Somit kann die quantitative Bildgebung klinische Studiendesigns verbessern und ‚behandelbare' Endpunkte für pharmakologische und neurorehabilitative Interventionen bieten, welche neurodegenerative Prozesse mildern und die Erholung fördern.

Chapter 1:

General introduction

Etiology of spinal cord disorders

Spinal cord disorders are life-changing conditions that may cause permanent impairment in motor control, sensory function, and autonomic regulation of the body with no cure available (Dietz and Fouad, 2014). Further long-term consequences of spinal cord injury include psychosocial aspects (e.g. life satisfaction) (Post and van Leeuwen, 2012) and economic independence (Young and Murphy, 2009). In addition, spinal cord disorders are a significant public health issue with a lifetime impact on society allocable to the costs due to hospitalization, rehabilitation, and further health challenges in the chronic stages of injury (World Health Organization & International Spinal Cord Society, 2013). The spectrum of etiologies of cord damage is manifold and is typically classified into traumatic or non-traumatic injuries (e.g. tumor or spondylosis). Traumatic spinal cord injury (SCI) is caused by immediate damage to the spinal cord and is mainly due to road traffic accidents, sport accidents, falls, or assaults (DeVivo, 1997). In contrast, non-traumatic SCIs are frequently caused by spondylosis of the spinal column, neoplastic tumors, infections, or vascular and autoimmune disorders (Moore and Blumhardt, 1997) and have different time profiles of disease evolution (i.e. from acute to chronic stage) and different trajectories of neuronal damage. Consequently, a holistic research approach in spinal cord disorders is needed to improve early diagnostics, to develop effective treatments, and to guide interventional decision making, that finally helps to improve the patient's quality of life. Due to the heterogeneity of spinal cord disorders and underlying mechanisms, the present thesis focused on neurodegeneration and reorganization in traumatic SCI and cervical spondylotic myelopathy (CSM) using non-invasive MRI imaging techniques.

Traumatic spinal cord injury

Traumatic SCI leads to immediate and permanent impairment in motor, sensory, and autonomic function below the level of lesion (Zariffa *et al.*, 2011). Prevalence of SCI is estimated being between 250 and 906 persons per million inhabitants, whereas the annual reported incidence is between 8 and 83 per million inhabitants (Wyndaele and Wyndaele, 2006; Singh *et al.*, 2014). The mean age at injury is 33 years with 3.8 times higher prevalence in male individuals (Wyndaele and Wyndaele, 2006).

The neurological impairments depend on the lesion level and the severity of disruption of the major ascending and descending fiber tracts and can be assessed using the International

Standards for Neurological Classification of Spinal Cord Injury (ISNCSCI) (Kirshblum *et al.*, 2011). Based on the level of the lesion, traumatic SCI can be grouped into tetra- and paraplegia. Tetraplegia is caused by a cervical SCI and occurs in a little more than half of all patients (Singh *et al.*, 2014) and is followed by sensory and motor loss within the upper and lower extremities. Lower lesions at the thoracic and lumbar levels cause paraplegia with loss in motor and sensory function in the lower extremities. Based on the lesion severity, SCI can be further described by the ASIA impairment scale (AIS) as motor and sensory complete (AIS A), motor complete and sensory incomplete (AIS B), motor and sensory incomplete (AIS C-D), and full recovery (AIS E) (Kirshblum *et al.*, 2011). In about one-half of all patients, lesions are clinically complete (AIS A) (Wyndaele and Wyndaele, 2006) and thus, no motor and sensory function below the lesion is preserved. In addition, around 34% of SCI patients develop below-level neuropathic pain with higher prevalence in tetraplegia (Siddall *et al.*, 2003).

During rehabilitation and within the first year after injury, patients show greatest recovery that levels off over time (Fawcett *et al.*, 2007). Functional and neurological recovery is more prominent in incomplete than in complete lesions due to spared neuronal fibers (Raineteau and Schwab, 2001; Curt *et al.*, 2008). Functional recovery can be achieved by developing compensatory strategies for activities of daily living (Curt *et al.*, 2008; Kalsi-Ryan *et al.*, 2014) and by reorganization of neuronal circuits. Neuronal plasticity contributes to recovery due to reorganization in spared as well as lesioned fiber tracts at the cortical (Raineteau *et al.*, 2002; Ghosh *et al.*, 2010; Rosenzweig *et al.*, 2010; Zörner *et al.*, 2014) and spinal level (Bareyre *et al.*, 2004; Courtine *et al.*, 2008; Filli and Schwab, 2015). Compensation and reorganization are both promoted by neurorehabilitation to achieve better functional outcome (Dietz and Fouad, 2014). The lesion level and severity have implications on the functional outcome and the rehabilitative strategies (Dietz and Curt, 2006). Thus, priorities of recovery are different for tetra- and paraplegics and need to be addressed to their specific needs (Anderson, 2004). In tetraplegia, the focus to improve upper-limb function like regaining arm and hand function, has the highest clinical value to improve functional independence and quality of life (Anderson, 2004). The aim is therefore to maximize functional independence for self-care (e.g. feeding, bathing, dressing) and mobility (e.g. wheelchair use, transfers). In paraplegia, upper-limb function is not impaired and enables these patients to reach a high level of independence. Priorities of recovery in paraplegia are therefore sexual function, bladder and bower

management, trunk stability, pain management, as well as walking capability (Anderson, 2004). Activity-based neuroplasticity and lower-limb function can be supported by neurorehabilitation such as robot-supported locomotor trainings (Colombo *et al.*, 2001a; Vallery *et al.*, 2013) and virtual reality-augmentation (Villiger *et al.*, 2013).

Cervical spondylotic myelopathy

Cervical spondylotic myelopathy is one of the most frequent forms of spinal cord disorder causing functional impairment and sensory discomfort that leads to reduced independence and quality of life (Kalsi-Ryan, Karadimas, *et al.*, 2013). Prevalence and incidence remain unknown, mostly because of the unknown onset and the slow progression of spinal cord compression being clinically asymptomatic for many years. In 585 consecutively assessed patients with non-traumatic spastic para- and tetraparesis, CSM was the most common diagnosis (23.6%) (Moore and Blumhardt, 1997). The mean age is approximately 64 years with a 2.7 times higher prevalence in men than women (Northover *et al.*, 2012). Considering the global ageing, the prevalence may further increase (New *et al.*, 2013). Cervical spondylotic myelopathy is a risk factor for development of a central cord syndrome, the most common cervical SCI (van Middendorp *et al.*, 2010). Most damage occurs to the central gray matter and thus, causes predominantly motor impairment in the upper extremities and varying sensorimotor impairment below the level of lesion. Patients with CSM are thus predisposed to this condition (van Middendorp *et al.*, 2010; Kalsi-Ryan, Karadimas, *et al.*, 2013). Depending on the disease severity and duration, symptoms differ and may include numbness, clumsiness, gait impairment, pain, and sphincter dysfunction. Based on the clinical assessment using the modified Japanese Orthopedic Association scale (mJOA) (Benzel *et al.*, 1991), CSM can be defined as mild, moderate, and severe (Tetreault *et al.*, 2016). In patients with severe stenosis and symptoms, decompressive surgery is the therapeutic gold standard to improve neurologic and functional outcome, and to hinder disease progression (Holly *et al.*, 2008). In patients with less severe stenosis and absent or mild symptoms, conservative management (e.g. physiotherapy and pain management) is chosen (Toledano and Bartleson, 2013). Depending on the severity and level of paresis, physiotherapy and occupational therapy are applied to improve balance, gait training, and upper-limb function in patients after decompression, but also in patients with conservative management (i.e. no surgery) (Toledano and Bartleson, 2013). Due to the compression in the cervical segments and the damage to the central gray,

rehabilitation should prioritize the same goals as in tetraplegia (Anderson, 2004; Kalsi-Ryan, Singh, *et al.*, 2013).

Neurodegeneration above the lesion site

Pathology in traumatic spinal cord injury

Experimental animal models are used to understand the pathophysiological mechanisms after SCI that help us to understand disease progression and reveal treatment targets. So far, animal models and post-mortem human specimens provided detailed insights into the molecular and cellular mechanisms at the lesion site and remote thereof after traumatic SCI and CSM (Fehlings and Skaf, 1998; Kwon, 2004; Karadimas *et al.*, 2014). Traumatic SCI is caused by sudden impact of mechanical forces (i.e. flexion/extension, rotation, distraction, compression) to the spinal cord and results in the primary lesion of the myelon. This is followed by secondary damage to spared tissue through pathophysiological processes such as inflammation, ischemia by disruption of microvasculature and thrombosis, lipid peroxidation by free radicals, excitotoxicity, electrolyte imbalance, and cell death through apoptosis and necrosis (Kwon, 2004). Above the level of lesion, injured ascending axons (e.g. dorsal column) undergo Wallerian degeneration that is detectable several segments remote to the lesion as early as 12 days after injury in human SCI (Buss *et al.*, 2004). This process is accompanied by slow and delayed gradual degradation of myelin over years (George and Griffin, 1994; Buss *et al.*, 2004). Myelin proteins of the periaxonal membrane are removed first, whereas removal of outer myelin membrane proteins is delayed (Buss and Schwab, 2003; Buss *et al.*, 2005). Intact neurons lacking presynaptic input (e.g. dorsal column nuclei and thalamus) are prone to transneuronal degeneration that results in volumetric atrophy and to a lesser extent to neuronal loss (Jones and Pons, 1998; Woods *et al.*, 1999). Above the lesion, damaged descending neurons (e.g. corticospinal tract) undergo axonal dieback at the lesion site (Kerschensteiner *et al.*, 2005; Freund *et al.*, 2007; Ward *et al.*, 2014). Remote retrograde degeneration causes volumetric loss (i.e. atrophy) in cortical (Beaud *et al.*, 2008) and subcortical (Kwon *et al.*, 2002; Wannier-Morino *et al.*, 2008) motor regions, and to a lesser extent apoptosis (Hains *et al.*, 2003). Chronic progressive demyelination of intact fiber tracts is an additional pathophysiological process (Crowe *et al.*, 1997; Totoiu and Keirstead, 2005), but there is also evidence for remyelination thereafter (Guest *et al.*, 2005; Powers *et al.*, 2012, 2013). Less recognized is the fact of long-term brain neuroinflammation that results in chronic

microglia activation and changes in chemokine and cytokine levels (Felix *et al.*, 2012; Wu, Stoica, *et al.*, 2014; Wu, Zhao, *et al.*, 2014; Faden *et al.*, 2015). Neuronal loss (Wu, Stoica, *et al.*, 2014; Wu, Zhao, *et al.*, 2014), alteration in neurogenesis (Felix *et al.*, 2012), and molecular dysfunction at the receptor level (Knerlich-Lukoschus *et al.*, 2011) are the consequence of this inflammatory response. In addition, these inflammation-induced changes were associated with the development of neuropathic pain (Knerlich-Lukoschus *et al.*, 2011).

Pathology in cervical spondylotic myelopathy

Chronic progressive narrowing of the spinal canal and compression of the cervical cord in CSM is caused by degeneration of the vertebral bodies, intervertebral discs, and ligaments and results in mechanic stress (Karadimas *et al.*, 2014). Dynamic factors of mechanical stress by repetitive movements of the compressed spinal cord exacerbate disease progression (Fehlings and Skaf, 1998; Kalsi-Ryan, Karadimas, *et al.*, 2013; Toledano and Bartleson, 2013). As the compression site is mostly located at the vertebra level C5 or C6, most damage is expected to the spinal cord at the same level and its vicinity (Northover *et al.*, 2012). Nevertheless, CSM is often a multifocal disease caused by degeneration and narrowing of the spinal canal at several segments (Northover *et al.*, 2012). At the cellular and molecular level, consequences of sustained cord compression comprise the remodeling of microvasculature (Karadimas *et al.*, 2013) and the distribution of blood supply (Kurokawa *et al.*, 2011; Karadimas *et al.*, 2015), both causing ischemia, dysfunction of the blood spinal cord barrier (Karadimas *et al.*, 2013), neuroinflammation (Yu *et al.*, 2011; Karadimas *et al.*, 2013), and apoptosis of oligodendrocytes and neurons (Yu *et al.*, 2009, 2011). Despite originating focally, the consequences of CSM are not restricted to the site of stenosis. Structural and functional changes are evident along the neuroaxis (Holly *et al.*, 2009; Cui *et al.*, 2014).

Similar and distinct disease patterns in both spinal cord disorders

As depicted in the previous sections, similarities in terms of clinical representation of impairment and certain pathophysiological mechanisms exist between both spinal cord disorders. Clinical symptoms of both conditions are represented by motor, sensory, and autonomic dysfunction. Typical signs are impairment in upper and lower extremities, loss of fine motor control, paresthesia, pain development, and bladder/bowel dysfunction. At the time point of diagnosis, the clinical representation is less severe in CSM compared to SCI. Nevertheless, CSM is a progressive disease and can lead to paralysis and sensory loss (Kalsi-Ryan, Karadimas, *et al.*, 2013). The similarities in pathophysiological mechanisms in both spinal cord disorders include the mechanical factors of static and dynamic stress leading to ischemia, inflammation, excitotoxicity, and cell death (Fehlings and Skaf, 1998; Kwon, 2004). The onset and temporal progression of clinical representation and damage to neuronal and non-neuronal tissue is the main distinction between both spinal cord disorders. Thus, research in both disorders may be relevant to each other and may enable to create synergies that support the development of improved diagnostics and treatment applications. In other words, drugs, rehabilitation devices and outcome measures that were developed for one spinal cord disorder might be used to treat the other one. This surely improves the cost-benefit ratio and expands treatment options (Freund *et al.*, 2016). For instance, two phase III clinical trials are currently investigating the neuroprotective effects of riluzole in SCI (Fehlings *et al.*, 2016) and CSM (Michael G. Fehlings *et al.*, 2013). Another example is an upper-limb assessment tool (i.e. GRASSP) that was initially developed for tetraplegia (Kalsi-Ryan *et al.*, 2012, 2014) and is now suggested as an complementary outcome measure in CSM (Kalsi-Ryan, Singh, *et al.*, 2013). Nevertheless, it is important to emphasize the fundamental discrepancy between both disorders. In CSM compared to SCI, there is (1) no acute trauma causing immediate damage to the spinal cord, (2) a slow progression of the disease being asymptomatic for a long time period, and (3) no hemorrhagic necrosis (Karadimas *et al.*, 2014). The key targets to improve patient recovery after SCI are (1) neuroprotection (e.g. minocycline, riluzole) after injury to preserve neuronal tissue (Casha *et al.*, 2012; Fehlings *et al.*, 2016), (2) stem cell application that aims to preserve neuronal tissue and enhance regeneration (Curt, 2012), (3) induction of plasticity by facilitating axonal sprouting and growth (e.g. anti-Nogo-A, chondroitinase ABC) (Bradbury *et al.*, 2002; Zörner and Schwab, 2010), (4) altering spinal cord excitability by neurostimulation (Courtine *et al.*, 2011; Angeli *et al.*, 2014), in combination with (5) goal-

directed rehabilitation (Dietz, 2002; Dietz and Curt, 2006). In comparison, sensitive diagnostics and prognostics combined with early treatment options (e.g. surgery combined with neuroprotection) to hinder disease progression (Moon *et al.*, 2014; Karadimas *et al.*, 2015) are the key in disease management of CSM.

Computational neuroanatomy

Computational morphometry to investigate atrophy and plasticity

In the early days, MRI entered the clinics as a non-invasive diagnostic imaging technique. Nowadays, MRI and computational morphometry (e.g. voxel-based morphometry) are establishing themselves more and more in daily routine in clinics and have helped to gain insights into sub clinical changes and define diagnosis (Barkhof *et al.*, 2009; Frisoni *et al.*, 2010; Huber *et al.*, 2015) (e.g. McDonald diagnostic criteria for multiple sclerosis that have resulted in earlier diagnosis with higher specificity and sensitivity (Polman *et al.*, 2011)). Neurodegeneration and -plasticity above the level of injury can be assessed non-invasively by using computational morphometry. Computational morphometry provides MRI-based measures of disease-specific patterns of atrophy (Jurkiewicz *et al.*, 2006; Wrigley, Gustin, *et al.*, 2009; Freund *et al.*, 2013) and training- or learning-induced plasticity (Maguire *et al.*, 2000; Gaser and Schlaug, 2003a; Draganski *et al.*, 2004; Zatorre *et al.*, 2012). There are several principal methods to investigate brain morphometry that include (1) voxel-based morphometry (VBM), (2) tensor-based morphometry (TBM), (3) voxel-based cortical thickness (VBCT), (4) surface-based morphometry, and (5) deformation-based morphometry (Ashburner and Friston, 2004). The first three methods are briefly introduced as they were integral to this thesis.

VBM is a technique to measure structural differences among subjects or populations by comparing the local composition of brain tissue types (i.e. gray matter (GM), white matter (WM), and cerebrospinal fluid (CSF)) (Ashburner and Friston, 2000). All MRI data have to be spatially normalized into the same stereotactic space and segmented into GM, WM, and CSF (Ashburner and Friston, 2005). To preserve the total amount locally within each tissue type during normalization, tissue types are modulated by adjusting for the relative volume change (e.g. when doubling a volume of GM in a specific region, the intensity will be scaled down by the factor 2). In general, VBM is used in cross-sectional study designs to assess local volumetric

atrophy or plasticity between groups (Maguire *et al.*, 2000; Jurkiewicz *et al.*, 2006). Nevertheless, local brain tissue compositions can also be studied using "longitudinal VBM" (Draganski *et al.*, 2004).

Typically, TBM is used in longitudinal settings to assess atrophy or plasticity over time (Freund *et al.*, 2013). Tensor-based morphometry is a technique to compare relative volumes locally among subjects or populations by comparing the Jacobian determinants that encode relative volumetric expansion and contraction due to local stretching and shearing during registration (Ashburner and Friston, 2004). The Jacobian determinants are calculated from the deformation fields that are estimated during within-subject longitudinal registration of each image to the subject-specific midpoint average (Ashburner and Ridgway, 2013). Nevertheless, TBM can also be used in cross-sectional studies when deformations from each image to the equivalent points of the template are estimated (Lambert, Chowdhury, *et al.*, 2013).

VBCT provides complementary cortical information about the gray matter thickness (Hutton *et al.*, 2008). Following the segmentation of the MRI data into GM, WM, and CSF, the thickness between the inner and outer GM border is calculated. VBCT and VBM show concurring results, VBCT is, however, more specific to cortical thickness, whereas VBM provides a mixture of measures including cortical surface and thickness (Hutton *et al.*, 2009).

In all morphometric methods, smoothing is applied to account for the inexact nature of spatial normalization and inter-subject variability of the CNS, to increase the validity of parametric statistical tests by making the data more normally distributed, and to meet the assumption for Gaussian Random Field Theory to account for multiple comparisons (Ashburner and Friston, 2000, 2004). Mass univariate statistics (e.g. t-tests, analysis of covariance) can then be applied to assess within- and between-subject variability at either the voxel-level or at the cluster-level. Cluster-level inference was introduced to increase sensitivity by taking the spatial extent of brain activity or changes of structure into account and thus lowering the number of independent statistical tests (Friston *et al.*, 1994). Therefore, an initial cluster-defining threshold needs to be defined. It is important to note that an appropriate threshold is crucial to control for the family-wise error, otherwise the rate of false positives increases dramatically (Eklund *et al.*, 2016). However, the problem of multiple testing needs to be

addressed by using Gaussian Random Field Theory (Worsley *et al.*, 1992) or any other valid method (e.g. Bonferroni, False Discovery Rate).

Advanced quantitative MRI to investigate ultra- and microstructure

The underlying microstructure (e.g. axonal integrity, myelin and iron content) can be assessed by quantitative MRI (qMRI). MRI tissue properties (i.e. relaxation times, proton density, exchange processes between tissue compartments) can be quantified by qMRI using physical models that are unbiased and facilitate multicenter and longitudinal study designs (Weiskopf *et al.*, 2013). In the central nervous system, these physical parameters mainly depend on the macromolecular (i.e. myelin) and iron content, as brain tissue contrast is mainly reflected by these two contributors (Stüber *et al.*, 2014). Correlation models revealed relationships between qMRI metrics that describe relaxation and magnetization transfer behavior of protons in their microenvironments and tissue properties. Magnetization transfer (MT) was related to myelin content (Mottershead *et al.*, 2003; Schmierer *et al.*, 2004; Turati *et al.*, 2015), longitudinal relaxation rate (R1) to myelin, water, and iron content (Rooney *et al.*, 2007; Stüber *et al.*, 2014; Callaghan *et al.*, 2015; Harkins *et al.*, 2015), and effective transverse relaxation rate (R2*) to iron content (Langkammer *et al.*, 2010; Stüber *et al.*, 2014).

Another quantitative MRI technique is diffusion tensor imaging (DTI) that takes advantage from diffusion weighted imaging (Pierpaoli and Basser, 1996) and provides information about microstructure including fiber alignment and white matter integrity. DTI indices of fractional anisotropy (FA), radial diffusivity (RD), axial diffusivity (AD), and mean diffusivity (MD) can be calculated after robust tensor fitting and motion and eddy current artefact correction. FA has been related to axonal count and myelin content (Schmierer, Wheeler-Kingshott, *et al.*, 2007; Gouw *et al.*, 2008), decreased AD with axonal degeneration (Zhang *et al.*, 2009), and increased RD with demyelination (Klawiter *et al.*, 2011). Biophysical modelling of qMRI data will propel the field of in-vivo histology MRI (hMRI) yielding biological metrics such as myelin and iron density, fiber orientation, and axonal g-ratio that were only accessible by ex-vivo histology (Weiskopf *et al.*, 2015). In addition, advanced multi-shell diffusion models such as neurite orientation dispersion and density imaging (NODDI) (Zhang *et al.*, 2012) that use different diffusion gradients seem to be promising for clinical research.

Spinal cord imaging

Ultra- and microstructural changes are not limited to the brain, but can also be quantified in the spinal cord (Wheeler-Kingshott *et al.*, 2014). The same techniques as described above can be applied to the spinal cord, but they are technically more challenging. Spinal cord imaging is still in its infancy and challenged by the complicated environment of surrounding bone structure and air-filled tissue (i.e. lungs), physiological noise of cardiac cycle, flow of cerebrospinal fluid and respiration, the small cross-sectional cord dimension, and close-by implants stabilizing the spinal canal causing imaging artefacts and signal drop out (Stroman *et al.*, 2014). Nevertheless, spinal cord imaging has been applied successfully in SCI and CSM (Cohen-Adad *et al.*, 2011; Freund *et al.*, 2013; Martin *et al.*, 2016). In spinal cord disorders, advanced MRI techniques show high potential in developing quantitative MRI biomarkers at the spinal level. They assess early changes even in asymptomatic subjects in which no irreversible damage did occur (e.g. CSM), predict outcome, and may be used as surrogate outcome measures in clinical trials to complement clinical assessments (Martin *et al.*, 2016).

Neurodegeneration above the lesion revealed by in-vivo computational neuroanatomy

Traumatic spinal cord injury

Trauma-induced ultra-structural and macroscopic changes due to neurodegeneration were investigated after SCI in both the motor and sensory system in the brain (Jurkiewicz *et al.*, 2006; Wrigley, Gustin, *et al.*, 2009; Gustin *et al.*, 2010; Freund *et al.*, 2013; Mole *et al.*, 2014; Jutzeler *et al.*, 2016). Macroscopic decline was already observed within the first 40 days after injury in the motor system including the primary motor cortex and corticospinal tract and progressed within the first year (Freund *et al.*, 2013). Atrophy was accompanied by ultra-structural reductions of myelin-sensitive MRI readouts (i.e. MT and R1) in the same areas and beyond. This early sensorimotor system atrophy is supported by other studies in chronic human SCI within the motor (Wrigley, Gustin, *et al.*, 2009; Freund *et al.*, 2011; Jutzeler *et al.*, 2016) and sensory system (Jurkiewicz *et al.*, 2006; Mole *et al.*, 2014; Jutzeler *et al.*, 2016). Crucially, atrophy was related to neurological and functional impairment (Freund *et al.*, 2013) and below-level neuropathic pain (Mole *et al.*, 2014; Jutzeler *et al.*, 2016).

The spinal cord above the lesion site is vulnerable to neurodegeneration as discussed in the previous sections. Assessment of MRI-based spinal cord measures at the level of vertebra C2/C3 above the lesion level is widely used in the SCI community (Cohen-Adad *et al.*, 2011; Freund *et al.*, 2011, 2013; Lundell *et al.*, 2011; Jutzeler *et al.*, 2016) and has several anatomical advantages: (1) CSF space is wide and thus the CSF to cord contrast is maximized, (2) intra-subject variability is small reducing repositioning errors, (3) disc protrusions are uncommon at this site, and (4) the location is accessible by MRI as it is remote to the implants stabilizing the lesion site that cause signal dropout (Losseff *et al.*, 1996). Cross-sectional cord area is linearly decreasing within the first year of injury (Freund *et al.*, 2013) and is reported to be reduced by up to 30% in chronic SCI (Freund *et al.*, 2011; Lundell *et al.*, 2011; Jutzeler *et al.*, 2016). These changes are further described by more detailed morphometric shape reductions in the anterior-posterior (APW) and left-right width (LRW) (Lundell *et al.*, 2011; Jutzeler *et al.*, 2016). At the micro- and ultra-structural level, differences between individuals with SCI and healthy controls were detected using diffusion and magnetization transfer imaging techniques (Cohen-Adad *et al.*, 2011). Crucially, trauma-induced changes in the spinal cord relate to clinical impairment. More atrophy was associated with worse functional independence (i.e.

SCIM) at 12 months (Freund *et al.*, 2013) and development of neuropathic pain (Jutzeler *et al.*, 2016). Morphometric measures of shape changes in APW and LRW correlated with sensory and motor scores, respectively, and were in good correspondence with the locations of main sensory (i.e. posterior column) and motor tracts (i.e. corticospinal tracts) (Lundell *et al.*, 2011). Spinal cord MRI metrics sensitive to micro- and ultra-structure (i.e. diffusion tensor imaging (DTI), magnetization transfer ratio (MTR)) in the ventrolateral and dorsal columns were related to corresponding clinical impairment of motor and sensory function, respectively (Cohen-Adad *et al.*, 2011).

Cervical spondylotic myelopathy

Standard clinical MRI, next to presentation of clinical symptoms, is indispensable in the diagnosis of CSM (Kalsi-Ryan, Karadimas, *et al.*, 2013) and helps (1) to identify the structural causes of CSM, (2) to determine the extent of cord compression and canal compromise (Fehlings *et al.*, 1999) and (3) to estimate the impact on neuronal tissue (i.e. signal intensity change) (Nouri *et al.*, 2015). These conventional measures are related to impairment and postoperative recovery and are used to assist decision making for surgical interventions (Arvin *et al.*, 2011, 2013; Nouri *et al.*, 2015), but still remain controversial (Ellingson *et al.*, 2014; Karpova *et al.*, 2014). Nevertheless, quantitative MRI methods may be promising to detect early changes of cord pathology in asymptomatic and mildly affected patients and therefor guide early interventional decision making. Using advanced MRI techniques, DTI and tractography at the compression site showed reduced fractional anisotropy (Ellingson *et al.*, 2014) and increased fiber density (Ellingson *et al.*, 2015) and were related to clinical impairment. Furthermore, column-specific degeneration was found in the anterior, posterior, and lateral columns using DTI (Cui *et al.*, 2014; Wen, Cui, Mak, *et al.*, 2014). Still, little is known about the structural integrity above the level of stenosis. Up to now, only MR spectroscopy revealed axonal and neuronal loss and ischemia based on reduced N-acetylaspartat and the presence of lactate peaks at this level (Holly *et al.*, 2009). Assessing the spinal cord integrity at vertebral level C2 is of interest due to the good CSF to cord contrast and the small intra-subject variability (Losseff *et al.*, 1996). In addition, this level (1) is rarely compressed and therefore its anatomical structure is well preserved and (2) potentially allows measuring conjoined effects from multifocal compression sites that contribute to impairment.

Diaschisis

Widespread changes have been observed along the neuroaxis in traumatic SCI and CSM. In traumatic SCI, neurodegeneration is evident in the spinal cord above the lesion site (Cohen-Adad *et al.*, 2011; Freund *et al.*, 2011, 2013; Lundell *et al.*, 2011; Jutzeler *et al.*, 2016) and in the brain (Jurkiewicz *et al.*, 2006; Wrigley, Gustin, *et al.*, 2009; Gustin *et al.*, 2010; Freund *et al.*, 2013; Mole *et al.*, 2014; Jutzeler *et al.*, 2016). In cervical spondylotic myelopathy, most studies have investigated the changes at the lesion site. However, there is evidence for neurodegenerative processes remote to the compression site (Holly *et al.*, 2009; Cui *et al.*, 2014; Wen, Cui, Mak, *et al.*, 2014; Ellingson *et al.*, 2015). These remote changes in SCI and CSM are suggestive for antero- and retrograde fiber degeneration (Jones and Pons, 1998; Woods *et al.*, 1999; Hains *et al.*, 2003; Buss *et al.*, 2004; Beaud *et al.*, 2008; Ghosh *et al.*, 2012). The phenomenon of remote changes in the CNS has been first described in stroke. Functional recovery that followed a focal lesion was thought to be the results of remote disruptive effects that were wearing off over time (Finger *et al.*, 2004). To describe this phenomenon, Constantin von Monakow introduced the term 'diaschisis' in 1914. Diaschisis is defined as a remote neurophysiological alteration in the CNS due to a lesion (Carrera and Tononi, 2014). This definition applies to spinal cord disorders as there is evidence for neurodegeneration above the level of lesion in SCI and CSM.

Potential clinical use of neuroimaging biomarkers

In spinal cord disorders, translation of scientific discovery from preclinical research to clinical trials and finally human application is challenging (Steeves, 2015). Thus, improvements in (1) patient stratification and selection (Steeves *et al.*, 2007; Tanadini *et al.*, 2014, 2015) and in (2) complementary outcome measures sensitive to subclinical improvements (Steeves *et al.*, 2007) should be achieved. These gaps may be filled by advances in quantitative MRI and computational neuroanatomy (Weiskopf *et al.*, 2015) that are now offering an exciting opportunity to develop MRI-based surrogate markers that could be used to improve diagnostics, to complement clinical assessments, to guide therapeutic strategies, and to predict future outcome (Martin *et al.*, 2016). The development of these promising quantitative MRI surrogate markers is supported by a growing community such as the Quantitative Imaging Biomarker Alliance (QIBA) which provides a larger framework including guidelines and recommendations to assist researchers and regulatory agencies (Kessler *et al.*,

2015; Raunig *et al.*, 2015). The potential of surrogate markers, but also their pitfalls, for efficient clinical trial designs is also acknowledged by the Food and Drug Administration (FDA) (Katz, 2004). MRI-based surrogate markers are widely used in clinical assessments and interventional studies in multiple sclerosis (Barkhof *et al.*, 2009) and Alzheimer disease (Frisoni *et al.*, 2010). Thus, the development and application of quantitative neuroimaging biomarkers seem to be feasible and promising - particularly for efficient clinical trial designs in spinal cord disorders (Cadotte and Fehlings, 2013) and in the decision making for surgical interventions in asymptomatic or mild CSM (Kalsi-Ryan, Karadimas, *et al.*, 2013).

Aims of the thesis

The overall objective of this thesis was to investigate neurodegeneration and reorganization in spinal cord disorders. The following aims were addressed specifically:

1) Tracking sensory system atrophy and myelin changes in the cord and brain in individuals with acute traumatic SCI and how these changes relate to functional and neurological impairment **(chapter 2)**
2) Investigation of atrophy and myelin changes in brainstem pathways and nuclei in individuals with chronic SCI and their relationship to impairment **(chapter 3)**
3) Assessment of brain plasticity during intensive virtual-reality augmented lower limb neurorehabilitation in individuals with chronic incomplete SCI **(chapter 4)**
4) Investigation of above stenosis neuronal degeneration in individuals with CSM **(chapter 5)**

Chapter 2:

Tracking sensory system atrophy and outcome prediction in spinal cord injury

Patrick Grabher[1], Martina F. Callaghan[2], John Ashburner[2], Nikolaus Weiskopf[2,3], Alan J. Thompson[4], Armin Curt[1] & Patrick Freund[1, 2, 3, 4]

[1]Spinal Cord Injury Center Balgrist, University Hospital Zurich, University of Zurich, Zurich, Switzerland

[2]Wellcome Trust Centre for Neuroimaging, Institute of Neurology, University College London, London, United Kingdom

[3]Department of Neurophysics, Max Planck Institute for Human Cognitive and Brain Sciences, Leipzig, Germany

[4]Department of Brain Repair and Rehabilitation, Institute of Neurology, University College London, London, United Kingdom

The original article was published in *Ann Neurol* 2015; 78:751-761

Abstract

Objective: In patients with sub-acute spinal cord injury (SCI), the motor system undergoes progressive structural changes rostral to the lesion, which is predictive of motor outcome. The extent to which the sensory system is affected and how this relates to sensory outcome is uncertain.

Methods: Changes in the sensory system were prospectively followed by applying a comprehensive MRI protocol to fourteen patients with sub-acute traumatic SCI at baseline, two months, six months, and twelve months, combined with a full neurological examination and comprehensive pain assessment. Eighteen controls underwent the same MRI protocol. T1-weighted volumes and myelin-sensitive magnetization transfer saturation (MT) and longitudinal relaxation rate (R1) mapping provided data on spinal cord and brain morphometry and microstructure. Regression analysis assessed the relationship between MRI readouts and sensory outcomes.

Results: At twelve months from baseline, sensory scores were unchanged and below-level neuropathic pain became prominent. Compared with controls, patients showed progressive degenerative changes in cervical cord and brain morphometry across the sensory system. At twelve months, MT and R1 were reduced in areas of structural decline. Sensory scores at twelve months correlated with rate of change in cord area and brain volume and decreased MT in the spinal cord at twelve months.

Interpretation: This study has demonstrated progressive atrophic and microstructural changes across the sensory system with a close relation to sensory outcome. Structural MRI protocols remote from the site of lesion provide new insights into neuronal degeneration underpinning sensory disturbance and have the potential as responsive biomarkers of rehabilitation and treatment interventions.

Introduction

Traumatic spinal cord injury (SCI) leads in most incidences to instantaneous loss of sensory input below the level of injury and permanent paralysis (Zariffa *et al.*, 2011). No effective treatments are currently available, though limited motor and sensory recovery can be promoted by intensive rehabilitation with the greatest improvements occurring during the first year after injury (Furlan *et al.*, 2011). During this time, disabling sensory discomfort and neuropathic pain below the level of lesion frequently develops as a secondary complication in SCI patients, severely impacting on patients' quality of life and functional independence (Siddall and Loeser, 2001; Siddall *et al.*, 2003). The underlying mechanisms influencing sensory impairment and its outcomes are thought to relate to structural changes including axonal degeneration and demyelination (Buss and Schwab, 2003), transneuronal atrophy (Jones and Pons, 1998), but also rewiring (Ghosh *et al.*, 2009) and hyper-excitability of neuronal circuits (Yague *et al.*, 2011).

Within the descending motor system, progressive structural changes have been directly linked to the recovery of muscle strength and functional independence during the first year following SCI (Freund *et al.*, 2013). However, the structural correlates and time course of changes in sensory impairment and emergence of neuropathic pain within the injured spinal cord, as well as the brain, are less well defined. Cross-sectional studies in chronic SCI have shown that sensory impairment and neuropathic pain below the level of the lesion correlated with structural (Miyanji *et al.*, 2007; Wrigley, Gustin, *et al.*, 2009; Gustin *et al.*, 2010; Cohen-Adad *et al.*, 2011; Lundell *et al.*, 2011; Mole *et al.*, 2014) and functional changes (Stroman *et al.*, 2002; Cadotte *et al.*, 2012) within the sensory system. However, such cross-sectional studies in chronic SCI do not allow for assessment of the spontaneous evolution of structural and functional changes attributable to (i) the acute onset of deafferentation (Jain *et al.*, 2000; Aguilar *et al.*, 2010; Chen *et al.*, 2012), (ii) spontaneous partial sensory recovery or (iii) relearning of compensatory approaches relevant for activities of daily living (i.e. visual inputs) (Villiger *et al.*, 2015). Therefore, there is only limited knowledge about the temporal dynamics and specificity of trauma-induced structural changes and their link to the arising sensory impairment and outcome and below-level neuropathic pain within the spinal cord, brainstem, and brain (Garcia-Larrea and Peyron, 2013).

Recent advances in quantitative neuroimaging of the spinal cord and brain provide the possibility of monitoring temporal changes of the macro- as well as the microstructure from the earliest onset of spinal cord injury (Huber *et al.*, 2015; Weiskopf *et al.*, 2015). In a longitudinal prospective design, we used advanced MRI outcome measures to assess the spontaneous time course of structural progressive changes within the sensory system above the spinal level of the lesion (i.e. cervical cord and brain). We measured cross-sectional spinal cord area including both anterior-posterior width (APW) and left-right width (LRW) to provide detailed insights into morphometric cord changes (Lundell *et al.*, 2011). At the level of the brain, we applied tensor-based morphometry to assess dynamic volumetric changes (Ashburner and Ridgway, 2013) and voxel-based quantification of magnetization transfer saturation (MT) and longitudinal relaxation rate (R1) maps (Weiskopf *et al.*, 2011) to gain information about myelin integrity at twelve months follow-up. We hypothesized that specific macro- and microstructural changes appear in the sensory system early after traumatic SCI and that volumetric decreases would be associated with the extent of sensory impairment/outcome and the development of neuropathic pain below the level of injury.

Material and Methods

Subjects and study design

Fourteen patients with a sub-acute (< 2 months post-injury) traumatic SCI (Table 1) and 18 healthy control subjects were recruited at the University Hospital Balgrist between July 2010 and June 2013. All patients fulfilled the following inclusion criteria: Sub-acute (<2 months post-injury) traumatic SCI without head and brain lesions, no pre-existing neurological, mental or medical disorders affecting functional outcome, and no contradictions to MRI.

ID	Age at injury (years)	Injury		ISNCSCI grade at baseline	Initial site of impairment (motor/sensory)	ISNCSCI pinprick		ISNCSCI light touch	
		Type	Severity			Baseline Left/Right	12 months Left/Right	Baseline Left/Right	12 months Left/Right
1	19	Fall	Complete	A	C5/C4	13/13	16/17	12/12	16/17
2	23	Fall	Incomplete	B	C7/C6	18/20	19/18	34/35	35/37
3	70	Fall	Incomplete	B	T10/T10	37/38	NA*	40/38	NA*
4	75	Fall	Incomplete	D	T12/T12	52/50	NA**	56/55	NA**
5	44	Fall	Incomplete	D	T11/T11	56/53	55/51	56/51	55/51
6	42	Fall	Complete	A	C5/C5	10/10	10/8	13/14	9/11
7	71	Fall	Incomplete	B	C7/C8	16/20	22/19	42/43	56/56
8	20	MVA	Complete	A	C5/C5	10/9	15/11	10/11	29/24
9	30	MVA	Incomplete	B	C7/C8	17/18	18/19	33/31	35/35
10	52	Fall	Incomplete	D	T9/T9	45/44	45/45	48/47	45/45
11	42	MVA	Incomplete	D	C5/C4	53/51	56/41	52/52	56/42
12	29	Fall	Complete	A	T11/T11	44/44	38/40	43/43	41/41
13	70	MVA	Complete	A	T7/T7	28/37	31/37	35/37	31/36
14	52	MVA	Incomplete	B	C6/C6	19/19	30/14	32/33	33/34

Table 1: Clinical and behavioral data of 14 patients with sub-acute traumatic spinal cord injury. All patients were male, only patient 3 was female. ISNCSCI = International Standards for the Neurological Classification of Spinal Cord Injury. MVA = motor vehicle accident. *No sensory testing was performed. ** Patient died.

A comprehensive and detailed clinical protocol and pain questionnaire was performed on patients at baseline, two months, six months, and twelve months to assess their sensory and motor impairments. This protocol included the International Standards for the Neurological Classification of Spinal Cord Injury (ISNCSCI) protocol (Kirshblum *et al.*, 2011) for motor, light touch and pinprick score, and the Spinal Cord Independence Measure (SCIM) (Anderson *et al.*,

2008). Using the European Multicenter Study about Spinal Cord Injury (EMSCI) pain questionnaire (V4.2, http://www.emsci.org/) (Hassanpour *et al.*, 2012; Widerström-Noga *et al.*, 2014), we assessed multiple aspects of pain (e.g., onset, duration, maximal and average pain intensity, quality of pain (e.g. nociceptive or neuropathic)) at each time point. To be classified as below-level neuropathic pain, ongoing pain had to be located three or more segments below the level of lesion. Pain intensity was assessed using an 11-point numeric rating scale with "0" indicating no pain to "10" indicating worst pain imaginable pain.

All participants underwent a comprehensive MRI protocol at the same time points. The relationship between SCIM and ISNCSCI motor scores and structural changes have been reported previously in a subgroup of the present study cohort (Freund *et al.*, 2013). Informed written consent was obtained from all participants before participation. The study protocol was in accordance with the Declaration of Helsinki and was approved by the local Ethics Committee of Zurich (EK-2010-0271).

Image acquisition

Participants were scanned with a 3T Magnetom Verio MRI scanner (Siemens Healthcare, Erlangen, Germany) operating with a 16-channel radio-frequency (RF) receive head and neck coil and RF body transmit coil. All participants were carefully positioned in the same position all the time by the radiographers to obtain high reproducibility across participants and time points to exclude any bias related to potential gradient non-linearity over time at the level of the spinal cord.

T1-weighted (T1w) structural whole-brain volumes including the cervical cord to C5 were collected at each time point. At twelve months, we acquired additional data using a multi-parameter mapping (MPM) quantitative MRI (qMRI) protocol (Weiskopf *et al.*, 2011). Data collected using this protocol can be used to compute maps of the longitudinal relaxation rate (R1)(Rooney *et al.*, 2007) and magnetization transfer saturation (MT) (Helms *et al.*, 2008). These metrics are physical MRI parameters, respectively describing the relaxation and magnetization transfer behavior of protons within their micro-environments. Both processes are enhanced by the presence of macromolecular content, e.g. myelin. As such, they are sensitive to tissue microstructure and provide quantitative measures that can be used for

multicenter studies and give information about myelin, water, and iron content (Weiskopf *et al.*, 2013). All image volumes were checked for artefacts.

For each subject, a 3D T1w scan (MPRAGE) (Tardif *et al.*, 2009) with 176 partitions was acquired at 1 mm isotropic resolution in 9 minutes using the following parameters: field of view of 224 x 256 mm^2, matrix size of 224 x 256, time of repetition (TR) of 2420 ms, echo time (TE) of 4.18 ms, inversion time (TI) of 960 ms, flip angle α=9°, and readout bandwidth of 150 Hz per pixel.

The quantitative MPM data were derived from three differently contrast weighted 3D multi-echo FLASH volumes acquired with 1mm isotropic resolution and a field of view of 240 x 256 mm^2 (matrix size of 240 x 256) with 176 partitions in a total scan time of 23 minutes. To reduce the overall acquisition time, parallel imaging with a speed up factor of 2 was used in the phase-encoding direction (anterior-posterior) using a generalized auto-calibration partially parallel acquisition algorithm (GRAPPA). Additionally, a partial Fourier acquisition with a 6/8 sampling factor was used in the partition direction (left-right). Predominantly T1-weighting was achieved with TR=25 ms and α=23° while PD-weighting was achieved with TR=25 ms and α=4°. Magnetization transfer weighting (TR=37 ms, α=9°) was achieved by applying an off-resonance RF pulse prior to non-selective excitation. The readout bandwidth was 480 Hz per pixel. Seven equidistantly spaced echoes were acquired with TE ranging from 2.46 ms to 17.22 ms for all volumes. One additional echo was acquired at 19.68 ms for both the PD-weighted (PDw) and T1w volumes.

Image analysis

Changes to the macro- and microstructure of the cervical cord

We investigated remote trauma-induced structural changes within the spinal cord at cervical level C2/C3. In addition to the already reported cross-sectional spinal cord area (Freund *et al.*, 2013), we here assessed its change in the shape, which we parameterized with APW and LRW, since reductions in these are related to sensory and motor impairment, respectively (Lundell *et al.*, 2011).

We used JIM 6.0 (Xynapse systems, Aldwincle, UK) to extract 10 contiguous and reformatted axial slices of 3 mm at the C2/C3 level from the structural MPRAGE T1w volume. The cross-sectional cord area was then calculated automatically with an active-surface model (Horsfield

et al., 2010). An ellipse was fit to the boundary of this spinal cord area in Matlab (The Mathworks Inc., Natick, MA, USA) to extract APW (elliptical short axis) and LRW (elliptical long axis).

To assess changes to the myelin content at the identical cervical cord level, we used in-house Matlab scripts based on nearest-neighbor region growing to define the cord volume (stopping criterion: 40% drop in parameter value) within the MT map followed by the same ellipse fitting procedure. This region of interest for the spinal cord was superimposed on the R1 maps and used to extract the mean quantitative parameters from the MT and R1 maps (processing of quantitative maps is explained in the next section).

Changes to the macro- and microstructure of the brain

We used tensor-based morphometry, implemented in SPM12 (Wellcome Trust Centre for Neuroimaging, University College London, London, UK), to investigate dynamic volumetric brain changes in patients and controls over time. This was performed with the MPRAGE T1w images obtained at baseline, two months, six months, and twelve months. For each participant, the four volumes were aligned longitudinally to their midpoint average using inverse-consistent 3D non-linear registration (Ashburner and Ridgway, 2013). This generated Jacobian determinant maps for each time point, as well as the participant's average image (both in terms of shape and intensity). Unified segmentation was used to segment the average image into gray matter, white matter, and cerebrospinal fluid (Ashburner and Friston, 2005). The Jacobian determinant maps were transformed to MNI (Montreal Neurological Institute) space using deformations derived from the fast diffeomorphic image registration algorithm (Dartel) (Ashburner, 2007). The spatially normalized Jacobian maps were finally smoothed with an isotropic Gaussian kernel filter with 2 mm full width at half maximum (FWHM). The processed data encoded volumetric expansion and compression in each participant (Freund *et al.*, 2013).

We used voxel-based quantification (Draganski *et al.*, 2011; Weiskopf *et al.*, 2011) to investigate the cross-sectional differences in myelin integrity between patients and controls at twelve months. MT-weighted (MTw), PDw and T1w FLASH volumes were used to calculate quantitative parameter maps of MT and R1, which are sensitive to microstructural features of the tissue (Weiskopf *et al.*, 2015). While MT maps are primarily sensitive to macromolecular

content, most notably myelin (Helms *et al.*, 2008, 2009), R1 maps are additionally sensitive to free water content, axon diameter, and iron content (Rooney *et al.*, 2007; Harkins *et al.*, 2015).

UNICORT was used for bias estimation and correction of RF transmit field inhomogeneity effects in the R1 maps (Weiskopf *et al.*, 2011). The MT maps for each participant were segmented into gray matter, white matter, and cerebrospinal fluid using unified segmentation (Ashburner and Friston, 2005). The transformation to the MNI space was performed using Dartel (Ashburner, 2007). Finally, the MT and R1 maps were warped to the MNI space with the participant-specific flow fields from the MT maps obtained with Dartel and smoothed with an isotropic Gaussian kernel filter with 3 mm FWHM. The VBQ approach was used for this normalization process to minimize partial volume effects (Draganski *et al.*, 2011).

Because we were interested in trauma-induced degeneration in the ascending sensory system, we defined specific regions of interest. The subcortical and cortical regions of interest were defined as one single ROI encompassing the bilateral anterior cingulate cortex (ACC), thalamus, primary (S1) and secondary somatosensory cortex (S2), and insula to include the main sensory and pain modulatory structures (Murray and Mishkin, 1984; Ogino *et al.*, 2007; Ray *et al.*, 2008; Eippert *et al.*, 2009; Mole *et al.*, 2014) using the anatomy toolbox for SPM (Eickhoff *et al.*, 2005). The brainstem and cerebellum were defined as a further region of interest using the SUIT toolbox for SPM (Diedrichsen, 2006). Regions were chosen according to whether they contain/receive ascending sensory pathways (Jahn *et al.*, 2008; Moulton *et al.*, 2010; Benarroch, 2013; Tattersall *et al.*, 2014).

Statistical analysis

Stata 13 (StataCorp LP, Texas, USA) was used for statistical analysis of all non-brain data. We estimated the rates of change of clinical impairments in patients with linear regression models, with time as predictor. To accommodate non-linear recovery, time was modelled on a logarithmic scale. We assessed the rate of change of the spinal cord parameters using linear regressions in all participants. A group indicator, group x time, and time x time interaction were included in the regression model to compare the rates of change and to accommodate quadratic effects. Age, sex and their interaction with time were used to diminish any confounding (linear) effects. Two-sample t-tests were used to assess MT and R1 differences between patients and controls in the spinal cord at twelve months.

Linear regression models in SPM12 were used to assess longitudinal brain volume changes in gray and white matter, and the microstructure at twelve months, in the defined regions of interest. The analyses included a group indicator and time. Age was treated as a covariate of no-interest. Statistical parametric maps were initially thresholded with an uncorrected voxel threshold of p=0.001. To account for multiple testing only clusters surpassing a corrected cluster threshold of p=0.05 FWE- corrected based on Gaussian Random Field Theory were considered as significant (unless otherwise stated for peak-voxel) (Friston *et al.*, 1994) and reported in the Results. One-tailed t-tests with a significance threshold of $p<0.05$ were used in each voxel of interest to test for decreases in patients and to compare the integrity of myelin between controls and patients, using the 12 month MT and R1 data. To ensure that each voxel was analyzed only once either in the GM or WM segments, explicit masks for each subspace were generated by assigning each voxel with a probability greater than 20% to the tissue class with the highest probability (Callaghan *et al.*, 2014). After characterizing the average group effects, we explored regional structural correlates of sensory function. We used linear regression models to examine associations between the individual MRI-derived metrics (e.g. spinal cord and brain metrics) as predictors and clinical outcomes at twelve months in patients as dependent variables. Age and lesion-level were modelled as confounds. Only significant associations are reported.

Results

Fourteen patients with sub-acute traumatic spinal cord injury (13 men and one woman), with a mean age of 45.6 years (SD 20.0), and 18 healthy participants (12 men and six women), with a mean age of 34.1 years (SD 9.5) were enrolled in this study (Table 1). There was no statistically significant difference between the mean ages in the two groups (Mann-Whitney-U-Test p=0.138). Eight patients suffered from a tetraplegia (three with a complete lesion) and six from paraplegia (two with a complete lesion) according to the ISNCSCI classification.

The mean interval from the time of injury to the baseline scan was 45.93 days (SD 18.38), to the second scan 96.64 days (38.09), to the third scan 209.46 days (59.14), and to the last scan 380.54 days (109.32). In total, 122 datasets were included, of which 32 were acquired at baseline, 29 at two months, 31 at six months and 30 at twelve months. Thus 95.3% of planned assessments were accomplished.

Besides the improvements in ISNCSCI motor score and SCIM score (as reported for this patient cohort earlier (Freund *et al.*, 2013)), patients did not recover on the ISNCSCI pinprick (increase of 0.046 per log month, p=0.967) and ISNCSCI light touch (increase of 1.439 per log month, p=0.324) score. Neuropathic pain below the lesion emerged in six patients and their pain intensity increased over time on the EMSCI pain questionnaire (mean pain intensity increased by 0.71 per log month 95% CI 0.072 - 1.341, p=0.029).

Changes to the macro- and microstructure of the cervical cord

In addition to progressive decrease in overall cord area at C2/C3 above the lesion level in patients (Freund *et al.*, 2013), we found spatially specific dynamic shape changes of the APW and LRW at the identical level (Figure 1A and B) between patients and controls ($p<0.001$). In patients, the decrease of the APW was 0.022 mm per month (95% CI -0.041 to -0.003, p=0.023) and LRW decreased by 0.034 mm per month (95% CI -0.059 to -0.010, p=0.005). In controls the cord metrics did not change over time (p=0.238 for cord area, p=0.136 for APW, p=0.412 for LRW). In patients, the rate of decrease was similar between the APW and LRW (p=0.520). At the cervical cord level at twelve months, myelin-sensitive MT and R1 were reduced in patients (MT: 2.65 %, CI 2.40-2.90 %, p=0.003; R1: 0.848 s^{-1}, CI 0.769-0.926 s^{-1}, p=0.012) compared to controls (MT: 3.08 %, CI 3.00-3.16 %; R1: 0.968 s^{-1} CI 0.916-1.020 s^{-1}) by 14.96% and 12.41%, respectively (Figure 1C and D).

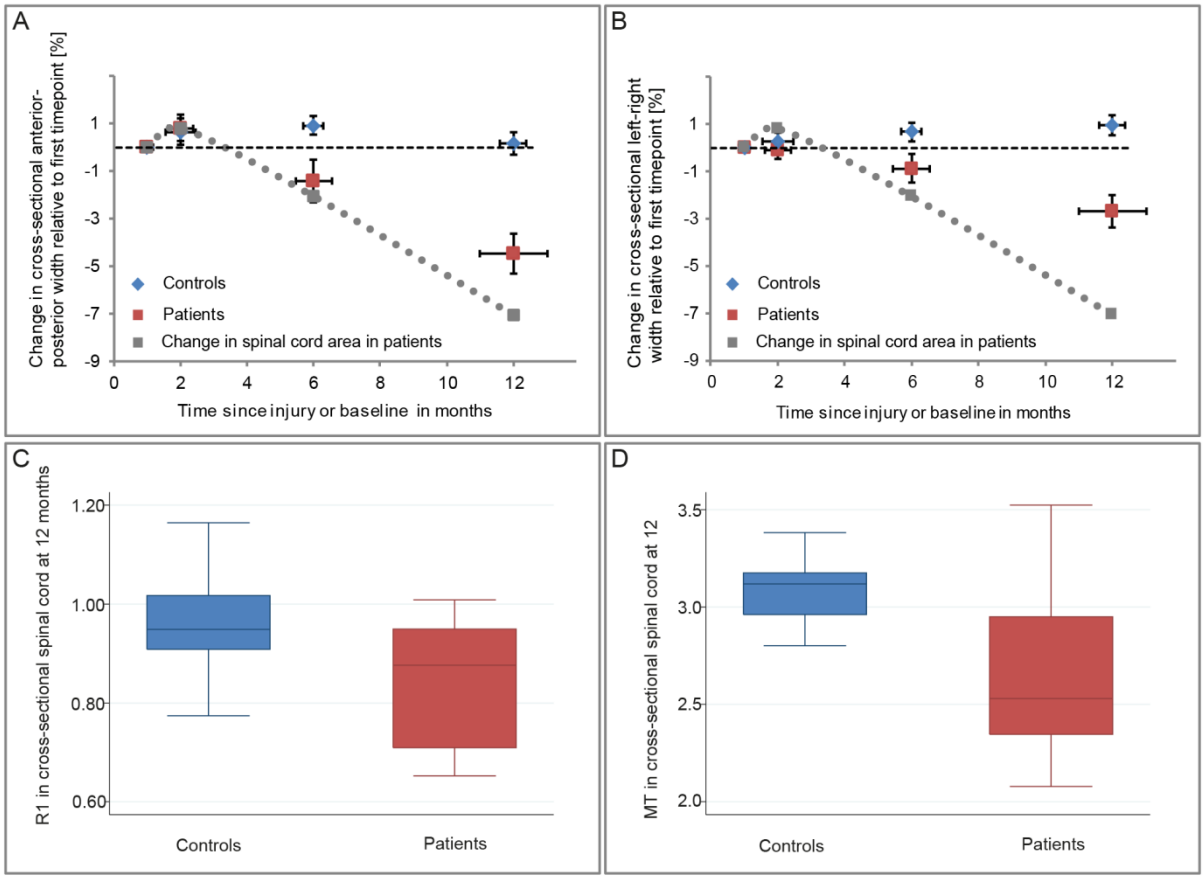

Figure 1: Longitudinal shape and cross-sectional microstructural changes of the spinal cord above the lesion level at C2/C3. (A) Shrinkage of the anterior-posterior width (APW) in patients compared to controls. (B) Shrinkage of the left-right width (LRW) in patients. No change was detected in controls. Vertical error bars show standard error (SE) for change in APW and LRW and horizontal error bars show SE for scan intervals. (C&D) Reduction of mean R1 and MT respectively at cervical C2/C3 level in patients compared to controls. Note that the results from the cross-sectional cord area change has been reported previously (Freund *et al.*, 2013) and are shown only for illustrative purposes.

Changes to the macro- and microstructure in the brain

Progressive focal brain volume decreases of up to 3% in the right thalamus (x: 20, y: -35, z:2, z-score 4.20, p=0.037, cluster extent=287; x:2, y:-5, z:8, z-score 3.82, p=0.019, cluster extent=358) , left thalamus (x:-20, y:-30, z=9, z-score 3.98, p<0.001, cluster extent=1324), right ACC (x:17, y:30, z:3, z-score 3.89, p=0.003, cluster extent=586), left ACC (x:-15, y:28, z:-1, z-score 3.62, p=0.010, cluster extent=432), left insula (x:-38, y:-24, z:17, z-score 3.85, p<0.001, cluster extent=1028), left S2 (x:-54, y:7, z:5, z-score 4.09, p<0.001, cluster extent=842), and pons (x:2, y: -39, z:-31, z-score 4.62, p<0.001, cluster extent=926) developed over time in patients compared to controls (Figure 2).

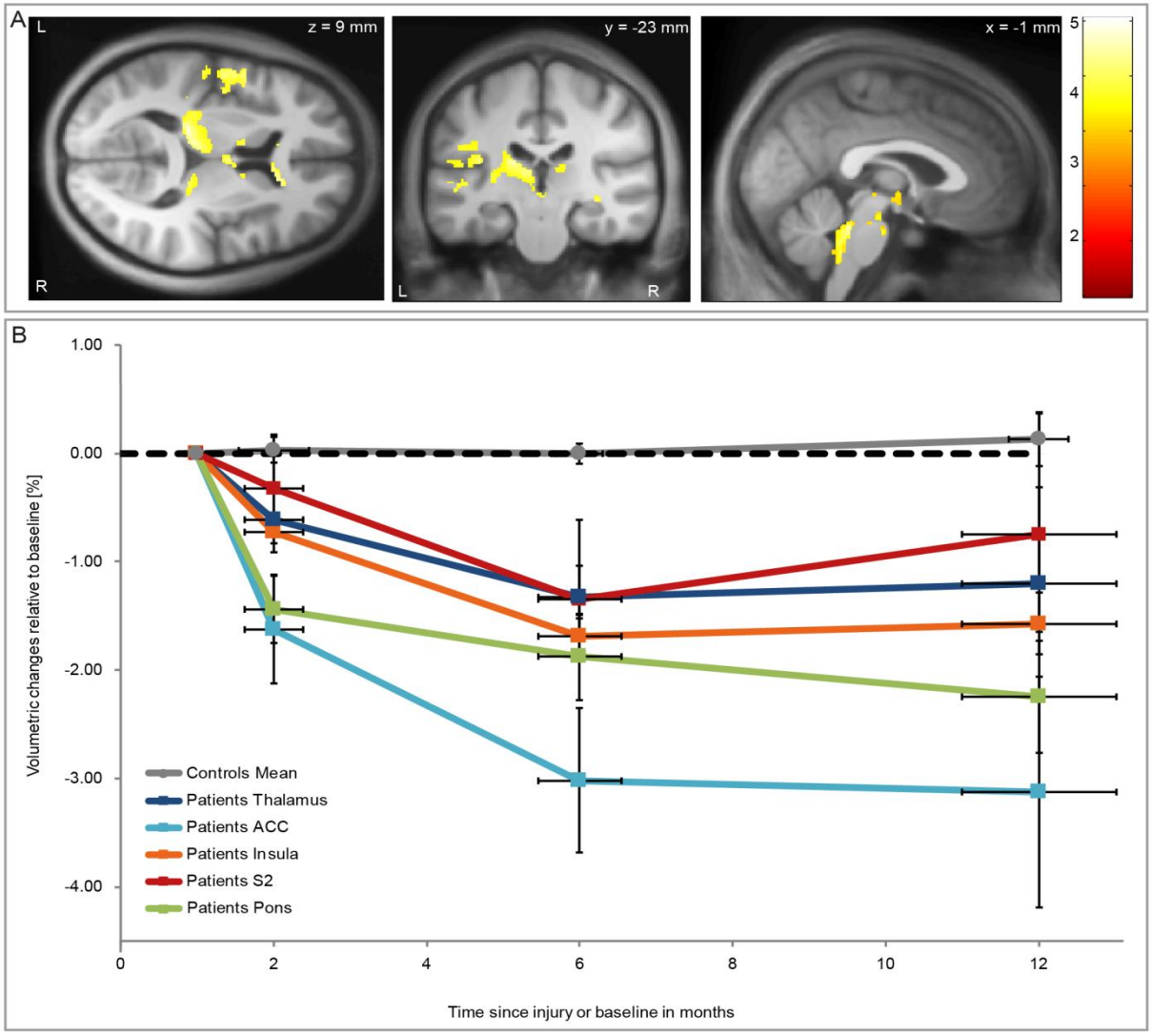

Figure 2: Longitudinal volumetric decreases in subcortical and brainstem gray and white matter shown by tensor-based morphometry. (A) Overlay of statistical parametric maps (uncorrected p<0.001, for illustrative purposes) showing volumetric decreases in gray and white matter. The color bar indicates the t-score. (B) Illustration of progressive volumetric changes relative to baseline extracted from selected areas of interest. Vertical error bars show SE for volumetric change in selected area of interest and horizontal error bars show SE for scan intervals.

At twelve months, myelin-sensitive R1 was reduced in the thalamus by up to 19% (x: 0, y:-26, z:-3, z-score 4.10, p<0.001, cluster extent=959). R1 was also reduced by 20% in the left (x:9, y:-45, z:-30, z score 4.39, p<0.001, cluster extent=1940) and by 17% in the right cerebellum (x: 2, y:-53, z:-14, z score 4.31, p<0.001, cluster extent=3124). The latter cluster is extending into the brainstem (e.g. medulla oblongata, pons, and midbrain). Myelin-sensitive MT was reduced by 14% in the spinal cord dorsal columns (x:0, y: -50, z:-66, z score 4.80, p=0.045, cluster extent=51, only significant at peak-voxel) (Figure 3).

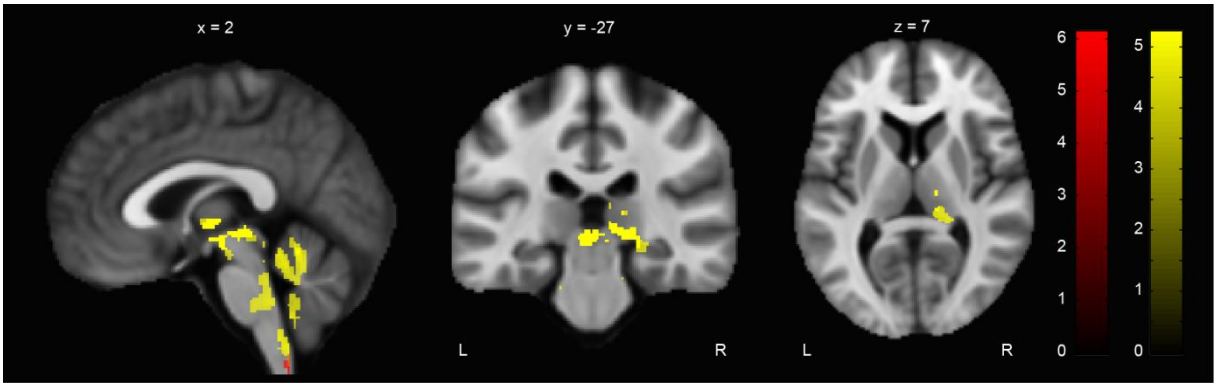

Figure 3: Changes in microstructure at twelve months revealed by voxel-based quantification. Overlay of statistical parametric maps (uncorrected p<0.001, for illustrative purposes) showing reduced MT (red) and R1 (yellow) in patients compared to controls at twelve months in thalamus, cerebellum with a cluster extending into the brainstem (i.e. medulla oblongata, pons, and midbrain), and medulla oblongata (i.e. dorsal column). These reductions suggest microstructural changes in patients because MT and R1 are both sensitive to myelin.

Association between structural changes and clinical outcomes

ISNCSCI pinprick scores at twelve months were associated with rate of cord area decrease (p=0.020, r^2=0.76) (Figure 4A). ISNCSCI pinprick scores at twelve months were associated with rate of volumetric changes in the right cerebellum (x:2, y:-47, z:-18, z-score 5.80, p<0.001, cluster extent=197; x:12, y:-62, z:-16, z-score 4.87, p=0.017, cluster extent=75) (Figure 5A and B) and ISNCSCI light touch scores with rate of volumetric changes in the dorsal columns at the level of the medulla oblongata (x:14, y:-29, z:-42, z-score 4.07, p=0.023, cluster extent=31; x:-8, y:36, z:-48, z-score 3.88, p=0.016, cluster extent=76; x:5, y:-45, z:-63, z-score 4.76, p=0.026, cluster extent=76, latter cluster only significant at peak-voxel) (Figure 5A and C), respectively. At twelve months, ISNCSCI pinprick scores were associated with spinal cord MT (p=0.005, r^2=0.82) (Figure 4B).

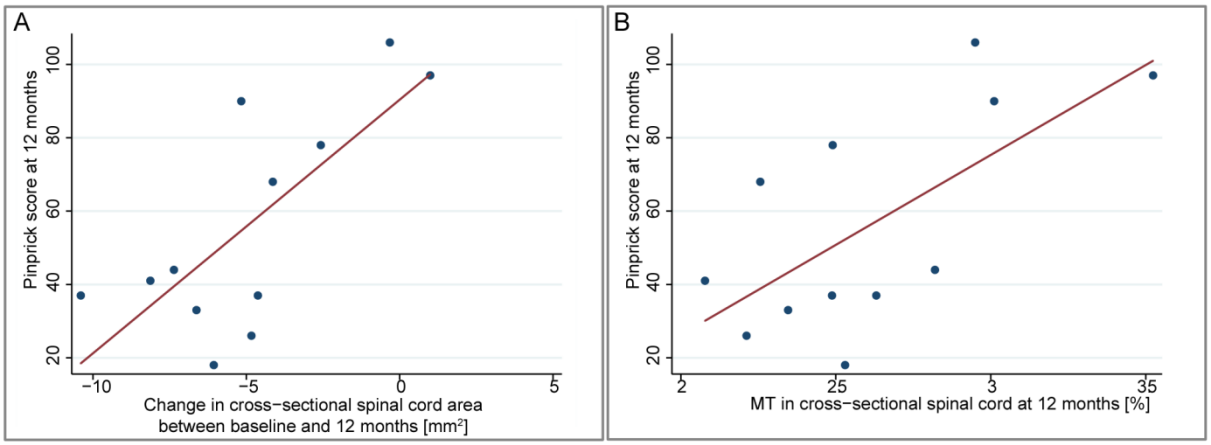

Figure 4: Correlations between structural changes in spinal cord and sensory outcome. Correlation between pinprick score and change in cross-sectional spinal cord area between baseline and twelve months (A) and MT at twelve months (B).

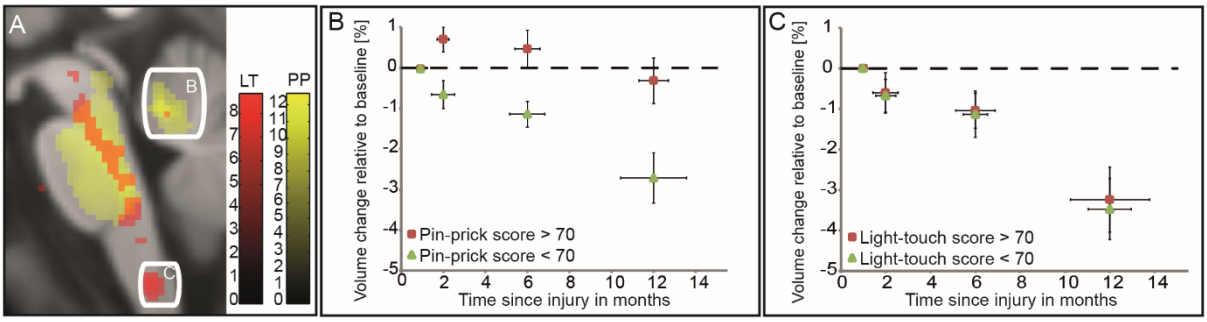

Figure 5: Correlation between progressive volumetric changes in the brain and sensory outcome. (A) Overlay of statistical parametric maps (uncorrected p<0.001, for illustrative purposes) showing a correlation between cerebellum and pinprick score at twelve months (yellow, data of peak-voxel plotted in B) and between the medulla oblongata and light touch score at twelve months (red, data of peak-voxel plotted in C). The color bars indicate the corresponding t-scores. (B) Greater volumetric decreases over time in patients with lower pinprick outcome at twelve months. (C) No difference in volumetric decreases over time in patients with lower light touch outcome at twelve months. Vertical error bars show SE for volumetric change in selected area of interest and horizontal error bars show SE for scan intervals. Arbitrary threshold for clinical outcome at twelve months was set to 70 (for illustrative purposes).

Discussion

This study shows progressive volumetric decreases along the sensory system from the earliest stage after spinal cord injury. The evaluation of myelin-sensitive MR supports the hypothesis that the observed volumetric changes relate to changes in the underlying myelo-architecture. From the clinical perspective, the observed structural changes in the cord and brain were related to the extent of sensory outcome but were not related to neuropathic pain. Thus, both the motor (Freund *et al.*, 2013) and sensory systems are susceptible to atrophy early after injury. Therefore the MRI changes could be considered as complementing the clinical assessment for monitoring sensory impairment and outcome during the course of rehabilitation and treatment interventions following SCI.

Evolution of structural changes from the spinal cord to the brain

During the first year after traumatic spinal cord injury, the cord area declines by 7% (Freund *et al.*, 2013) with a reduction of up to 30% fifteen years post-injury (Freund *et al.*, 2011; Lundell *et al.*, 2011). Besides the overall reduction of cord area, morphometric changes may provide further insight into tract specific changes, as reductions of the APW have been associated with sensory impairment and the LRW with motor function in chronic SCI (Lundell *et al.*, 2011). Here, we assessed the progressive shape changes of the cord (i.e. APW and LRW). In agreement with the observations in chronic SCI patients (Lundell *et al.*, 2011), shape deformations occurred both in the APW and LRW. The change in the APW might reflect anterograde degeneration occurring along the dorsal columns (Jain *et al.*, 2000; Lundell *et al.*, 2011; Chen *et al.*, 2012) in parallel to retrograde degeneration of the descending tracts (e.g. corticospinal tracts) captured by the LRW (Lundell *et al.*, 2011). The reductions of myelin-sensitive MT and R1 parameters –at the same cord level– and of diffusion tensor metrics in the chronic injured spinal cord (Cohen-Adad *et al.*, 2011; Freund, Schneider, *et al.*, 2012) may reflect on-going changes of the myelin architecture that in turn contribute to the shape changes.

At the level of the brain, we found progressive volumetric decreases in areas involved in sensory processing (e.g. brainstem, thalamus, ACC, S2, and insula) between baseline and twelve months. Alterations in structure and function in these areas (Jain *et al.*, 2000; Gustin *et al.*, 2010, 2014; Widerström-Noga *et al.*, 2013) have been associated with impaired sensory processing and sensory discomfort in patients with SCI (Garcia-Larrea and Peyron, 2013).

Similar to findings in the spinal cord, myelin-sensitive R1 and MT paralleled the volumetric changes observed in the thalamus, cerebellum, and medulla oblongata comprising the dorsal columns. The bilateral decrease of both volume and myelin-sensitive MR parameters within the same cortical areas is suggestive of on-going structural changes responding to the spinal cord injury which in the present SCI cohort caused equally severe impairments on either side of the body. These changes are likely to involve changes at the level of cellular metabolism, blood flow and functional depression inducing a state of hypo-activity and shrinkage of sensory neurons and their axons (Moxon *et al.*, 2014). In accordance with motor system atrophy during the first year after injury (Freund *et al.*, 2013), the magnitude of atrophy within the sensory system was evident in both incomplete and complete paraplegic and tetraplegic patients. This finding is of interest, as patients with a very chronic SCI show level-dependent spinal atrophy – with more pronounced atrophic changes in those patients with higher lesion levels (Lundell *et al.*, 2011). Thus, level-dependent atrophy (i.e. lesions in the cervical cord impact the structural integrity of a greater number of fibers and neurons than a comparable thoracic lesion) may only become distinguishable at later disease stages of SCI. However, we are aware that the sample size of our study is rather small and weak effects might not have been detected. To detect the full spectrum of potential changes, future multi-center studies with the advantage of collecting large sample size are required. Our results provide the necessary motivation and evidence for conducting such expensive studies.

Clinical associations with structural changes

Crucially, the rate of volume change and the reduction of myelin-sensitive structural measures in the cord and volume changes in the brain related quantitatively to sensory deficits. In other words, faster atrophy and greater decreases in myelin-sensitive markers were seen in ascending spinal pathways and sensory specific brain areas in patients with greater loss of pain (pinprick) and light touch (brush) sensation. At the cervical cord and the medulla oblongata level, long distance Wallerian degeneration of primary afferents within the spinothalamic tracts as wells as dorsal columns is a likely pathophysiological substrate underlying the clinicopathological associations of pinprick and light touch (Kaas, H.-X. Qi, *et al.*, 2008; Zhang *et al.*, 2009). Within the brainstem and cerebellum – both receivers of afferent spinal inputs (Jain *et al.*, 2000; Moulton *et al.*, 2010) – the interpretation of the association between trauma-induced atrophy rate and light touch and pinprick outcome is more complex. In

addition to Wallerian degeneration of ascending fiber pathways that arise from the spinal cord, transsynaptic changes affecting the structure and function of sensory relay nuclei in the brainstem and neurons within the cerebellum (e.g. Purkinje Cells) occurs as a consequence of deafferentation (Kaas *et al.*, 1999; Jain *et al.*, 2000; Villiger *et al.*, 2015). The relationship between greater cerebellar atrophy rate and worse pinprick outcome is therefore interesting, as the cerebellum may also be involved in trauma-induced maladaptive processing of afferent sensory inputs (e.g. nociception) (Cerminara *et al.*, 2009) alongside its role as an comparator for errors in somatosensory processing (Apps and Garwicz, 2005) resulting in motor impairment (Moulton *et al.*, 2010). Thus, a trauma dependent altered structure function relationship due to deafferentation could explain why patients with greater sensory dysfunction (i.e. worse protopathic sensation) show more severe atrophy. The shape changes (APW, LRW) of the cord could not be associated with specific sensory outcomes. Therefore, the rather gross geometrical changes (APW, LRW) along the axis might only become responsive to sensory impairment in the very chronic phase of injury (Lundell *et al.*, 2011).

The clinical standard to determine the degree of sensory disability (i.e. epicritic and protopathic sensation) after spinal cord damage is the testing of light touch and pinprick sensation, respectively. Somatosensory (Kuhn *et al.*, 2012) and contact heat evoked potentials (Haefeli *et al.*, 2013) have been shown to provide complementary insights into the pathophysiology underlying sensory deficits as they reveal subclinical afferent sparing beyond pinprick and light touch sensation. Thus future serial studies will integrate these complementary measures as they have the potential to reveal pathology to anatomically distinct pathways with greater resolution (i.e. dorsal columns and spinothalamic tract) (Ellaway *et al.*, 2011).

Although neuropathic pain developed in this patient group over time, neither the onset nor the intensity of neuropathic pain was linked to neurodegeneration (e.g. reduction in volume decline and myelin) during the first year of injury. While loss of sensory input is generally induced by neural damage and disconnection within ascending sensory pathways (Jain *et al.*, 2000; Chen *et al.*, 2012), most important mechanisms underlying neuropathic pain in the sub-acute phase of injury originate in the brain with complex interactions of the spinal and supraspinal neuronal circuits (Wrigley, Press, *et al.*, 2009; Makin *et al.*, 2013; Mole *et al.*, 2014). Studies focusing on the chronic phase were able to associate structural changes in brain

regions with nociceptive processing (i.e. thalamus, prefrontal cortex, insular cortex, amygdala, and premotor cortex) although the ultimate mechanisms remain unclear (Wrigley, Press, *et al.*, 2009). Future multimodal studies integrating serial structural and functional MRI and electrophysiological assessments of pain are needed to address this issue further.

Limitations

Our study had some limitations. Firstly, controls were on average 12 years younger than patients. We included age as a covariate in all statistical analyses to exclude any (linear) age-related effects, although the relationship between age and cord area is not significant (Callaghan *et al.*, 2014). Moreover, our analysis revealed that the brain volume trajectories were not significantly associated with age nor did the adjustment of age influence the latter significantly. However, the validity of the adjustment can only be asserted confidently for patients and controls under 55 years of age, since there were no controls older than 55 years. Secondly, while computational morphometry can reveal disease-specific changes over time, it is not biologically specific. In this study, these morphometric changes were paralleled by changes in qMRI metrics that are sensitive to underlying tissue microstructure. Measures of MT provide information about the macromolecular content of the microstructural environment. Although not a direct measure of myelin, post mortem validation has shown high correspondence between MT-based measures and myelin staining (Schmierer *et al.*, 2004; Turati *et al.*, 2015), indicating that myelin is a significant contributor to this measure. While there are multiple contributors to the measured R1, including water and iron content, the contribution from macromolecular components has been shown to dominate (Rooney *et al.*, 2007; Callaghan *et al.*, 2015). Therefore we interpret the changes observed in this study as being consistent with axonal demyelination that contributes to volumetric changes within the sensory system. Thirdly, the aim to define compartments of the spinal cord to distinguish ascending and descending pathways is not completely accurate as tracts located laterally also transmit ascending information (e.g., spinocerebellar and spinothalamic tracts). Finally, the mean intervals between the MRIs in patients during follow-up varied, but importantly as a result, the dropout rate was minimal (compliance of 95%). We note that we accounted for this variability in the linear trajectory analyses of cord and brain MRI parameters by explicitly modelling the timing of the MRI acquisitions for all subjects.

Conclusion

The neuroimaging biomarkers applied for the first time were sensitive to reveal dynamic volumetric changes of the sensory system at both spinal cord and supraspinal level that are likely to be associated with changes in myelin architecture. Importantly, slower rates of atrophy were associated with less severe sensory disturbance. These findings indicate that not only the motor but also the sensory system undergoes remote (spinal and supraspinal) changes which complement clinical measures of recovery, although the underlying pathophysiological mechanisms are yet to be elucidated.

Acknowledgments

We would like to thank all participants who spent their valuable time, all colleagues involved in this study, and the staff of the Department of Radiology at the University Hospital Balgrist.

Funding

The SRH Holding and the Clinical Research Priority Program "NeuroRehab" of the University of Zurich funded this study. The Wellcome Trust Centre for Neuroimaging is supported by core funding from the Wellcome Trust 091593/Z/10/Z.

Author Contributions

Patrick Grabher contributed substantially to the data analysis and interpretation of the results. He was writing the research article. Martina Callaghan and John Ashburner were involved in data analysis. Nikolaus Weiskopf was involved in the study design and data analysis. Alan Thompson and Armin Curt were involved in the study design. Patrick Freund contributed substantially to the conception and design of the study, to the data analysis and interpretation. He was writing the research article. All authors revised the research article.

Conflict of Interest

PG, MFC, JA, NW, AC, AT, and PF have no commercial relationships to disclose for this study.

Chapter 3:

Relationship between brainstem neurodegeneration and clinical impairment in traumatic spinal cord injury

Patrick Grabher[1], Claudia Blaiotta[2], John Ashburner[2], & Patrick Freund[1, 2, 3, 4]

[1]Spinal Cord Injury Center Balgrist, University Hospital Zurich, University of Zurich, Zurich, Switzerland

[2]Wellcome Trust Centre for Neuroimaging, Institute of Neurology, University College London, London, United Kingdom

[3]Department of Neurophysics, Max Planck Institute for Human Cognitive and Brain Sciences, Leipzig, Germany

[4]Department of Brain Repair and Rehabilitation, Institute of Neurology, University College London, London, United Kingdom

This article is in preparation (targeted journal: NeuroImage Clinical)

Abstract

Background: Brainstem networks are pivotal in sensory and motor function and play a crucial role in recovery following experimental spinal cord injury (SCI).

Objective: To quantify macroscopic and ultra-structural measures of neurodegeneration and their relation to clinical impairment in major brainstem pathways and nuclei in traumatic SCI.

Methods: Quantitative MRI data of 30 individuals with chronic traumatic SCI (15 with tetraplegia and 15 with paraplegia) and 23 healthy subjects were acquired using a multi-parameter mapping protocol. Patients were neurological assessed. We calculated quantitative maps of myelin-sensitive magnetization transfer saturation (MT) and longitudinal relaxation rate (R1), as well as iron-sensitive effective transverse relaxation rate (R2*). We constructed brainstem tissue templates using a multivariate Gaussian mixture model and assessed volume decrease (i.e. atrophy), myelin loss, and iron accumulation across the brainstem pathways and major nuclei (i.e. corticospinal tracts (CSTs), medial lemniscus (ML), red nucleus and periaqueductal gray (PAG)). We assessed the relationship between structural changes within brainstem pathways and nuclei and clinical impairment using regression analysis.

Results: Volume loss was detected in the CSTs and in the ML at the level of the medulla ($p=0.017$). Myelin-sensitive MT and R1 were reduced in the PAG (MT: $p=0.001$), the CSTs (MT: $p=0.039$, R1: $p=0.003$ & $p=0.025$), the dorsal medulla (R1: $p<0.001$), the pontomedullary junction (R1: $p=0.020$ & $p=0.038$) and the dorsal pons (R1: seven clusters). No iron-sensitive changes were detected. Lower pinprick score related to more myelin loss in the PAG ($p=0.015$), whereas lower functional independence was related to more myelin loss in the vestibular ($p=0.038$) and pontine nuclei ($p=0.034$).

Discussion: Neurodegeneration, indicative by volume and myelin loss, is evident in major brainstem pathways and nuclei following traumatic SCI; the magnitude relating to clinical impairment. Thus, quantitative MRI protocols offer new targets which may be used as neuroimaging biomarkers in treatment trials.

Introduction

Traumatic spinal cord injury (SCI) is a devastating condition and causes in most patients permanent sensorimotor loss and autonomic dysfunction, with no cure currently available (Dietz and Curt, 2006). Usually patients show some degree of recovery which levels off within two years after injury (Fawcett *et al.*, 2007). Using computational neuroimaging approaches, rapid and dynamic trajectories of neurodegenerative processes have been identified above the level of injury that accompanied the recovery. Crucially, the magnitude of cord and cortex degeneration was associated with greater clinical impairment (Freund *et al.*, 2013, 2015; Grabher *et al.*, 2015).

Besides neurodegeneration at the spinal and cortical level (George and Griffin, 1994; Hains *et al.*, 2003; Beaud *et al.*, 2008; Ghosh *et al.*, 2012; Jirjis *et al.*, 2015), retrograde and transneuronal degeneration has been shown in experimental SCI in brainstem pathways (Jones and Pons, 1998; Woods *et al.*, 1999; Jirjis *et al.*, 2015) and nuclei (Jones and Pons, 1998; Woods *et al.*, 1999; Kwon *et al.*, 2002; Wannier-Morino *et al.*, 2008; Carter *et al.*, 2011). The brainstem is phylogenetically highly conserved in mammals and plays a key role in motor (Lemon, 2008) and sensory function (Jones and Pons, 1998). Crucially, structural reorganization of brainstem pathways and nuclei have been associated with functional recovery following experimental SCI (Zaaimi *et al.*, 2012; Zörner *et al.*, 2014). Important substructures of the motor system entail the rubrospinal system (i.e. execution of precise limb movements), the vestibulospinal system (i.e. balance and posture), the reticular formation (i.e. initiates and coordinates limb movements and postural support), and the corticospinal system (i.e. skilled motor function) (Lawrence and Kuypers, 1968a, 1968b; Markham, 1987; Whishaw *et al.*, 1998; McCrea and Rybak, 2008), while the dorsal column nuclei and medial lemniscus (ML) (Kaas, H. Qi, *et al.*, 2008; Liao *et al.*, 2015) and the periaqueductal gray (PAG) (Benarroch, 2012) are involved in sensory processing and pain modulation. Thus, understanding trauma-induced processes affecting the brainstem pathways and nuclei might offer crucial insights into neurodegenerative processes and plasticity, and offer eloquent relationships with clinical measures that assess motor and sensory function (Kirshblum *et al.*, 2011). However, the brainstem is understudied in human SCI due to difficulties in imaging this densely packed structure in a reliable and repeatable fashion. First attempts using neuroimaging approaches provided evidence of brainstem atrophy (i.e. volume loss) (Wrigley,

Gustin, *et al.*, 2009; Freund, Wheeler-Kingshott, *et al.*, 2012; Freund *et al.*, 2013; Grabher *et al.*, 2015) and plasticity (i.e. volume increases) during intensive training (Villiger *et al.*, 2015) in human SCI.

Recent improvements in quantitative MRI (qMRI) techniques now allow to quantify the underlying ultra-structural changes (Weiskopf *et al.*, 2015) and segmenting individual brainstem pathways and nuclei (Lambert, Lutti, *et al.*, 2013). This is possible because different MR contrasts (magnetization transfer saturation (MT), longitudinal relaxation rate (R1), effective transverse relaxation rate (R2*)) can be used to calculate quantitative maps which are sensitive to myelin (Mottershead *et al.*, 2003; Schmierer *et al.*, 2004; Turati *et al.*, 2015) and iron (Langkammer *et al.*, 2010; Stüber *et al.*, 2014) and for multiparametric brainstem tissue segmentation (Lambert, Lutti, *et al.*, 2013). First studies show strong indications that myelin loss accompanies atrophic changes in the cord and cortex thus offering complementary insights into the sequela of SCI (Cohen-Adad *et al.*, 2011; Freund *et al.*, 2013; Grabher *et al.*, 2015).

Here, we combined voxel-based quantification and multiparametric tissue segmentation to address our hypotheses that after traumatic chronic SCI (1) atrophy and demyelination are evident in major brainstem pathways and nuclei and, (2) that the extent of atrophy, myelin loss and iron accumulation relates to impairment, lesion level and severity.

Material and methods

Participants and study design

We recruited 30 individuals with a chronic traumatic SCI and 23 healthy participants at the University Hospital Balgrist between August 2011 and May 2015. Fifteen patients were tetraplegics and fifteen paraplegics. No participant reported a history of medical, neurological, or psychiatric disorders and all subjects were eligible for MRI examinations.

Patients underwent a comprehensive clinical protocol including (1) the International Standards for Neurological Classification of Spinal Cord Injury (ISNCSCI) (Kirshblum *et al.*, 2011) to assess upper and lower extremity motor score (UEMS and LEMS), light touch (LT), and pinprick (PP), lesion level and severity (i.e. ASIA impairment scale (AIS)), and (2) the Spinal Cord Independence Measure (SCIM) (Catz *et al.*, 2007).

All participants gave informed written consent prior to study enrolment. The study protocol was in accordance with the Declaration of Helsinki and approved by the Ethics Committee of the Canton Zurich (reference number: EK-2010-0271).

Image acquisition

Structural whole-brain data including the cervical cord up to vertebra C5 were acquired on a 3T Magnetom MRI scanner (Siemens Healthcare, Erlangen, Germany) in all participants. The system was equipped with a 16-channel radiofrequency (RF) receive head and neck coil and RF body transmit coil. A multiecho 3D FLASH (fast low-angle shot) sequence with the following parameters was used within a whole-brain multi-parameter mapping (MPM) qMRI protocol (Helms *et al.*, 2008; Weiskopf *et al.*, 2013): field of view (FoV) of 240 x 256 mm^2, matrix size 240 x 256, isotropic resolution of 1 mm^3, GRAPPA parallel imaging in phase-encoding direction (anterior-posterior) with speed-up factor of 2, partial Fourier acquisition with 6/8 sampling factor in partion direction (left-right), and a readout bandwith of 480 Hz per pixel. Different weightings were predominantly achieved by choosing repetition time (TR) and flip angle (α): (1) T1-weighted (T1w): 25 ms / 23°, (2) PD-weighted (PDw): 25 ms / 4°, and (3) MT-weighted (MTw): 37 ms / 9° with off-resonance RF pulse prior to excitation. Echoes were acquired at seven equidistantly echo times (TE) from 2.46 ms to 17.22 ms for all volumes and an additional echo at 19.68 ms for PDw and T1w.

Image pre-processing

The acquired T1w, PDw, and MTw echoes were first averaged to increase the signal to noise ratio (SNR) and then used to calculate quantitative maps of MT and R1 (Helms *et al.*, 2009; Draganski *et al.*, 2011; Weiskopf *et al.*, 2011) in MATLAB (MathWorks, Natick, MA). R2* was calculated from the log signal of the PDw echoes. For correction of RF transmit field inhomogeneity, UNICORT was used (Weiskopf *et al.*, 2011).

Brainstem template generation

Before generating the brainstem tissue probability maps (TPMs), we extracted the brainstem from all individual quantitative maps from a longitudinal qMRI dataset of 29 subjects over four time points (Freund *et al.*, 2013, 2015; Grabher *et al.*, 2015) by label propagation using a set of brain labels (Neuromorphometrics Inc., Somerville, USA). Subsequently, whole-brain deformation fields were derived by segmenting the MT maps (Ashburner and Friston, 2005) and then applying a diffeomorphic image registration algorithm (Ashburner, 2007). The derived deformation fields enabled the extracted qMRI brainstem data to be transformed to the MNI space.

We then used a multivariate Gaussian mixture model to generate brainstem TPMs (Hasselblad, 1966). Such a model assumes that the observed image intensities are drawn from a set of multivariate Gaussian probability density functions, where each Gaussian captures the intensity distribution of one single tissue type. Additionally, we introduced locally-varying, unknown tissue priors, which are learned directly from the observed data, thus providing a set of population-specific, average-shaped TPMs (Lambert, Lutti, *et al.*, 2013). The statistical Gaussian mixture model was fit to the spatially normalized qMRI brainstem data, using the Expectation-Maximization algorithm (Moon, 1996) to obtain *maximum likelihood* or *maximum a posteriori* estimates of the model parameters, for probabilistic latent variable models. The resulting seven brainstem TPMs are shown in Figure 6 and contained, amongst others, the red nucleus (RN), cerebral crus including the corticospinal tracts (CSTs), and PAG. Anatomical locations were validated using a high-field MRI brainstem atlas (Naidich *et al.*, 2009). The tissue probability maps were subsequently aligned and merged with the whole brain TPMs provided with SPM12 (http://www.fil.ion.ucl.ac.uk/spm/) (subsequently referred to as modified TPMs), so as to allow a more accurate alignment of the brainstem tissue maps with the individual scans, during the following processing steps. In fact, information derived

from the tissues surrounding the brainstem (i.e. gray and white matter) can be effectively used to drive the registration of the individual volumes to the population mean, therefore ensuring more accurate segmentation results.

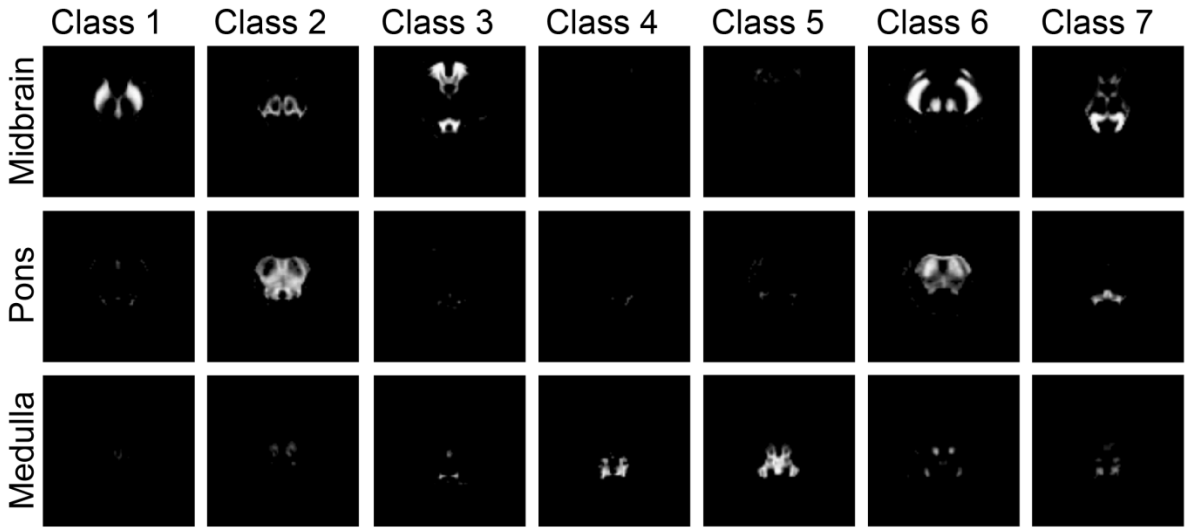

Figure 6: Seven within-brainstem tissue classes at different anatomical brainstem levels derived from multiparametric brainstem segmentation using a modified multivariate mixture of Gaussians. Prominent structures in tissue classes are: substantia nigra (class 1), pons (class 2 & 6), periaqueductal gray (class 3), and cerebral crus including corticospinal tracts and red nuclei (class 6).

Voxel-based morphometric and ultra-structural analysis of brainstem

We used our modified TPMs to segment the brain data (using MT and PDw data) of our study population (30 SCI and 23 controls) into gray matter, white matter, cerebrospinal fluid, plus the seven brainstem tissues for each subject (Ashburner and Friston, 2005). Then, a geodesic shooting registration algorithm (Ashburner and Friston, 2011) was used to create a common study population mean (Figure 7). The estimated deformation fields were used both to compute Jacobian determinant maps for tensor-based morphometry (TBM), and to warp the quantitative maps of MT, R1, and R2* into the study population mean space for voxel-based quantification (VBQ) (Draganski *et al.*, 2011). Due to the lack of gyrification of the brainstem and due to the highly accurate warping algorithm, no smoothing was applied to achieve higher spatial accuracy (Lambert, Lutti, *et al.*, 2013).

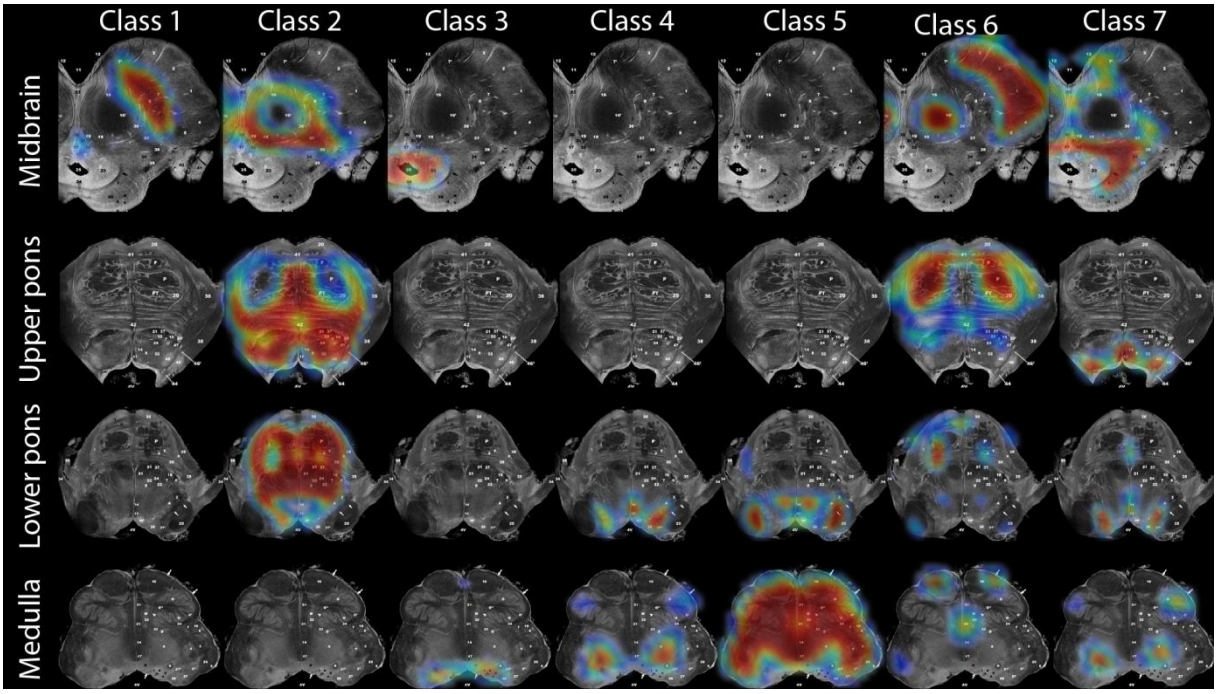

Figure 7: Overlay of the common study population brainstem mean onto the high-resolution histological sections from the Duvernoy brainstem atlas (Naidich *et al.*, 2009).

We used t-tests within the framework of general linear model (GLM) to assess morphometric and ultra-structural differences between individuals with SCI and healthy controls. We used regression models to assess the relationship between morphometric and ultra-structural measures and neurological and functional impairment (AIS, lesion level, LEMS; UEMS, LT, PP, SCIM). Covariates of no interest included age, total intracranial volume and scanner upgrade to control for linear effects in all GLMs (Barnes *et al.*, 2010). Cluster-inference within regions of interest (ROIs) derived from the seven brainstem TPMs was performed using a cluster-defining threshold of $p = 0.001$ and a family-wise error (FWE) corrected threshold of $p = 0.05$ using Gaussian Random Field theory to account for multiple comparisons (Friston *et al.*, 1994). Only significant results ($p < 0.05$) corrected for FWE are reported. The ROIs (i.e. brainstem TPMs) were used to increase sensitivity for pathophysiological processes and specificity for anatomical locations in brainstem sub-structures (e.g. CST, RN, and PAG).

Results

Patients' characteristics

The mean age of patients was 44.7 years (standard deviation (SD) 16.7, range 19.1 – 72.6) and their time since injury was 3.0 years (SD 5.4, range 0.7 – 23.8) (Table 2). Control subjects had a mean age of 36.9 years (SD 11.8, range 24.0 – 66.0) and was not statistically different (p=0.052). Neurological and functional outcomes of patients were as follow: UEMS 42.4 (SD 11.3, range 14 - 50), LEMS 15.1 (SD 20.5, range 0 - 50), PP 58.0 (SD 28.1, range 13 – 112), LT 68.3 (SD 26.0, range 16 – 112), and SCIM 57.9 (SD 25.7, range 19 - 100).

Atrophy and myelin loss in brainstem pathways and nuclei

Voxel-wise analysis revealed significant atrophy and myelin loss in patients compared to healthy controls within the brainstem (Figure 8, Table 3). Volume loss was observed in the CSTs and ML at the level of the medulla (p=0.017). Lower myelin-sensitive MT was evident in the left CST at the level of the medulla (p=0.039) and within the PAG (p=0.001). Lower myelin-sensitive R1 was observed in the CSTs at the level of the medulla (cluster 1: p=0.003; cluster 2: p=0.025) and bilaterally in the dorsal medulla (p<0.001), in the dorsal pontomedullary junction (cluster 1: p=0.020; cluster 2: p=0.038) and in the dorsal pons (7 clusters, Table 3). Iron-sensitive R2* did not reveal any significant changes in patients compared to controls.

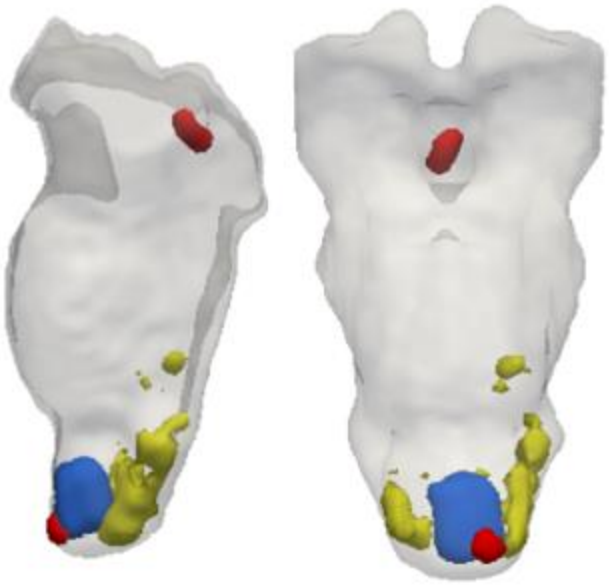

Figure 8: Atrophy and myelin loss in brainstem pathways and nuclei. Blue = Volume (Jacobians), Red = Myelin-sensitive MT, Yellow = Myelin-sensitive R1.

ID	Age (years)	Time since injury (months)	Completness	AIS	Site of impairment (motor/sensory)	ISNCSCI LEMS	ISNCSCI UEMS	ISNCSCI Pinprick	ISNCSCI Light Touch	SCIM
1	19	13.5	Complete	A	C6/C7	0	23	33	33	37
2	43	15.73	Complete	A	C6/C4	0	25	18	20	37
3	21	12.33	Complete	A	C6/C5	0	23	26	53	34
4	31	10.27	Complete	A	T10/T10	16	50	78	82	80
5	70	9.5	Complete	A	T7/T7	0	50	68	67	49
6	34	12.2	Complete	A	C7/C7	0	35	29	32	26
7	32	10.27	Complete	A	C6/C5	0	26	20	33	30
8	29	12.07	Complete	A	C5/C4	0	14	13	16	19
9	53	54.6	Complete	A	T3/T3	0	50	44	47	53
10	36	185.47	Complete	A	T12/T12	4	50	78	78	70
11	60	68.17	Complete	A	T1/T1	0	49	40	52	32
12	53	8.03	Complete	A	T9/T9	0	50	66	68	69
13	26	10.8	Complete	A	T4/T4	0	50	46	48	67
14	39	9.33	Complete	A	T7/T7	0	50	58	60	65
15	69	12.17	Incomplete	B	T11/T11	32	49	74	92	42
16	31	12.3	Incomplete	B	T1/C7	0	48	46	68	38
17	43	186.77	Incomplete	B	C6/C4	0	25	32	77	29
18	32	10.77	Incomplete	B	T11/T11	0	50	72	78	66

Table 2: (continued)

ID	Age (years)	Time since injury (months)	Completness	AIS	Site of impairment (motor/sensory)	ISNCSCI LEMS	ISNCSCI UEMS	ISNCSCI Pinprick	ISNCSCI Light Touch	SCIM
19	29	22.83	Incomplete	B	T6/T6	0	50	52	77	66
20	31	12.33	Incomplete	B	T4/T4	0	50	46	74	54
21	52	9.7	Incomplete	C	C7/C5	12	32	44	67	31
22	24	12.2	Incomplete	D	T1/C6	19	48	37	72	70
23	45	13.4	Incomplete	D	L3/L4	45	50	106	106	100
24	72	11.9	Incomplete	D	T1/T2	41	48	41	112	36
25	53	11.97	Incomplete	D	T10/T10	48	50	90	90	100
26	48	12.13	Incomplete	D	C5/C3	47	35	97	98	98
27	68	12.07	Incomplete	D	S1/L3	50	50	102	107	100
28	55	18.63	Incomplete	D	C3/C3	49	42	94	62	84
29	69	285	Incomplete	D	T1/C3	40	49	78	69	NA
30	73	11.97	Incomplete	E	T3/T3*	50	50	112	112	97

Table 2: Clinical and behavioural data of 30 patients with chronic traumatic spinal cord injury. * Initial level of injury. AIS = ASIA impairment scale. ISNCSCI = International Standards for the Neurological Classification of Spinal Cord Injury. NA = not available.

Clinical impairment relates to myelin changes

Lower R1 in the PAG was associated with lower PP in individuals with SCI (p = 0.015, cluster extent (k) = 13, Z score = 4.44, x = 0, y = -38, z = -7, n = 30, Figure 9A). Lower R1 in the left upper dorsolateral medulla (e.g. vestibular nucleus) (p = 0.038, k = 1, Z score = 3.24, x = -4, y = -45, z = -43, n = 29, Figure 9B) and left upper-mid ventrolateral pons (e.g. pontine nucleus) (p = 0.034, k = 12, Z score = 3.88, x = -13, y = -22, z = -23, n = 29, Figure 9C) was associated with lower SCIM (i.e. functional independence).

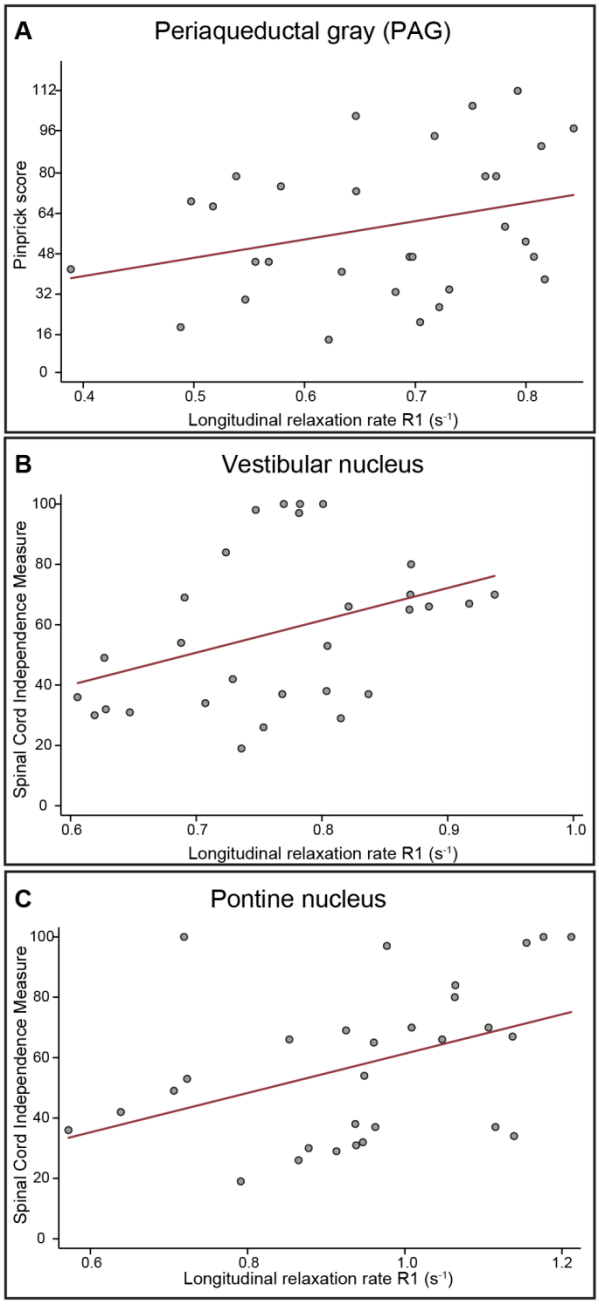

Figure 9: Correlation between ultra-structural integrity within the brainstem and neurological and functional impairment. Regression models from extracted peak-voxel within the significant cluster are shown for illustrative purposes only (not adjusted for age, scanner, and total intracranial volume).

Modality	P-value (FWE-corrected)	Cluster Extent (voxels)	Z Score	Coordinates (mm)			Anatomical location
				x	y	z	
Jacobian determinant (i.e. volume loss)							
	0.017	336	3.87	0	-39	-49	Cluster spanning the CSTs and medial lemniscus (medulla)
MT (i.e. myelin loss)							
	0.001	15	4.32	1	-28	-4	PAG
	0.039	8	4.5	-2	-38	-54	Left CST (medulla)
R1 (i.e. myelin loss)							
	<0.001	110	4.78	-8	-38	-27	Low-mid pons (left, dorsolateral)
	0.019	21	3.77	-8	-40	-29	Low-mid pons (left, dorsolateral)
	0.006	18	3.66	9	-43	-31	Low pons (right, dorsolateral)
	0.01	16	4.07	2	-41	-34	Low pons (dorsomedial)
	0.005	7	3.85	4	-42	-35	Low pons (right, dorsomedial)
	0.011	4	3.55	-2	-41	-36	Low pons (left, dorsomedial)
	0.024	2	3.41	-1	-39	-36	Low pons (left, dorsomedial)
	0.038	1	3.18	6	-44	-37	Pontomedullary junction (right, dorsolateral)
	0.02	13	3.82	2	-43	-39	Pontomedullary junction (right, dorsomedial)
	<0.001	485	5.11	-7	-44	-48	Medulla (bilateral, dorsal)
	0.025	12	4.99	4	-35	-49	Right CST (medulla)
	0.003	22	4.53	-1	-38	-54	CSTs (medulla)

Table 3: Group analysis showing volume loss and microstructural changes within the brainstem in individuals with SCI compared to healthy controls. CST = corticospinal tract, FWE = family-wise error, MT = magnetization transfer saturation, PAG = periaqueductal gray, R1 = longitudinal relaxation rate, TBM = tensor-based morphometry.

Discussion

This study revealed atrophy and myelin loss within major brainstem pathways and nuclei involved in motor and sensory (dys-) function in chronic traumatic SCI. Interestingly, atrophy was observed only in the CST and ML whereas myelin loss occurred also in areas containing brainstem nuclei. Crucially, the magnitude of myelin loss was related to the extent of motor and sensory impairment. Therefore, these structural alterations in the brainstem should be considered, if reproduced in longitudinal studies, as new targets to monitor impairment and complement assessments in clinical trials following SCI.

Tracking neurodegeneration in the brainstem

First, we confirmed atrophy, the endpoint of neurodegeneration, in the CST (Wrigley, Gustin, *et al.*, 2009; Freund *et al.*, 2011, 2013; Mole *et al.*, 2014) and show quantitative myelin loss in the same areas of atrophy which is suggestive of retrograde fiber degeneration (Hains *et al.*, 2003; Buss *et al.*, 2004; Beaud *et al.*, 2008; Ghosh *et al.*, 2012). Next to CST atrophy, we identified atrophic changes in the ML. Although we did not observe any myelin changes there, this is suggestive of anterograde degeneration (Jones and Pons, 1998; Woods *et al.*, 1999). Interestingly, we did no observe any macroscopic or ultra-structural changes in the rubrospinal system (i.e. RN). Phylogenetically, the formation of direct cortico-motoneuronal connections (i.e. CST) reaching as far as the lumbar enlargement (Lemon, 2008) has rendered the rubrospinal system less important for the control of movements in man where fibers terminate in the high cervical cord (Nathan and Smith, 1982; Hicks and Onodera, 2012). Conversely after experimental SCI, rubrospinal fibers which reach more caudally into the spinal cord (Lawrence and Kuypers, 1968b; Belhaj-saïf and Cheney, 2000) and the RN show signs of neurodegeneration (Kwon *et al.*, 2002; Wannier-Morino *et al.*, 2008; Carter *et al.*, 2011). Thus, these findings might illustrate the dominant role of the CST in processes of neurodegeneration and reorganization in the context of functional recovery after human SCI (Dietz and Fouad, 2014).

We observed myelin loss in the PAG after traumatic SCI. The PAG is part of the endogenous pain inhibition system and involved in motor function (Benarroch, 2012). Dysfunction of the PAG affects the pain modulating capacity of nociceptive dorsal horn neurons (Basbaum and Fields, 1979; Eippert *et al.*, 2009) and was related to neuropathic pain (Knerlich-Lukoschus *et al.*, 2011; Ho *et al.*, 2013), a condition that develops in about half of SCI patients (Siddall *et al.*,

2003). Furthermore, the PAG is orchestrating sensory and motor circuits and dysfunction changes cerebellar nociceptive and proprioceptive input and, consequently, the cerebellar motor system (Moulton *et al.*, 2010; Koutsikou *et al.*, 2015). We also observed myelin loss in the cerebellar peduncles that illustrate alterations in spinal and supraspinal input into the cerebellum. Interestingly, myelin loss in the PAG was associated with lower pinprick score. The PAG receives nociceptive input from the spinothalamic tract (Basbaum and Fields, 1979) which integrity can be assessed clinically by the pinprick assessment. Thus, the extent of degeneration in the PAG depends on the spinothalamic tract integrity. Myelin loss in the PAG therefore affects the pain circuitry and this is supported by the cerebellar changes which we have found to relate to pain (Grabher *et al.*, 2015). The role of myelin loss in the PAG and neuropathic pain needs to be elucidated in future studies to unravel the mechanisms that cause this devastating condition.

We further observed myelin loss in the ventromedial brainstem pathways involved in motor function in the dorsal pons and medulla, independent of atrophy. This is suggestive that the integrity of the microarchitecture of the vestibular and reticular system , -crucial for postural control and movement coordination (Markham, 1987; McCrea and Rybak, 2008)- is disturbed and might reflect reduced postural stability and increased risk of fall in SCI patients (Iles *et al.*, 2004; Liechti *et al.*, 2008). In addition, myelin loss in the medulla (i.e. vestibular nucleus) and pons (i.e. pontine nucleus) were related to lower functional independence (i.e. SCIM score). Previously, reduced microstructural integrity in the corticopontine fibers were reported in chronic human SCI (Wrigley, Gustin, *et al.*, 2009). Here we demonstrate that the magnitude of these changes relate to the functional impairment. Both the vestibular and corticopontine nuclei are important for postural control and cerebellar motor function (Markham, 1987; Moulton *et al.*, 2010). Thus, their integrity is crucial to maintain independence in activities of daily living and postural stability (Iles *et al.*, 2004; Liechti *et al.*, 2008).

Interestingly, we did not observe iron accumulation caused by myelin breakdown (Hametner *et al.*, 2013; Sauerbeck *et al.*, 2013) causing detrimental inflammation in the CNS (Felix *et al.*, 2012; Kroner *et al.*, 2014; Faden *et al.*, 2015). This may be due to rather small effects of iron accumulation in supraspinal regions compared to the spinal cord, where more iron is released by breakdown of hemoglobin after hemorrhage (Sauerbeck *et al.*, 2013). Longitudinal

assessment of iron accumulation after acute SCI will shed more light into these mechanisms with greater sensitivity to subtle effects.

The lesion height and severity determines the amount of damaged nerve fibers (Fehlings and Tator, 1995), as reflected in measures of cross-sectional cord area (Lundell *et al.*, 2011; Jutzeler *et al.*, 2016). Interestingly, we did not find any association between loss of structural integrity and lesion level/severity (i.e. AIS) in this cohort, and therefore also no differences between cervical and non-cervical lesions. Nevertheless, myelin loss was related to clinical impairment that *per se* reflects lesion level and severity.

No relationships between clinical impairments and atrophy were observed. This might be due to fact that volume loss is rather unspecific to the underlying pathological processes and points to the importance of quantitative markers of myelin and iron.

Limitations

We note the following limitations of this study. The anatomical locations of brainstem ROIs (i.e. TPMs) and findings in SCI compared to healthy controls were carefully confirmed using a high-field MRI atlas (Naidich *et al.*, 2009). The lack of specificity for pathological mechanisms influencing relaxation times and the small anatomical structures compared to resolution may conceal small effects and may be approached by high-resolution hMRI techniques (Weiskopf *et al.*, 2015). The scanner was upgraded during the study period (from Verio to Skyra^{fit}). Data from both patients and controls were acquired on both systems (the same ratio in each group) to minimize potential confounding effects due to the scanner upgrade thereby accounting for this confound in both cohorts. The cross-sectional study design allows us to only assess differences in MRI readouts between SCI and healthy controls, but not the underlying trajectories of structural changes. This design is also less sensitive, as higher between-subject variability may conceal weak effects. To overcome this limitation, we aim to develop a longitudinal analysis pipeline to assess trajectories of structural change in brainstem pathways and nuclei in acute SCI.

Conclusion

Refined qMRI methods enable to track spatially specific neurodegeneration and structural reorganization in the brainstem following traumatic SCI. Next to measures of atrophy that are rather insensitive and unspecific to the underlying pathology, we show myelin loss across the brainstem. Therefore, these clinically relevant structural brainstem alterations, obtained with a qMRI protocol, could serve as neuroimaging biomarkers to monitor treatment efficacy and complement clinical assessments in clinical trials following SCI.

Acknowledgements

We would like to thank all volunteers participating in this study and the staff of the radiology department at University Hospital Balgrist, Switzerland.

Funding

The SRH Holding and the Clinical Research Priority Program "NeuroRehab" of the University of Zurich funded this study. The Wellcome Trust Centre for Neuroimaging is supported by core funding from the Wellcome Trust [091593/Z/10/Z]. Open access of this publication was supported by the Wellcome Trust.

Contributions

Patrick Grabher contributed substantially to the conception and design of the study, data acquisition, methods development, data analysis and interpretation. He wrote the research article. Claudia Blaiotta and John Ashburner were substantially involved in the methods development and revising the manuscript. Patrick Freund contributed to the conception and design of the study and data interpretation. He made substantial contributions in writing and revising the research article.

Conflicts of Interest

We declare no conflicts of interest.

Chapter 4:

Relationship between structural brainstem and brain plasticity and lower-limb training in spinal cord injury: a longitudinal pilot study

Michael Villiger[1,2*], Patrick Grabher[1*], Marie-Claude Hepp-Reymond[3], Daniel Kiper[3], Armin Curt[1], Marc Bolliger[1], Sabina Hotz-Boendermaker[1], Spyros Kollias[4], Kynan Eng[3] & Patrick Freund[1,5,6]

[1]Spinal Cord Injury Center Balgrist, University of Zurich, Zurich, Switzerland

[2]University College Physiotherapy Thim van der Laan, Landquart, Switzerland

[3] Institute of Neuroinformatics, University of Zurich and ETH Zurich, Zurich, Switzerland

[4] Institute of Neuroradiology, University Hospital Zurich, University of Zurich, Zurich, Switzerland

[5] Department of Brain Repair and Rehabilitation, Institute of Neurology, University College London, London, UK

[6] Wellcome Trust Centre for Neuroimaging, Institute of Neurology, University College London, London, UK

[*] Shared first authorship

The original article was published in *Front Hum Neurosci* 2015; 9:1–10

Abstract

Rehabilitative training has shown to improve significantly motor outcomes and functional walking capacity in patients with incomplete spinal cord injury (iSCI). However, whether performance improvements during rehabilitation relate to brain plasticity or whether it is based on functional adaptation of movement strategies remain uncertain. This study assessed training improvement-induced structural brain plasticity in chronic iSCI patients using longitudinal MRI.

We used tensor-based morphometry (TBM) to analyze longitudinal brain volume changes associated with intensive virtual reality (VR)-augmented lower limb training in nine traumatic iSCI patients. The MRI data was acquired before and after a 4-week training period (16-20 training sessions). Before training, voxel-based morphometry (VBM) and voxel-based cortical thickness (VBCT) assessed baseline morphometric differences in nine iSCI patients compared to 14 healthy controls.

The intense VR-augmented training of limb control improved significantly balance, walking speed, ambulation, and muscle strength in patients. Retention of clinical improvements was confirmed by the 3-4 months follow-up. In patients relative to controls, reductions in VBM of white matter volume within the brainstem and cerebellum and VBCT showed cortical thinning in the primary motor cortex. Over time, TBM revealed significant improvement-induced increases in the left middle temporal and occipital gyrus, left temporal pole and fusiform gyrus, both hippocampi, cerebellum, corpus callosum, and brainstem in iSCI patients.

This study demonstrates structural plasticity at the cortical and brainstem level as a consequence of VR-augmented training in iSCI patients. These structural changes may serve as neuroimaging biomarkers of VR-augmented lower limb neurorehabilitation in addition to performance measures to detect improvements in rehabilitative training.

Introduction

Complete spinal cord injury leads to permanent impairments of motor, sensory, and autonomic function. However, in the majority of cases, sensorimotor functions are partially preserved below the lesion level due to an anatomically incomplete lesion, resulting in an incomplete spinal cord injury (iSCI) (Wyndaele and Wyndaele, 2006). Intensive neurorehabilitation therapy improves clinical outcome, but little is known about the relationship between training intensity and behavioral outcome, or about their neural underpinnings. The ability to relearn successfully a motor action depends on the key concepts for motor learning, i.e. repetition, performance feedback and motivation (Holden, 2005). Virtual reality (VR)-augmented neurorehabilitation interventions in patients with chronic iSCI have shown to improve motor function and neuropathic pain (eg. (Villiger *et al.*, 2011, 2013)). VR provides interactive, multimodal sensory stimuli and immediate environment feedback to motivate the patient. Furthermore, adjustments of the VR-presented motor tasks aim to prevent or reduce fatigue and demotivation (Holden, 2005; Adamovich *et al.*, 2009; Bohil *et al.*, 2011). However, the neurophysiological mechanisms underlying performance improvements in patients with acute and chronic iSCI are uncertain.

To date, training-dependent functional neuroplasticity in humans has been investigated using transcranial magnetic stimulation (TMS), positron emission tomography (PET) and functional magnetic resonance imaging (fMRI). Long-term motor training induces decreases in task-related activity in cortical motor areas, indicating economization processes (Walz *et al.*, 2014) and changes in functional connectivity (Sampaio-Baptista *et al.*, 2014). Recently, structural and functional cortical connectivity changes were associated with motor training (Taubert *et al.*, 2011). Cortical modulation was assessed with TMS in training of upper (Pascual-Leone *et al.*, 1995; Classen *et al.*, 1998; Koeneke *et al.*, 2006; Kantak *et al.*, 2013) and lower extremities (Perez *et al.*, 2004). Classen et al. (1998) showed that simple thumb training could change the movement direction evoked by TMS indicating reorganization of neuronal networks. Crucially, computational morphometry has shown training-dependent (i.e. juggling) dynamic volumetric changes in brain tissue in motor learning associated cortical areas in healthy controls (Draganski *et al.*, 2004). Patients with Parkinson's disease – trained on a balance task – showed improvements that were related to local brain volume increases in cortical and cerebellar regions involved in balance control and motor learning (Sehm *et al.*, 2014). These increases in

brain volume occurred within the first weeks of training during which the greatest improvements occurred. Thus, improvements in ambulatory function might depend on similar mechanisms in iSCI patients who have to relearn movement patterns using spared fibers that most probably were involved in different motor tasks prior to spinal cord injury (Ghosh *et al.*, 2010).

Morphometric brain changes are conventionally assessed using voxel-based morphometry (VBM) and voxel-based cortical thickness (VBCT). Both procedures were developed for cross-sectional detection of gray and white matter volume changes between two groups (Ashburner and Friston, 2000; Hutton *et al.*, 2008). Recently, tensor-based morphometry (TBM) was developed to assess dynamic volumetric changes over time (Ashburner and Ridgway, 2013). TBM has successfully shown its potential in longitudinal studies characterizing changes induced by SCI trauma, inflammation in multiple sclerosis, and in neurodegeneration such as Alzheimer's and Parkinson's diseases (Tao *et al.*, 2009; Freund *et al.*, 2013; Hua *et al.*, 2013; Tessa *et al.*, 2014).

In the present study, we applied computational morphometry (VBM, VBCT) to detect volumetric bi-directional differences between chronic iSCI patients and controls at baseline. Over time in iSCI patients, we used TBM to assess the relationship between VR motor-training induced performance improvements and local brain volume increases in brain areas responsive to motor training during a similar balance task in in healthy and diseased subjects (Taubert *et al.*, 2010; Sehm *et al.*, 2014).

Material and Methods

Participants and study design

Nine iSCI outpatients (mean age 55.1 years, standard deviation (SD) 15.8, range 28-71 years, 4 females) from the University Hospital Balgrist (Zurich, Switzerland) were included in the study between August 2010 and March 2012 (Table 4). Inclusion criteria were: clinically incomplete, chronic SCI (time since injury > 1 year), motor level of lesion below C4, ability to sit in a chair without assistance and support systems (e.g. securing belt), and motor functions below the level of lesion corresponding to the American Spinal Cord Injury Association Impairment Scale (AIS) (Marino *et al.*, 2003). Exclusion criteria were psychiatric or other neurological disorders, head injuries causing cognitive or visual impairment, spasticity limiting performance of lower limb movements, and medication influencing ability to attend the therapy for 45 minutes. Furthermore, patients with depressive symptoms (score >14 in the Beck Depression Inventory) were excluded (Hassanpour *et al.*, 2012). Neuropathic pain was classified into at-level and below-level SCI neuropathic pain based on the most recent taxonomy (Bryce *et al.*, 2012) and was assessed on an 11-point numeric rating scale from 0 (no pain) to 10 (worst pain imaginable).

Patient	Age (years)	Gender	Etiology	Level of lesion	AIS classification	Level of pain	Years since injury
P1	70	M	ME	C8	D	-	2
P2	60	F	ME	T4	D	Below-level	2
P3	28	M	T	C6	D	-	5
P4	71	F	ME	T12	D	At-level	3
P5	61	M	T	C4	D	At- and below-level	4
P6	30	M	ME	C5	D	Below-level	3
P7	62	M	ME	T9	D	-	5
P8	67	F	T	T12	D	-	1
P9	47	F	ME	C7	D	Below-level	4

Table 4: Characteristics of patients with spinal cord injury. Gender: M = male; F = female. Etiology: T = trauma; ME = medical etiology. Level of lesion: C = cervical; T = thoracic level SCI. AIS classification D: sensory-motor incomplete, with the average strength of the muscles below the level of lesion equal to or above 3 (i.e. movement over the full range of motion against gravity). Level of pain: at-level pain is defined as pain located within the dermatome and 3 dermatomes below the lesion level, and not in any lower dermatomes, unless the pain is thought to be caused by damage to the cauda equine. Below-level pain is defined as pain present more than 3 dermatomes below the lesion level, and the lesion or disease must affect the spinal cord and that the pain is believed to arise as a result of this damage.

Fourteen healthy subjects participated in the control group (mean age 47.1 years, SD 14.4, range 25 - 61 years, 7 females). Their mean age was not significantly different from iSCI patients (Mann–Whitney U = 34.5, nc = 14, np = 9, P = 0.07, two-tailed). They had normal or corrected-to-normal visual acuity and no history of psychiatric or neurological disorder.

SCI and healthy participants were informed of the purpose of the study and gave written consent. The experimental protocol was in accordance with the Declaration of Helsinki and performed with the approval of the local Ethics Committee (EK-24/2009).

Patients underwent four weeks of intensive VR-augmented lower limb training. Before and after the training period a structural volumetric 3D MRI data set was acquired in patients. Retention of the performance improvements was assessed in a 3-4 month follow-up session. The 14 control subjects were invited to a single MRI session using the same imaging protocol as the patients to reveal any baseline differences (increases and decreases) in local brain volume between both groups. Controls did not partake in the VR-enhanced motor training.

The patients with iSCI were trained with the VR movement tasks 16-20 times during 4 weeks (4-5 x 45 min. per week). The training used a VR-augmented therapy system for lower limbs combining action observation, imagination and execution. The system and the motivating training tasks are shown and described in more detail by Villiger et al. (2011; 2013). In short, the movements of the patient's real lower limbs are transferred in real time to the virtual lower limbs using sensory modules with accelerometers, attached to the patients' shoes. The virtual lower limbs are presented in a first-person perspective on a large monitor (132 cm diagonal). Clinically relevant interactive games for training foot and leg movements were used for 3 x 2 minutes each in a sitting or standing position. These games were:

Footbag: A simple exercise in which the patient juggles a ball between the left and right foot, using dorsiflexion of the ankle (tibialis anterior contraction, approx. 70 per 2 min. per leg), an exercise to reduce foot dragging. The trajectory of the ball in the air between the left and right feet is pre-set.

Hamster splash: Hamsters run up to the patient's toes. The patient's task is to perform a dorsal flexion of the ankle (approx. 30 per 2 min. per leg) to launch each hamster into a swimming

pool. Launching the hamsters higher (faster ankle movement) is rewarded by a higher score and more elaborate hamster movements (somersaults, swimming patterns).

Star kick: The patient performs a knee extension (approx. 24 per 2 min. per leg) by kicking a ball towards displayed stars. For every hit, the patient receives a score reward.

Planet drive: Cars are moving on a highway towards the virtual feet. The patient's task is to avoid touching the cars by displacing the foot and legs sideways (approx. 8 per 2 min. per leg).

During each training session, patients rated their enjoyment, motivation, and attention level on an 11-point numeric rating scale from 0 (worst) to 10 (best).

Behavioral data

Outcomes for lower limb motor functions in patients with iSCI were assessed at four different time points: 1 month prior to baseline scan, at baseline (immediately before training), after one month of training (post-training), and 3-4 months after the last training session (follow-up). Patients were assessed on 1) the '10 meter walking test' (10MWT) gait speed test (self-selected speed) (van Hedel *et al.*, 2005, 2006), 2) the 'Berg balance scale' (BBS) assessment of balance during functional activities (14 balance items) from 0 (no balance) to 4 (good balance) (Berg *et al.*, 1995), 3) the 'lower extremity motor score' (LEMS) from 0 (complete paralysis) to 50 (normal strength)(Marino *et al.*, 2003), and 4) the 'spinal cord independence measure' (SCIM mobility) from 0 (no mobility) to 40 (normal mobility) (Catz *et al.*, 2007).

Statistical analysis of behavioral data

We used Stata 13 (StataCorp LP, College Station, TX; www.stata.com) to assess changes in behavioral data. In order to estimate rates of clinical recovery (patients only) linear mixed models were used with the clinical measure (10MWT, BBS, LEMS, and SCIM) as response variable and time as predictor. All time points and all participants were included.

MRI data acquisition

The structural volumetric MRI images were acquired at baseline in all participants and following training in patients. A 1.5T whole-body MRI scanner equipped with an 8-channel SENSE™ head coil (Philips Medical Systems, Eindhoven, The Netherlands) was used to acquire 3D T1-weighted (T1w) (TFE sequence) (repetition time (TR) = 20 ms, echo time (TE) = 4.6 ms, flip angle (α) = 20°, field of view (FoV) = 220x220 mm^2, 210 slices, voxel size = 0.98x0.98x0.75

mm^3). Total scan time was 11 min. 36.4 s for each subject. All images were controlled for movement artefacts prior to processing.

MRI data analysis

Voxel-based morphometry (VBM) and voxel-based cortical thickness (VBCT)

VBM (Ashburner and Friston, 2000) and VBCT (Hutton *et al.*, 2008), implemented in SPM12 (Wellcome Trust Centre for Neuroimaging, University College London, London, UK), were applied to assess differences in white matter and gray matter volumes and cortical thickness between the iSCI patients and the healthy controls prior to training (Ashburner and Friston, 2000). In brief, for VBM the T1w anatomical images were segmented into gray matter, white matter and cerebrospinal fluid using unified segmentation (Ashburner and Friston, 2005). The gray matter and white matter segments were then transferred to MNI (Montreal Neurological Institute) space using the diffeomorphic non-linear image registration algorithm (Dartel) (Ashburner, 2007). Finally, the gray matter volumes were scaled (i.e. "modulation") in order to preserve the local tissue volumes and smoothed using an isotropic Gaussian kernel with 6 mm full width at half maximum (FWHM). For VBCT, the segmented maps of gray matter, white matter, and cerebrospinal fluid (created in the pre-processing steps of the VBM analysis) were used to create a cortical thickness map for each subject (Hutton *et al.*, 2008). Cortical gray matter boundaries were extracted from these maps to estimate the cortical thickness for each voxel. To increase the spatial resolution of narrow cerebrospinal fluid spaces, the input tissue segments were sub-sampled from 1 mm to 0.5 mm using trilinear interpolation. The thickness value at each voxel was then calculated as the distance between the inner and outer borders of the local gray matter(Hutton *et al.*, 2009). VBCT maps were then warped into the MNI space and smoothed using the same FWHM Gaussian kernel with a correction to preserve (i.e. no modulation) local cortical thickness (Hutton *et al.*, 2008).

Tensor-based morphometry (TBM)

Using inverse-consistent 3D non-linear image registration, implemented in SPM12, we longitudinally aligned the MRI volumes collected before and after training to their half-way average (Ashburner and Ridgway, 2013) to obtain Jacobian determinant maps, as well as half-way T1w average images for each subject. The half-way average images were subsequently segmented into gray matter, white matter, and cerebrospinal fluid using unified segmentation (Ashburner and Friston, 2005). The Jacobian determinant maps were transformed to the MNI

space using deformations derived from Dartel. These aligned maps revealed volumetric expansion and compression for each of the subjects.

Statistical analysis

For the VBM/VBCT analysis, used to assess impairment related structural brain changes prior to study onset, three general linear models (GLM) were constructed for the whole brain (for gray matter, white matter, and cortical thickness), consisting of a group identifier, age, and total intracranial volume (TIV) to account for any confounding (non-specific) effects. For the cortical changes (VBM of gray matter and VBCT of cortical thickness), the sensorimotor cortex was additionally chosen as search volume to increase sensitivity (Freund *et al.*, 2011). Two-tailed two-sample t-tests were used to assess volume differences in patients compared to controls at baseline.

For TBM analysis, linear regression models were constructed to identify volumetric changes that are associated with individual performance improvements (i.e. 10MWT, LEMS, BBS, and SCIM) across the training period. Individual performances of the lower limb motor functions were assessed before and after the four weeks training. As the study duration was short and age has shown not to have disadvantageous effects on rehabilitation associated performance improvements (Furlan *et al.*, 2010), we did not include age as a covariate in the TBM analysis (Freund *et al.*, 2013). Pain reduction during training was included as covariate of no interest in TBM models to overcome possible confounds, because training with visual aspect has shown reductions in SCI neuropathic pain scores (e.g. (Moseley, 2007; Villiger *et al.*, 2013)). Regression models were tested for positive correlations between volume changes and improvements in performance.

The associated p-values were corrected for multiple comparisons of all voxels analyzed using Gaussian random field theory. Only significant results ($P < 0.05$, Family Wise Error (FWE) corrected) are reported.

Results

Patient characteristics and motivational factors

All patients completed the training and were classified as AIS D. Five patients suffered from neuropathic pain. The clinical characteristics are summarized in Table 4. On average, during each VR training session around 300 repetitions of ankle movements and 75 knee movements (over 5000 and 1200 per leg respectively during a month) were performed. A survey at the end of every training session indicated that patients enjoyed the VR-augmented lower limb tasks (mean 9.5, SD 0.9, range 7.7-10) and maintained a high level of motivation (mean 8.5, SD 1.2, range 6.9-10) and attention (mean 8.6, SD 1.2, range 6.4-10).

Behavioral data

No significant changes occurred between the period of time one months before training and at baseline (pre-training) (10MWT: 0.01s, P = 0.999, CI -0.43 to 0.43; BBS: -0.15, P = 0.856, CI -1.73 to 1.44; LEMS: -0.03, P=0.965, CI -1.18 to 1.13; SCIM: -0.25, P = 0.617, CI -1.22 to 0.72). During the entire training period, patients spent a total mean training time of 413.8 min. (SD 43.2, range 344-480). Over time, all iSCI patients exhibited training-induced improvements in performance (see Figure 10). Specifically, iSCI patients showed a significant improvement in the 10MWT (-1.33 s, P < 0.001, CI -1.77 to -0.90), BBS (3.11, P < 0.001, CI 1.51 to 4.72), LEMS (3.00, P < 0.001, CI 1.81 to 4.19), and SCIM (1.89, P = 0.001, CI 0.81 to 2.97) in the post-training compared to the pre-training. The performance at follow-up was still significantly improved compared to pre-training in the 10MWT (-0.93 s, P < 0.001, CI -1.37 to -0.49), BBS (2.67, P = 0.010, CI 0.65 to 4.69), LEMS (2.78, P = 0.002, CI 1.03 to 4.52), and SCIM (1.89, P = 0.002, CI 0.71 to 3.07). They did not significantly change when compared to post-training in the 10MWT (0.41 s, P = 0.068, CI -0.03 to 0.84), BBS (-0.44, P = 0.587, CI -2.05 to 1.16), LEMS (-0.22, P = 0.715, CI -1.42 to 0.97), and SCIM (0.00, P = 1.000, CI -1.08 to 1.08).

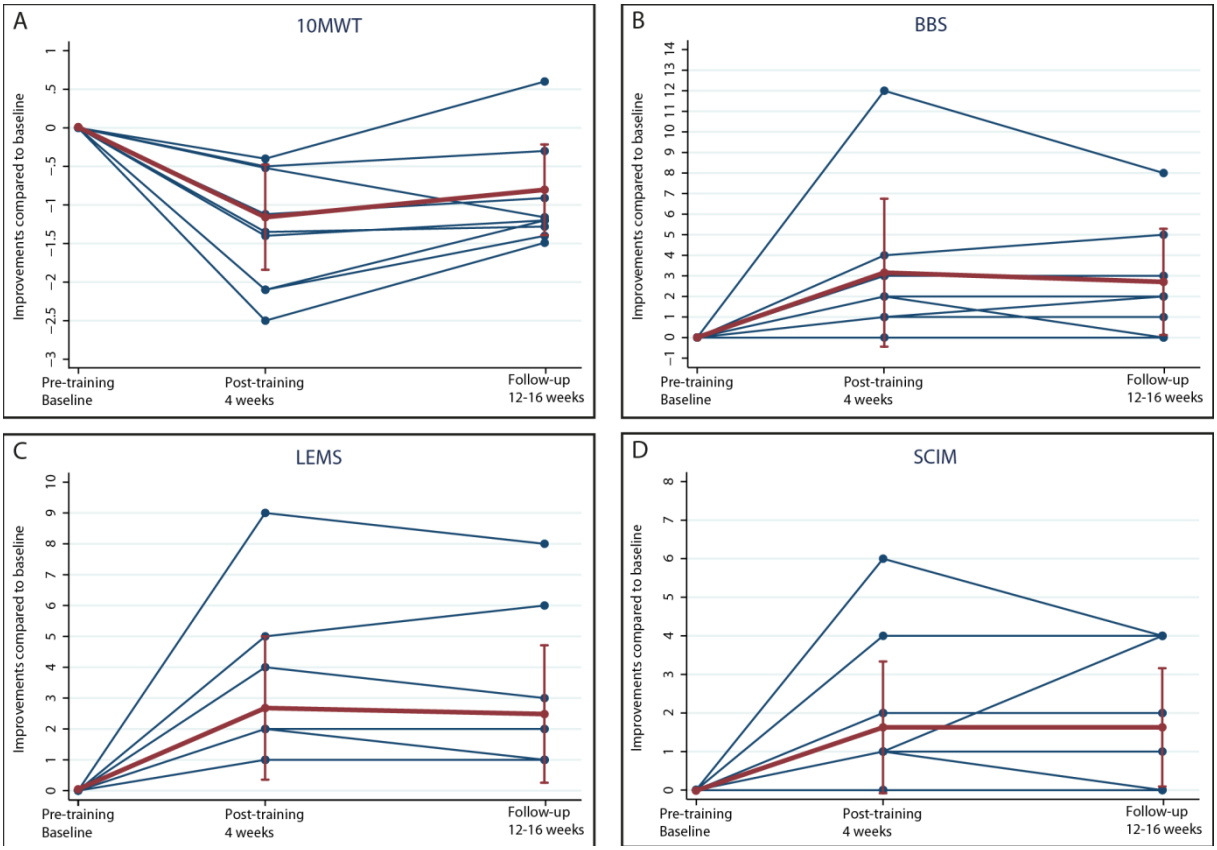

Figure 10: Performance improvements. Improvements of (A) 10 meter walking test (10MWT), (B) Berg balance scale (BBS), (C) lower extremity motor score (LEMS) and (D) spinal cord independence measure (SCIM) in patients with incomplete spinal cord injury (iSCI) after 16-20 interactive training sessions during four weeks (post-training) and 12 to 16 weeks after training (follow-up). Individual results (blue) and means with standard deviations (red) are shown.

Cross-sectional structural changes (MRI data) prior to training - VBM and VBCT

At baseline, VBM of white matter volume revealed significant reductions in the cerebellum (lobule IX, Z score 3.95, $P < 0.001$) and brainstem (medulla oblongata, Z score 4.88, $P < 0.001$) in patients compared to controls (Table 5 and Figure 11, left). No alteration in VBM of gray matter volume was detected in patients compared to controls.

VBCT of cortical thickness (Table 5 and Figure 11, right) revealed thinner cortical thickness in the left primary motor cortex of iSCI patients compared to controls when analyzing the sensorimotor cortex as region of interest (Z score 3.63, $P < 0.001$), but not at whole brain. No volumetric and cortical thickness increases were detected in patients compared to controls.

Region	Z score	P value (cluster, FWE-corrected)	Cluster extent (voxel)	MNI coordinates		
				x (mm)	y (mm)	z (mm)
VBM						
Brainstem (medulla oblongata)	4.88	< 0.001	300	-6	-48	-61
Cerebellum (lobule IX)	3.95	< 0.001	353	-6	-51	-31
VBCT						
Primary motor cortex*	3.63	< 0.001	46	-23	-30	59

Table 5: VBM/VBCT volume decreases (e.g. atrophy) at whole brain before training between patients and healthy controls. *Analysis was performed in the sensorimotor cortex to increase sensitivity (Freund *et al.*, 2011). VBM = voxel-based morphometry; VBCT = voxel-based cortical thickness.

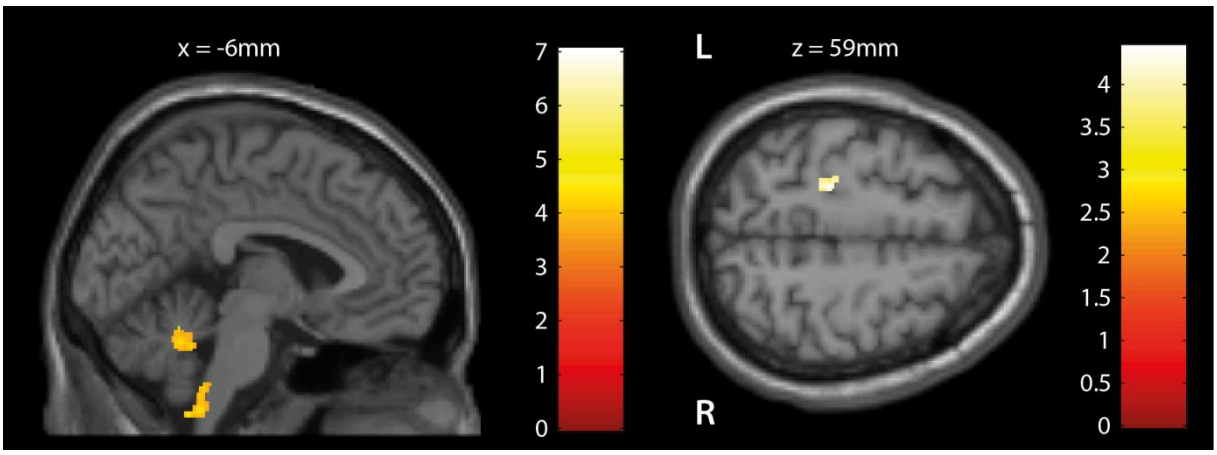

Figure 11: Cross-sectional structural changes (VBM/VBCT) - Statistical parametric maps (thresholded at P < 0.001 uncorrected, for illustrative purposes) showing volume reductions in patients with incomplete spinal cord injury (iSCI) compared with controls. (Left) Voxel-based morphometry (VBM): cerebellum and pyramids and (right) voxel-based cortical thickness (VBCT): left primary motor cortex. The color bars indicate the t-scores.

Longitudinal structural changes (MRI data) - TBM

Over the course of training, the iSCI patients' improvements in performance correlated positively with dynamic changes in local volume in several brain regions (Table 6 and Figure 12). Related to the BBS scores, the changes were located in the right cerebellum (lobule V, Z score 4.70, P = 0.037; lobule VI, Z score 4.58, P = 0.002), left middle occipital gyrus (Z score 4.28, P = 0.034), both hippocampi (Z score 4.27, P < 0.001; Z score 4.17, P < 0.001), the left temporal pole (Z score 4.00, P < 0.001), corpus callosum (Z score 4.12, P < 0.001), and two brainstem regions (pons, Z score 4.16, P < 0.001; midbrain, Z score 4.09, P = 0.003). For the LEMS, a positive correlation between volumetric changes and improvements were found in the left middle temporal gyrus (Z score 4.05, P < 0.001). The SCIM scores were positively correlated with longitudinal volume changes in the left cerebellum (lobule VI, Z score 5.17, P < 0.001; lobules I-IV, Z score 4.77, P = 0.003) and left fusiform gyrus (Z score 4.52, P < 0.001). No significant correlations between the behavioral and structural changes were found for the 10MWT.

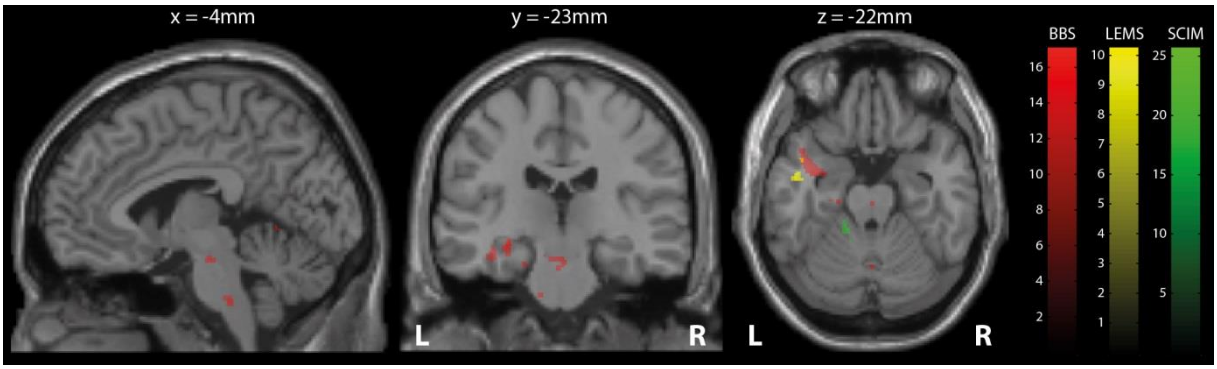

Figure 12: Longitudinal structural changes (TBM). Overlay of statistical parametric maps (thresholded at P < 0.001 uncorrected, for illustrative purposes) showing correlations between volume increases measured by tensor-based morphometry (TBM) and clinical improvements in balance (BBS, red), lower extremity motor score (LEMS, yellow), and spinal cord independence measure (SCIM, green). The corresponding t-scores are indicated by the color bars. Correlations are shown in brainstem (left), hippocampus (middle), and left temporal gyrus and cerebellum (right). Pain reduction was included as covariate of no interest.

Region	Z score	P value (cluster, FWE-corrected)	Cluster extent (voxel)	MNI coordinates		
				x (mm)	y (mm)	z (mm)
BBS						
Right cerebellum (lobule V)	4.70	0.037	59	3	-57	0
Right cerebellum (lobule VI)	4.58	0.002	93	8	-68	-13
Left middle occipital gyrus	4.28	0.034	60	-39	-65	-1
Right hippocampus	4.27	<0.001	122	27	-5	-40
Left hippocampus	4.17	< 0.001	159	-30	-18	-18
Brainstem (pons)	4.16	< 0.001	129	-8	-32	-43
Corpus callosum	4.12	<0.001	143	-24	-6	36
Brainstem (midbrain)	4.09	0.003	89	-9	-17	-16
Left temporal pole	4.00	< 0.001	833	-35	4	-36
LEMS						
Left middle temporal gyrus	4.05	<0.001	324	-45	-2	-15
SCIM						
Left cerebellum (lobule VI)	5.17	<0.001	169	-15	-60	-27
Left cerebellum (lobules I-IV)	4.77	0.003	87	-14	-39	-21
Left fusiform gyrus	4.52	< 0.001	265	-30	-75	-10

Table 6: Correlations between TBM longitudinal volume increases and performance improvements in patients. TBM = tensor-based morphometry; BBS = Berg balance scale; LEMS = lower extremity motor score; SCIM = spinal cord independence measure.

Discussion

This study reveals specific structural brain changes associated with motor performance improvements following intensive VR-augmented lower limb training in chronic iSCI patients. As anticipated, intensive training over a period of four weeks resulted in improvements in ambulation (e.g. 10MWT) and postural stability/control (e.g. BBS) (Deliagina *et al.*, 2008). Overall independence in their daily life improved, as shown by the higher SCIM scores. The success of this intensive VR-augmented training with over 5000 ankle movements and 1200 knee movements per leg during a month of training was reflected by high ratings for enjoyment, motivation, and attention. Crucially, motor performance improvements relate to increases in local brain volume in areas relevant for locomotion. These findings allow us to address the question to what extent motor performance improvements during rehabilitation are reflected by brain plasticity.

Using longitudinal structural MRI data, it has been shown repeatedly that training improvements in healthy controls can be related to increases in cortical volume in humans (Driemeyer *et al.*, 2008; Taubert *et al.*, 2010; Landi *et al.*, 2011; Sagi *et al.*, 2012; Sehm *et al.*, 2014) and monkeys (Quallo *et al.*, 2009). These changes occur rather rapidly (within weeks) and the effects are stronger when a new task was learned as opposed to a refinement of an already learned task (Driemeyer *et al.*, 2008; Quallo *et al.*, 2009). Moreover, these structural brain changes are dynamic, demonstrating increases during the initial phase of learning and decreases at later stages (Taubert *et al.*, 2010; Sehm *et al.*, 2014). Only a few studies have assessed this phenomenon in neurological disorders (Burciu *et al.*, 2013; Sehm *et al.*, 2014). Using TBM, we demonstrate dynamic structural brain plasticity associated with motor learning in several cortical and subcortical areas in patients with chronic iSCI. These brain regions correspond with those involved in the learning of balance tasks in the healthy and diseased brain and occurred within the first weeks (Sehm *et al.*, 2014).

In particular, the iSCI patients exhibited an expansion of gray matter volume in the temporal lobe that was associated with improvements in balance (BBS) and muscle strength (LEMS) of the lower limbs. The responsiveness of the temporal lobe is similar to that observed during upper limb training in healthy subjects who were trained over 3 months to learn a classic three-ball cascade juggling routine (Draganski *et al.*, 2004). Furthermore, our VR training, which demanded high levels of spatial memory capacities, induced structural changes within

the hippocampus. These results are in line with hippocampi volume increases associated with spatial memory and learning in a cohort of London taxi drivers memorizing navigation patterns (Maguire *et al.*, 2000). In addition, functional MRI studies have shown that the hippocampus is also involved in encoding (Schendan *et al.*, 2003) and consolidation of motor skills (Albouy *et al.*, 2008). The increase in gray matter volume due to VR-augmented lower limb training in the cerebellum most likely reflects improved adaptation of postural movement (Houk *et al.*, 1996; Rabe *et al.*, 2009; Burciu *et al.*, 2013). An increase in volume was induced in the brainstem, but only little is known about the anatomical plasticity of key locomotor regions in this area. In a recent study with rats, Zörner et al. (2014) observed that anatomical plasticity in defined brainstem motor networks significantly contributed to functional recovery after injury of the central nervous system.

While the analysis of the MRI data can show dynamic changes over time, it cannot explain the microstructural neuronal processes underlying learning-induced brain volumetric changes (Draganski and May, 2008). Thus, the dynamic gray and white matter volume increases observed in our cohort of iSCI patients may be attributable to several factors such as synaptogenesis, astrocytic hypertrophy, neurogenesis, angiogenesis and myelin formation (for review, see (Markham and Greenough, 2004)).

In accordance with previous structural MRI studies, white matter volume in the cerebellum, medulla oblongata, and cortical thickness in the primary motor cortex were reduced in iSCI patients when compared to controls (Freund *et al.*, 2011, 2013). At a microstructural level, these atrophic changes are related to axonal degeneration and demyelination (Cohen-Adad *et al.*, 2011; Freund, Schneider, *et al.*, 2012; Freund, Wheeler-Kingshott, *et al.*, 2012). Interestingly, we observed training-induced increases in local brain volume in key areas of locomotion (i.e. brainstem and cerebellum) adjacent to areas that showed volume reductions as assessed by VBM. Future quantitative MRI studies using myelin-sensitive readouts will elucidate whether training can reverse atrophy by promoting structural integrity.

Our study had few limitations. Although we carefully selected and assessed the patients clinically, the sample size was rather small (n=9, 18 MRI assessments). Therefor our study might have been insensitive to detecting small changes with week effect sizes. Moreover, the lack of a SCI control group for the VR-augmented training means that the training induced

changes in trained patients might have occurred not only as part of the training but also as part of a placebo effect (e.g. secondary effect due to participation in the training study). However, the locations of the brain volume changes were strongly overlapping with those shown to be responsive during motor training in healthy subjects and neurological impaired patients and therefore we are confident that the findings relate to performance improvements rather than spontaneous recovery. Moreover, the clinical outcome measures were shown to be stable one month prior to training commencement indicating that the observed behavioral improvements were training-induced rather than occurring spontaneously.

Conclusion

Overall, our present pilot study demonstrates a close link between structural changes in spatially distinct, task-specific areas of the central nervous system related to performance improvements during motor learning in patients with chronic iSCI. Novel neuroimaging measures of dynamic structural changes in response to training hold significant potential to provide complementary information regarding the intensity and specificity of functional training programs which, while applied routinely in SCI patients, may require adjustment in terms of their intensity and specificity for the individual patient. The hope is that neuroimaging measures of structural changes will establish itself as means to reveal the effectiveness of rehabilitation interventions in addition to, and beyond clinical outcome measures. Although routine clinical outcome measures are utmost important to value the outcome of rehabilitation interventions, they are limited to disclose if the trainings where effective enough to sufficiently engage the CNS to allow for any improved outcome.

Acknowledgments

Thanks to Pawel Pyk, Jeremy Spillmann and Bruno Meilick for their technical support, to Chris Schmidt for his critical review of a former version of this manuscript and to all participants for their generous help.

Funding

This research was supported by the International Foundation for Research in Paraplegia (IRP), Clinical Research Priority Program (CRPP), Neuro-Rehab UZH, Swiss National Science Foundation (SNF; Grant Number 51NF40-144619/PMPDP3-124282), OPO Foundation Zurich, the Neuroscience Center Zurich (ZNZ) and Wings for Life (WFL-CH-007/14).

Author contributions

Michael Villiger was involved in the study design, data acquisition, data interpretation, and writing the research article. Patrick Grabher contributed substantially to data analysis and data interpretation. He wrote the research article. Marie-Claude Hepp-Reymond, Daniel Kiper, Armin Curt, Marc Bolliger, Sabina Hotz-Boendermaker, Spyros Kollias and Kynan Eng were involved in the study design. Patrick Freund contributed substantially to data analysis and interpretation and writing the manuscript. All authors revised the research article.

Competing financial interests

There is a commercial interest of two authors (Kiper and Eng) relevant to the subject of the manuscript. All other authors declared no potential conflicts of interest with respect to the research, authorship, and/or publication of this article.

Chapter 5:

Voxel-based analysis of gray and white matter degeneration in cervical spondylotic myelopathy

Patrick Grabher[1], Siawoosh Mohammadi[2,3], Aaron Trachsler[1], Susanne Friedl[1], Gergely David[1], Reto Sutter[4], Nikolaus Weiskopf[3,5], Alan J. Thompson[6], Armin Curt[1] & Patrick Freund[1,3,5,6]

[1]Spinal Cord Injury Center Balgrist, University Hospital Zurich University of Zurich, Zurich, Switzerland

[2]Department of Systems Neuroscience, University Medical Center Hamburg-Eppendorf, Hamburg, Germany.

[3]Wellcome Trust Centre for Neuroimaging, Institute of Neurology, University College London, London, United Kingdom.

[4]Department of Radiology, University Hospital Balgrist, Zurich, Switzerland

[5]Department of Neurophysics, Max Planck Institute for Human Cognitive and Brain Sciences, Leipzig, Germany.

[6]Department of Brain Repair and Rehabilitation, Institute of Neurology, University College London, London, United Kingdom

The original article was published in *Sci Rep* 2016; 6:24636

Abstract

In this prospective study, we made an unbiased, voxel-based analysis to investigate above-stenosis spinal degeneration and its relation to impairment in patients with cervical spondylotic myelopathy (CSM).

Twenty patients and 18 controls were assessed with high-resolution MRI protocols above the level of stenosis. Cross-sectional areas of gray matter (GM), white matter (WM), and posterior columns (PC) were measured to determine atrophy. Diffusion indices assessed tract-specific integrity of PC and lateral corticospinal tracts (CST). Regression analysis was used to reveal relationships between MRI measures and clinical impairment.

Patients showed mainly sensory impairment. Atrophy was prominent within the cervical WM (13.9%, p=0.004), GM (7.2%, p=0.043), and PC (16.1%, p=0.005). Fractional anisotropy (FA) was reduced in the PC (-11.98%, p=0.006) and lateral CST (-12.96%, p=0.014). In addition, radial (+28.47%, p=0.014), axial (+14.72%, p=0.005), and mean (+16.50%, p=0.001) diffusivities were increased in the PC. Light touch score was associated with atrophy (R^2=0.3559, p=0.020) and FA (z score 3.74, p=0.003) in the PC, as was functional independence and FA in the lateral CST (z score 3.68, p=0.020).

This study demonstrates voxel-based degeneration far above the stenosis at a level not directly affected by the compression and provides unbiased readouts of tract-specific changes that relate to impairment.

Introduction

Cervical spondylotic myelopathy (CSM) is one of the most frequent spinal cord disorders leading to reduced independence and quality of life especially in the elderly (Kalsi-Ryan, Karadimas, *et al.*, 2013). Neurological impairment is mainly caused through chronic cord compression and deterioration of blood supply triggering degeneration of neural tissue in gray and white matter in the spinal cord at the level of stenosis (Yu *et al.*, 2011; Karadimas *et al.*, 2013). The time course of the stenosis and its relation to the emergence of clinical impairment is unknown, as a moderate cord stenosis might be clinically silent for many years. Decompressive surgery is the therapeutic gold standard in patients with clinically relevant cord stenosis (Holly *et al.*, 2008), while a conservative approach is chosen in those patients with a radiologically less severe stenosis and only mild symptoms. Recently, novel experimental neuroprotective approaches improving outcome were investigated by blocking Fas-mediated apoptosis (Yu *et al.*, 2011) and the application of a benzothiazole anticonvulsant (i.e. riluzole) (Moon *et al.*, 2014; Karadimas *et al.*, 2015) and results were encouraging. Hence, there is a pressing need to detect and monitor early subclinical pathologic changes to the microstructure of the spinal cord, allowing interventions before those changes cause clinical impairments. However, neuroimaging biomarkers that can quantify disease progression at a stage before major irreversible damage occurs, monitor treatment effects (beyond decompression of the cord) and predict outcome are lacking (Kalsi-Ryan, Karadimas, *et al.*, 2013).

Recent developments in imaging and post-processing techniques have significantly advanced the accuracy and sensitivity of spinal cord neuroimaging. For example the advent of a common anatomical spinal cord template (Fonov *et al.*, 2014), probabilistic tracts (Fonov *et al.*, 2014), and optimization of post-processing techniques (Mohammadi *et al.*, 2012) have now opened the avenue for unbiased voxel-based morphometry (VBM) analysis (i.e. without an a priori hypothesis) of volumetric as well as microstructural changes (Mohammadi *et al.*, 2012; Fonov *et al.*, 2014). This enables the spatial localization of cord pathology and the determination of its relation with clinical impairment (Naismith *et al.*, 2013; Toosy *et al.*, 2014).

In this study, we took advantage of high-resolution anatomical volumetric MRI to assess gray and white matter atrophy (i.e. Multiple Echo Data Image Combination (MEDIC)) and diffusion tensor imaging (DTI) to assess changes to the microstructural tissue properties. We

hypothesized that chronic cord compression results in remote and spatially localized morphometric changes (i.e. atrophy) within cervical gray and white matter as well as tract-specific changes above the level of stenosis in CSM patients and that the degree of remote degeneration relates to clinical impairment.

Material and methods

Subjects and study design

Twenty patients (six women) (Table 7) referred for a neurological evaluation due to CSM with a mean age of 52.0 ± 14.5 (SD) years and 18 gender-matched controls (six women) with a mean age of 44.4 ± 9.7 (SD) years were consecutively recruited for this study between July 2012 and September 2014 in the outpatient clinic at the University Hospital Balgrist, Switzerland. The mean age between both groups was statistically not different (Mann-Whitney U test: z=-1.61, p=0.1075). The participants fulfilled the following inclusion criteria: no other neurological or mental disorders affecting clinical outcome, age between 18 to 70 years, no MRI contradictions, and no pregnancy. The study protocols were in accordance with the Declaration of Helsinki and were approved by the local Ethics Committee of Zurich, the *'Kantonale Ethikkommission Zurich'* (ref. number: EK-2012-0343). All participants provided written informed consent.

Clinical examination

All patients received a comprehensive clinical examination including the modified Japanese Orthopedic Association (mJOA) scale (Benzel *et al.*, 1991) [max. 18 points], and additional outcome measures such as the ISNCSCI protocol for upper extremities (Kirshblum *et al.*, 2011) for motor score (UEMS) (e.g. pyramidal dysfunction) [max. 50 points], light touch (UELT) (e.g. posterior column dysfunction) [max. 32 points], and pinprick (UEPP) (e.g. spinothalamic dysfunction) [max. 32 points], Spinal Cord Independence Measure (SCIM) [max. 100 points]) (Anderson *et al.*, 2008), and the Graded Redefined Assessment of Strength, Sensibility and Prehension (GRASSP) protocol [max. 232 points] as ancillary outcome measure sensitive for upper extremities in CSM (Kalsi-Ryan, Singh, *et al.*, 2013) (sub-item for strength [max. 100 points], sensibility [max. 48 points], and prehension [max. 84 points]) (Kalsi-Ryan *et al.*, 2012). Based on the mJOA, CSM severity was identified as mild (mJOA≥15), moderate (mJOA=12-14), or severe (mJOA<12) (Michael G Fehlings *et al.*, 2013).

Image acquisition

All participants were scanned on a 3T Skyra MRI scanner (Siemens Healthcare, Erlangen, Germany) equipped with a 16-channel radio-frequency (RF) receive head and neck coil and RF body transmit coil. All participants wore an MRI-compatible stiff neck (Laerdal Medicals, Stavanger, Norway) to minimize motion artefacts and were carefully positioned by the

radiographers to acquire the data from the same position and to obtain high reproducibility between all participants.

A 2D sagittal T2-weighted turbo spin-echo sequence was used for anatomical assessment of cervical spinal cord covering the levels of stenosis. Following parameters were applied to acquire 20 slices within 2 minutes and 2 seconds: slice thickness 2.5 mm with 10% inter-slice gap, field of view (FOV) of 220x220 mm^2, matrix size of 384x384, time of repetition (TR) of 3760 ms, time of echo (TE) of 87 ms, flip angle α=160°, and readout bandwidth of 260 Hz per pixel.

A 3D high-resolution optimized T2*-weighted multi-echo sequence (multiple echo data image combination; MEDIC) (Schmid *et al.*, 2005) was applied to acquire five high-resolution axial 3D volumes of the cervical cord above the stenosis at C2/C3 level. Each volume consisted of twenty partitions and was obtained with a resolution of 0.25x0.25x2.50 mm^3 within 2 minutes and 8 seconds for each of the five volumes. Following parameters were applied: FOV of 162x192 mm^2, matrix size of 648x768, TR of 44 ms, TE of 19 ms, flip angle α=11°, and readout bandwidth of 260 Hz per pixel.

The acquisition of DTI data used a cardiac-gated monopolar sequence (based on finger pulse oximetry) (Morelli *et al.*, 2010) and the following parameters: 30 diffusion-weighted (DW) images (b = 500 s/mm^2), six T2- weighted images without diffusion weighting (b = 0), 5 mm slice thickness, with 10% inter-slice gap, 10 slices perpendicularly oriented to the spine, 5/8 Partial-Fourier Imaging in phase-encoding direction, phase oversampling 50%, and a cardiac trigger delay of 200 ms, 176 x 40 acquisition matrix, FOV of 133 x 30 mm^2, 0.8 x 0.8 mm^2 in-plane resolutions, TE of 73 ms, and TR of 350 ms. The gated data were acquired in blocks of two slices per cardiac cycle. The minimal time between successive triggers was 1800 ms. Reduced field of view was achieved by outer-volume suppression (Morelli *et al.*, 2010) using two spatial saturation pulses placed anterior and posterior to the spinal cord, along the phase-encoding direction (Heidemann *et al.*, 2009). To reduce fold-over artefacts due to insufficient outer volume suppression, the amplitude of the saturation pulse was adjusted for each subject individually. Each DTI dataset was acquired four times at the same C2/C3 position in the cervical spinal cord, resulting in 144 images for each subject. Altogether, this resulted in a total

acquisition time of about 6.2 minutes (as estimated by the sequence simulator), but could be longer depending on the participant's heart rate.

Processing of sagittal T2-weighted data of cervical spine

We used JIM 6.0 (Xynapse Systems, Aldwincle, UK) to calculate the maximum canal compromise (MCC) and maximum spinal cord compression (MSCC) using the midsagittal slice (Fehlings *et al.*, 1999; Nouri *et al.*, 2015). We calculated the signal change ratio from the region of hyperintensity or, if not applicable, from the level of greatest cord compression against an average reference on the spinal cord at C7/T1 and C2 using the ratio proposed by Nouri et al (Nouri *et al.*, 2015).

Processing of high-resolution structural data above the level of stenosis

We used a symmetric diffeomorphic algorithm (Ashburner and Ridgway, 2013), that is embedded in SPM12 (Wellcome Trust Centre for Neuroimaging, University College London, London, UK), to register the five 3D MEDIC volumes in each subject in order to account for non-rigid body motion effects and create an average volume for a better signal to noise ratio (SNR). Jim 6.0 was then used to merge the adjacent partitions to get 10 contiguous slices (to increase SNR) and to semi-automatically segment the cross-sectional cervical cord area using an active-surface model after setting a marker in the center of the cord in 10 contiguous slices (Horsfield *et al.*, 2010). The gray matter (GM) and posterior column (PC) were extracted manually in each slice. White matter (WM) was estimated by subtracting the GM from cervical cord area. The segmentation was performed by two independent investigators (PG and AT) and was reevaluated a second time with a gap of at least two weeks in between. Coefficient of variations (=standard deviation divided by mean) for cervical cord area, WM, GM, and PC were 0.6%, 1.9%, 6.9%, and 3.4% for inter-rater and 0.9%, 1.3%, 4.4%, and 1.4% for intra-rater variations, respectively.

Pre-processing and estimation of DTI data

The DTI data were interpolated to a higher in-plane resolution of 0.4 x 0.4 mm^2. Then, the data were corrected for motion and eddy current artefacts using a novel constrained 3D-affine registration (Mohammadi, Tabelow, *et al.*, 2015) that corrected for selected rigid-body subject motion and linear eddy current distortion parameters (details on linear eddy currents can be found in (Mohammadi *et al.*, 2010)). We restricted the 3D-affine registration to correct only

for in-plane x- and y-translation (mainly caused by subject motion and eddy currents) as well as for in-plane scaling and in-plane shearing along the y-direction (both mainly caused by eddy currents). We did not correct for rotation and through-plane shearing effects, which were less pronounced and less robust to estimate. To correct for residual artefacts associated with subject motion and physiological noise (Mohammadi, Hutton, *et al.*, 2013), we used robust fitting as implemented in the ACID toolbox (www.diffusiontools.com). Combining eddy current and motion correction with the robust tensor fitting approach has been shown to be particularly efficient to reduce intra-scan variability of DTI metrics (Mohammadi, Freund, *et al.*, 2013).

Post-processing and spatial normalization of DTI index maps

First, the in-plane field-of-view was chopped to 24 x 24 mm^2 for each DTI dataset to exclude non-spine tissue. Then, the following pathological relevant DTI index maps (Schmierer, Wheeler-Kingshott, *et al.*, 2007; Freund, Wheeler-Kingshott, *et al.*, 2012; Toosy *et al.*, 2014) were calculated: fractional anisotropy (FA), radial diffusivity (RD), axial diffusivity (AD), and mean diffusivity (MD). These DTI index maps were spatial normalized into the space of the AMU white and gray matter probabilistic tracts embedded within the MNI–Poly–AMU template (Fonov *et al.*, 2014) using the FA voxel-based statistics (FA-VBS) toolbox (Mohammadi *et al.*, 2012) with refined spatial normalization parameters, which specifically accounted for the anatomy of the spinal cord, i.e. the degree of freedom of the spatial transformation was reduced along the head-feed direction. To use optimal and complementary contrast information, we used the MD and FA contrast to drive the spatial normalization. Then, we performed additional manual slice-by-slice registration (shift and scaling along the phase-encoding direction) to refine to accuracy of the registration. Finally, all DTI index maps were smoothed using a Gaussian kernel with 0.5x0.5x5 mm^3 with full-width at half maximum (FWHM).

Statistical analysis

Stata 13 (StataCorp LP, Texas, USA) was used for statistical analysis of clinical and morphometric data. We used Mann-Whitney U tests to investigate age differences between patients and controls. We used ANCOVA with age as covariate of no interest to assess morphometric differences between patients and controls in cross-sectional cervical cord area, GM, WM, and PC. Linear regression models were used to determine associations between

bilateral clinical outcome measures for mJOA, UELT, UEPP, GRASSP sensibility, strength, and prehension, SCIM, MSCC, MCC, and signal change ratio and cross-sectional cervical cord area and between UELT and GRASSP sensibility and PC. Bilateral outcome measures were used because there is not landmark to separately segment left and right cross-sectional cervical cord measures separately. Age was included and treated as covariate of no interest to adjust for possible confounds of age in every statistical test. The level of significance was defined as α=0.050.

SPM12 was used for voxel-based statistics of the different DTI indices. To this end, we investigated the averaged DTI indices across the cross-section of the cervical cord (C2/C3) and verified the tract-specific location using the white matter spinal cord atlas that is embedded in the Spinal Cord Toolbox (Cohen-Adad *et al.*, 2014) for the posterior column (PC), lateral corticospinal tract (CST), and spinothalamic tracts. We used ANCOVA to investigate cross-sectional differences in DTI indices (e.g. FA, AD, RD, and MD) between patients and controls and adjusted for age within the groups.

Linear regression models were constructed for associations between unilateral clinical outcome measures for UELT, UEPP, GRASSP sensibility, strength, and prehension and DTI indices (except for mJOA, SCIM, MSCC, MCC, and signal change ratio as purely bilateral outcome measures). Age was included as a covariate of no interest in all linear regression models to adjust for possible confounds of age. All statistical parametric maps were initially thresholded with a cluster defining threshold of uncorrected $p<0.01$. Clusters surpassing a cluster threshold of $p=0.05$, corrected for family-wise error based on Gaussian Random Field theory, are reported (Friston *et al.*, 1994).

Results

Subjects

In patients, impairment was assessed on the modified Japanese Orthopedic Association (mJOA) score which identified ten patients suffering from mild (mJOA≥15 [max. 18]), nine from moderate (mJOA=12-14) and one from severe (mJOA<12) CSM. The upper-extremity International Standards for Neurological Classification of SCI (ISNCSCI) scores were (mean ± SD) 27.70 ± 4.07 for light touch (UELT) [max. 32], 27.30 ± 3.77 for pinprick (UEPP) [max. 32], and 49.70 ± 0.57 for motor score (UEMS) [max. 50]. The spinal cord independence measure (SCIM) was 97.85 ± 4.04 [max. 100]. The total Graded Redefined Assessment of Strength, Sensibility and Prehension (GRASSP) score was 220.74 ± 12.32 [max. 232], and the sub-items were 95.16 ± 6.83 for strength [max. 100], 42.57 ± 6.50 for sensibility [max. 48], and 83.26 ± 1.45 for prehension [max. 84]. Individual scores are shown in Table 7.

Conventional MRI measures at site of stenosis

The level of stenosis was at C5/C6 (n=13) for the majority of patients, twice at C3/4, once at C4/C5, three times at C6/7, and once at C7/C8. In patients, the maximum spinal cord compression (MSCC) was 17.33 ± 7.21% and maximum canal compromise (MCC) 37.36 ± 8.58%. Nine patients showed a T2 signal hyperintensity with a signal change ratio of 1.58 ± 0.32. Individual data are shown in Table 7.

ID	Gender	Age	Level Of Stenosis	mJOA	UEMS	UELT	UEPP	SCIM	GRASSP			MSCC (%)	MCC (%)	T2 Hyperintensity	Signal Change Ratio
									Strength	Sensibility	Prehension				
1	m	36	C5/6[a]	12	48	20	25	99	74	37	84	8.35	39.14	No	0.93
2	m	50	C5/6[a]	16	49	25	26	100	100	47	84	23.85	48.37	No	1.03
3	m	39	C3/4[a]	13	50	25	23	100	98	43	84	24.38	40.83	No	1.00
4	f	66	C5/6	12	49	32	32	96	95	37	84	14.14	36.67	Yes	1.33
5	m	69	C5/6[a]	17	50	32	32	100	99	44	84	16.31	39.59	No	1.12
6	m	68	C6/7[a]	17	50	32	32	100	NT	NT	NT	26.12	49.81	Yes	1.77
7	m	39	C5/6	16	50	32	25	100	100	46	84	29.33	52.72	No	1.13
8	m	34	C5/6	14	50	30	30	100	100	47	84	23.73	37.29	No	0.99
9	f	31	C5/6	16	50	27	27	100	100	48	84	11.40	34.04	Yes	1.55
10	f	47	C5/6[a]	16	50	31	31	100	100	48	84	12.84	39.94	Yes	1.35
11	m	63	C4/5[a]	12	50	24	24	95	94	41	84	13.82	30.67	Yes	1.81
12	m	74	C6/7[a]	14	50	32	32	88	89	42	84	22.62	43.01	Yes	1.34
13	m	32	C5/6[a]	16	50	20	20	100	100	48	84	1.13	27.14	No	1.03
14	m	66	C5/6	9	50	25	26	86	99	34	82	18.17	26.44	Yes	2.27
15	m	51	C5/6	15	50	27	27	96	92	44	81	17.07	36.32	No	1.00
16	f	53	C5/6	16	50	32	30	100	100	46	84	18.76	49.98	Yes	1.46
17	m	72	C7/T1[a]	14	50	26	22	100	98	41	83	25.82	32.07	No	1.05
18	f	37	C3/4[a]	14	49	30	30	99	93	46	79	16.03	23.00	Yes	1.31
19	f	58	C5/6[a]	16	49	29	29	100	93	48	84	15.64	34.96	No	1.00
20	m	55	C6/7	12	50	23	23	98	84	22	81	7.15	25.25	No	1.06

Table 7. Clinical and behavioural data of 20 patients with cervical spondylotic myelopathy. mJOA = modified Japanese Orthopaedic Association [max. 18 points]. UEMS = Upper extremity motor score [max. 50 points]. UELT = Upper extremity light touch [max. 32 points]. UEPP = Upper extremity pinprick [max. 32 points]. SCIM = Spinal Cord Independence Measure [max. 100 points]. GRASSP = Graded Redefined Assessment of Strength, Sensibility and Prehension [strength: max. 100 points, sensibility: max. 48 points, prehension: max. 84 points]. MSCC = Maximum Spinal Cord Compression. MCC = Maximum Canal Compromise. NT = Not tested. [a] Multisegmental degeneration of cervical spine.

Morphometric changes in the cervical cord above the site of stenosis

Volumetric as well as microstructural changes were observed in patients compared to controls above the level of stenosis at C2/C3. In patients, the cross-sectional cervical cord area was reduced by 12.8% (patients: 80.88 mm^2, CI 75.59-86.17 mm^2 vs. controls: 92.77 mm^2, CI 88.88-96.67 mm^2, p=0.0032), GM area by 7.2% (patients: 17.80 mm^2, CI 16.96-18.64 mm^2 vs. controls: 19.18 mm^2, CI 18.33-20.03 mm^2, p=0.0429), WM area by 13.9% (patients: 63.08 mm^2, CI 58.42-67.75 mm^2 vs. controls: 73.23 mm^2, CI 69.88-76.57 mm^2, p=0.0041) and PC area by 16.1% (patients: 18.86 mm^2, CI 17.30-20.41 mm^2 vs. controls: 22.49 mm^2, CI 21.06-23.92 mm^2, p=0.0051) (Figure 13).

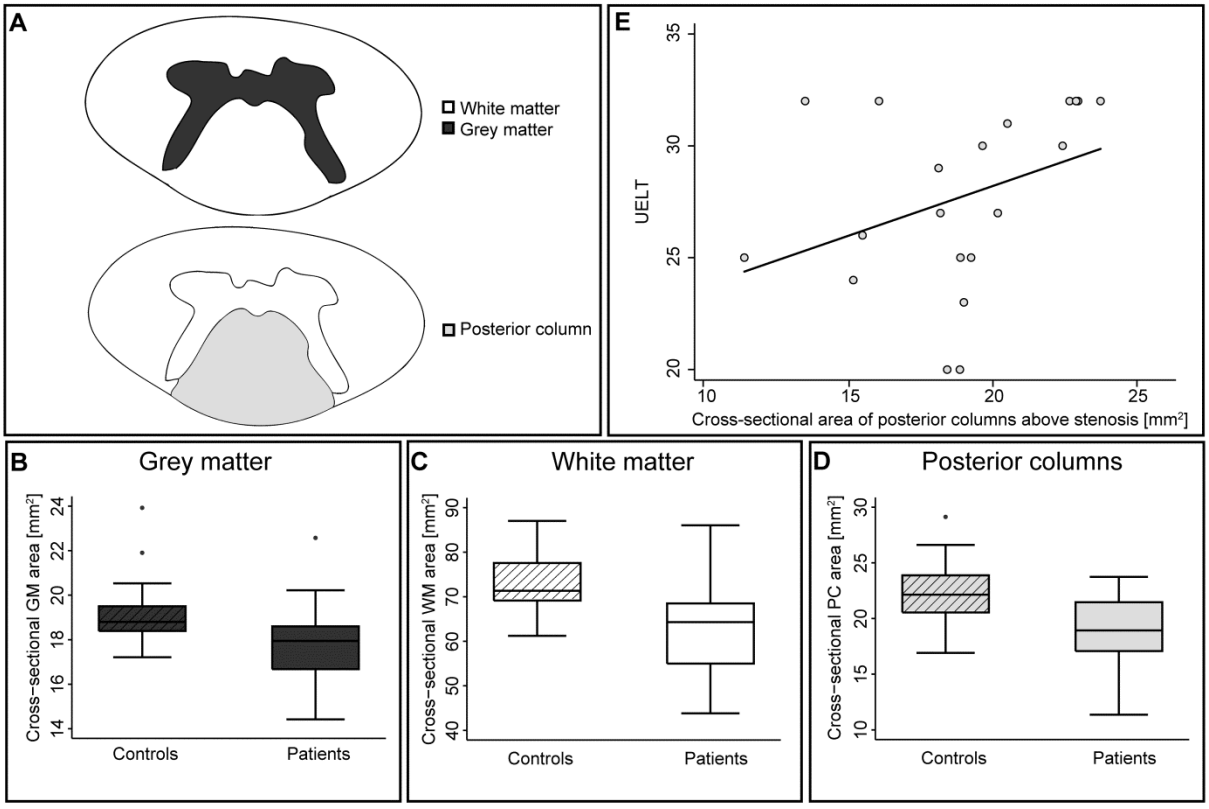

Figure 13 Morphometric changes in cervical spinal cord above compression site at C2/C3. (A) Schematic illustration of segmented cross-sectional cervical areas of gray matter, white matter, and posterior columns remote to compression. Significant reductions are shown for cross-sectional cervical cord area of gray matter (B), white matter (C), and posterior columns (D) in patients compared to controls. (E) Correlation between ISNCSCI upper extremity light touch (UELT) score and cross-sectional area of the posterior columns (for illustrative purposes, not adjusted for age).

Voxel-based analysis of the cervical cord DTI revealed reductions in FA in the lateral CST (-12.96%, patients: 0.57, CI 0.53-0.61 vs. controls: 0.66, CI 0.63-0.68; x:4.5, y:-20.5, z:8.0, z score 3.30, cluster extent=144, p=0.014, FWE corrected) and PC (-11.99%, patients: 0.59, CI 0.55-0.63 vs. controls: 0.67, CI 0.65-0.69;x:-2.0, y:-20.0, z:8.0, z score 4.08, cluster extent=174, p=0.006, FWE corrected) while AD (+14.72%, patients: 0.0019, CI 0.0019-0.0020 vs. controls 0.0017, CI 0.0016-0.0017; x:-1.0, y:-18.5, z:41.0, z score 3.91, cluster extent=228, p=0.005, FWE corrected), RD (+28.47%, patients: 0.00073, CI 0.00064-0.00082 vs controls 0.00057, CI 0.00053-0.00060; x:1.0, y:-18.0, z:14.0, z score=3.39, cluster extent=203, p=0.014, FWE corrected), and MD (+16.50%, patients: 0.00073, CI 0.00064-0.00082 vs. controls 0.00057, CI 0.00053-0.00060; x:2.0, y:-19.5, z:41.0, z score 3.80, cluster extent=379, p=0.001, FWE corrected) were all increased in the PCs in patients when compared to controls (Figure 14, Figure 15).

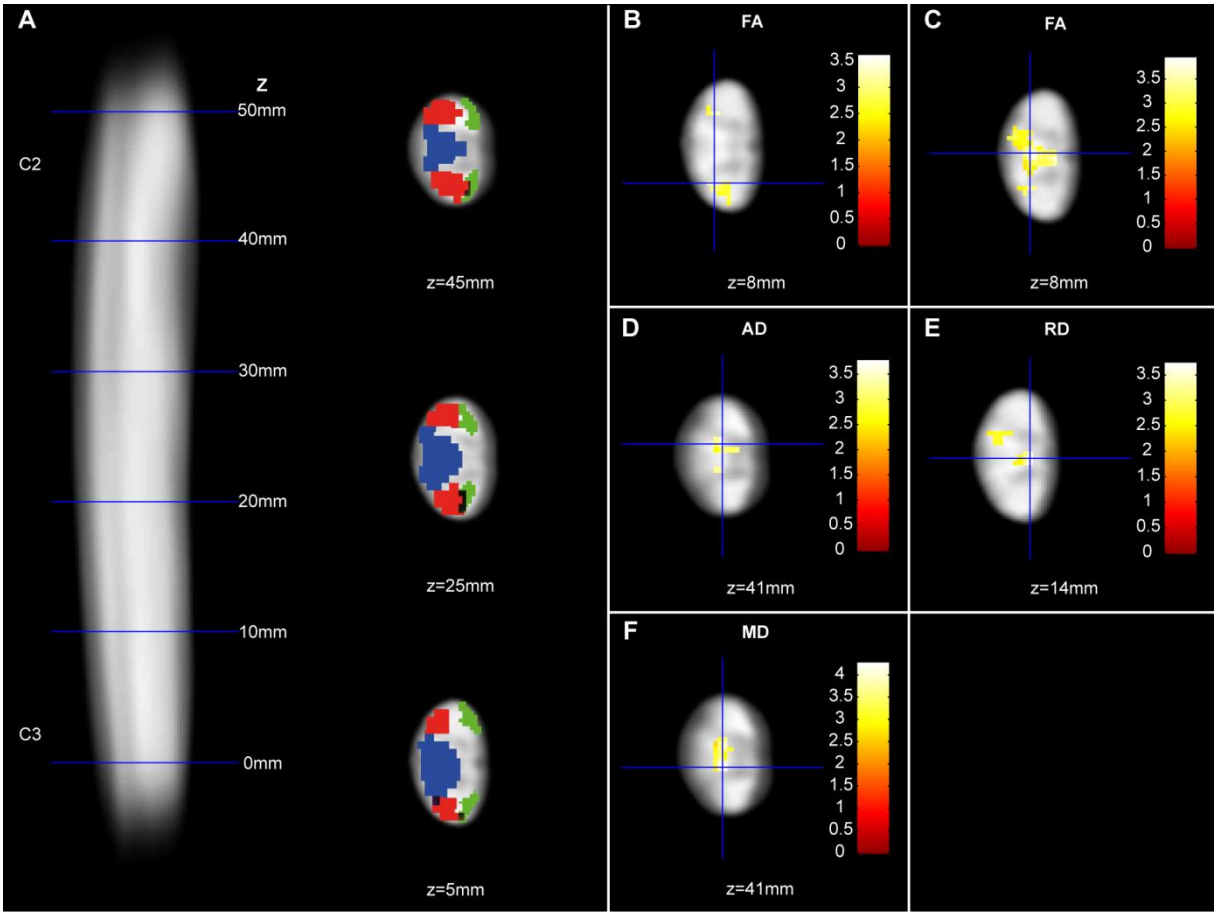

Figure 14: Tract-specific changes in microstructure above stenosis in patients with CSM compared to healthy controls. (A) Sagittal FA template of all subjects showing the cervical spinal cord at C2/C3 level and axial slices overlaid with regions of interest (lateral corticospinal tracts (CST) in red, posterior columns (PC) in blue, and spinothalamic tracts in green) for labeling of the anatomical position of the findings. (B-F) Overlay of statistical parametric maps ($p<0.01$ uncorrected, shown for descriptive purposes, masked by the lateral CST and PC, respectively) revealing microstructural changes in patients compared to controls. In patients compared to controls, fractional anisotropy (FA) was reduced in the right lateral CST (B). In the PC, FA was reduced (C) and axial (D), radial (E), and mean diffusivity (F) increased. Color bars indicate t-values. Axial slices are shown and their position is indicated by the z coordinate.

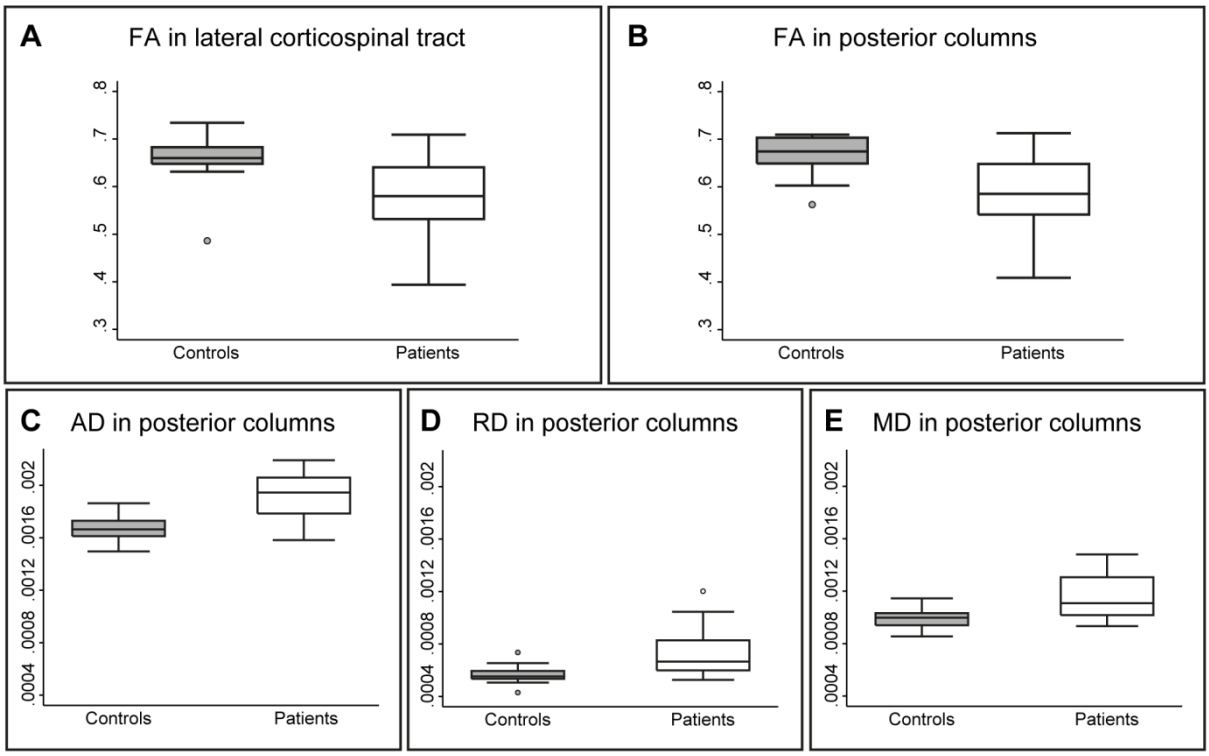

Figure 15: Quantification of tract-specific changes in microstructure above stenosis. In patients compared to controls, fractional anisotropy (FA) was reduced in the lateral CST (A) and PC (B), while AD (C), RD (D), and MD (E) were all increased in the PCs. Mean data were extracted from each significant cluster.

Clinical associations

In patients, significant associations were seen between macro- and microstructural MRI readouts and impairment. In particular, reduced PC area was associated with lower ISNCSCI UELT scores (R^2=0.3559, p=0.020) (Figure 13E). Furthermore, lower FA in the left PC was associated with lower left ISNCSCI UELT scores (x: 0.0, y:-18.5, z:19.0, z score 3.74, p=0.003, extent=198, FWE corrected) (Figure 16A). Lower FA in the left lateral CST was associated with lower SCIM score (x:-3.5, y:-21.5, z:-3.0, z score 3.68, p=0.020, extent=135, FWE corrected) (Figure 16B).

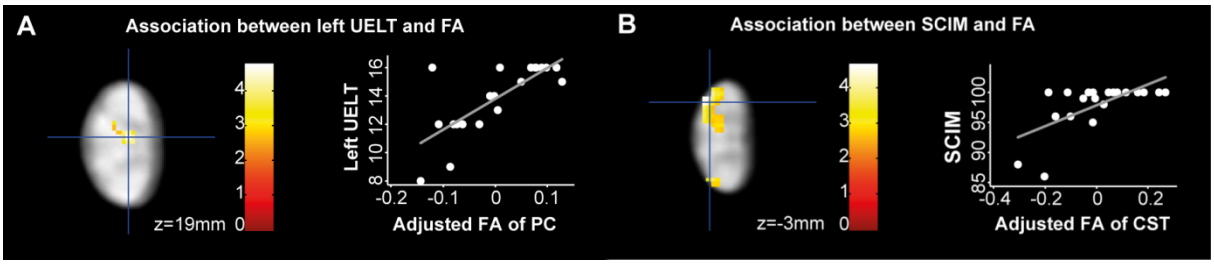

Figure 16: Associations between tract-specific microstructural readouts and clinical outcome above stenosis in patients with CSM. (A-B) Overlay of statistical parametric maps (p<0.01 uncorrected, shown for descriptive purposes, masked by the lateral corticospinal tract (CST) and posterior columns (PC), respectively) revealing associations between DTI indices and clinical outcome (left panel) between cervical level C2 and C3 (see Figure 14A for reference). Color bars indicate t-values. The right panels illustrate the corresponding regression models extracted from the peak-voxel within the significant cluster. Diffusivity parameters of the correlations are mean centered and adjusted for age. In particularly, (A) lower fractional anisotropy (FA) in left PC was associated with worse left ISNCSCI upper extremity light touch score (UELT) and (B) lower FA in the left lateral CST was associated with lower Spinal Cord Independence Measure (SCIM).

Discussion

This study in patients with CSM shows, next to conventional MRI measures (e.g. MSCC, MCC, signal change ratio) (Nouri *et al.*, 2015), for the first time remote and spatially localized morphological and microstructural changes of the spinal cord within the gray and white matter above the level of stenosis. In particular, there was gray and white matter atrophy, which was paralleled by tract-specific microstructural changes in major spinal pathways. Crucially, the degree of spinal cord pathology correlated with measures of clinical impairment of posterior column and pyramidal dysfunction. Thus, unbiased voxel-based analysis revealing spatially localized cord pathology provides complementary pathophysiological insights into rostral degenerative changes beyond the routine clinical work up (i.e. clinical examination, electrophysiology and radiology) of patients suffering from CSM.

Volumetric MRI provides information on (macro-structural) general tissue loss (e.g. atrophy) whereas DTI provides information on fiber orientation and tissue structure and thus is sensitive to microstructural tissue properties. While decreased FA has been associated with both axonal count (Gouw *et al.*, 2008) and myelin content (Schmierer, Wheeler-Kingshott, *et al.*, 2007), increased RD and decreased AD have been associated with demyelination (Klawiter *et al.*, 2011) and axonal degeneration (Zhang *et al.*, 2009), respectively.

This study found marked tissue loss (i.e. atrophy) of white and gray matter and tract-specific microstructural changes within major ascending and descending spinal pathways above the site of cord compression. The degree of atrophy above the site of stenosis was greater in the white matter (-13.9%) and less strong in gray matter (-7.2%). Changes in the spinal cord microvasculature (Karadimas *et al.*, 2013) and distribution of blood flow (Kurokawa *et al.*, 2011; Karadimas *et al.*, 2015), disruption of blood spinal cord barrier (Karadimas *et al.*, 2013), and neuroinflammation (Yu *et al.*, 2011; Karadimas *et al.*, 2013) could make motoneurons above the compression site vulnerable to degeneration and apoptosis and be potential mechanisms for gray matter atrophy.

Moreover, we found tract-specific decreased FA within the lateral CST and PC, and increased RD and MD in the PC as markers of axonal degeneration and demyelination (Schmierer, Tozer, *et al.*, 2007; Gouw *et al.*, 2008; Budde *et al.*, 2009; Zhang *et al.*, 2009; Cohen-Adad *et al.*, 2011; Klawiter *et al.*, 2011) next to the reported white matter atrophy. These findings are coherent

with other studies (Cui *et al.*, 2014; Wen, Cui, Liu, *et al.*, 2014; Zhou *et al.*, 2015). We found AD to be increased within the PC and these results are consistent with regards to the change of AD as shown in previous studies of CSM (Cui *et al.*, 2014; Rajasekaran *et al.*, 2014; Wen, Cui, Mak, *et al.*, 2014). This might be due to elevated fiber tract density due to compression and loss of surrounding structure, as reported at the lesion site in patients with CSM (Ellingson *et al.*, 2015), but also caudal and rostral to the compression site (Yu *et al.*, 2009), that manifests over time. AD has been shown to behave bi-directionally over time in patients with optic neuritis and in experimental spinal contusion studies (Ellingson *et al.*, 2008; Naismith *et al.*, 2009). In the latter AD decreased rapidly in rostrocaudal direction, but increased over time at the lesion site (Ellingson *et al.*, 2008). Nevertheless, in our study we report that the difference between patients with CSM and healthy controls in RD is nearly double as high as in AD which is suggestive that demyelination rather than axonal degeneration is occurring above the level of stenosis. It would be interesting to investigate our reported findings in other spinal cord pathologies at the same cervical level. Our conjoint analysis of macro- as well as microstructural changes are of interest because they suggest that a combination of pathological processes at the microstructural level including long distance retro- as well as anterograde fiber degeneration (i.e. axonal loss, demyelination) and potentially inflammation (Karadimas *et al.*, 2013) and to a lesser extent neuronal changes (i.e. apoptosis (Yu *et al.*, 2011; Karadimas *et al.*, 2013) and anterior horn cell loss (Fehlings and Skaf, 1998; Karadimas *et al.*, 2015)) occur several segments above the level of stenosis.

The magnitude of remote changes in terms of atrophy and microstructural changes resembles those observed in traumatic spinal cord injury (SCI) (Cohen-Adad *et al.*, 2011; Freund *et al.*, 2011, 2013; Lundell *et al.*, 2011; Freund, Wheeler-Kingshott, *et al.*, 2012; Grabher *et al.*, 2015). Although based on two very different underlying etiologies (abrupt onset in traumatic SCI, slowly developing symptoms in CSM), CSM and SCI clearly result in focal damage to the spinal cord with a combination of alpha-motoneuron damage (lesion of the central gray) as well as demyelination and axonal damage of long projecting spinal nerve fiber tracts (white matter damage) (Buss *et al.*, 2005; Kalsi-Ryan, Karadimas, *et al.*, 2013). Herein we provide converging evidence that both etiologies show remote cord pathology to a similar extent despite their striking difference in levels of disability. Given the marked degenerative changes above the site of stenosis, we anticipate atrophy and microstructural changes also to occur caudal to the

site of stenosis contributing to the frequently seen gait disturbance (Kalsi-Ryan, Karadimas, *et al.*, 2013).

Associations between clinical outcomes and cord pathology at the level of cord damage have been reported previously (Arvin *et al.*, 2013; Ellingson *et al.*, 2015; Nouri *et al.*, 2015). Here we show that the structural changes above the site of stenosis carried within specific tracts are related to measures of functional independence (i.e. SCIM) within the lateral CST and sensory deficits (i.e. UELT) within the PC. The latter finding is striking as it suggests that greater structural perturbations, most probably corresponding to a combination of pathologic processes, contribute to sensory impairment. In contrast, despite signs of marked structural integrity changes of the lateral CST, most patients had normal or only mild pyramidal impairment. In other words, good clinical scores but marked structural changes may portend risk for a progressive functional decline.

We note the following considerations and limitations of this study. Firstly, the average age difference between gender matched patients and healthy controls was 7.6 years though this difference was not statistically significant. In all models, we included age as a regressor of no interest to reduce effects of age on our results. Secondly, the segmentation of the cervical cord into gray matter and posterior columns was performed manually, but the inter-, and intra-rater coefficients of variation for the cervical cord were similar to those published (Yiannakas *et al.*, 2012). Finally, VBM-style analysis of spinal cord DTI is in its infancy (Naismith *et al.*, 2013; Fonov *et al.*, 2014; Toosy *et al.*, 2014) and as with the early days of exploring brain DTI, there are limitations associated with this method. For example, spatial mis-registration can lead to false positive or false negative results and thus reduce the reliability of this emerging post-processing method for spinal cord DTI (Mohammadi *et al.*, 2012). To reduce these, we performed an additional registration step to reduce residual mis-registrations that were not sufficiently removed by our proposed automated processing method. In future work advanced spatial normalization methods such as Dartel (Ashburner, 2007) could, if adopted to the spinal cord, help to improve registration quality and thus further advance VBM-style of analysis of DTI in the spinal cord.

Another important issue of spinal cord DTI is the fact that instrumental and physiological noise artefacts are larger in the spinal cord than in the brain. This can reduce the reproducibility of

spinal cord DTI metrics. To minimize artefacts, we applied sophisticated imaging and preprocessing methods. In particular, we reduced fold-over artefacts due to incomplete outer-volume suppression using 50% phase oversampling and by adjusting the amplitude of the saturation pulse manually for each subject. To minimize physiological noise artefacts, all patients were equipped with a stiff neck to reduce motion in the z-direction during scanning (Yiannakas *et al.*, 2012). Further, we used a pulse-triggered sequence and optimized pre-processing techniques (Mohammadi, Hutton, *et al.*, 2013) to mitigate the adverse effect of subject motion and other physiology-related artefacts (e.g. heart-beat or breathing). To assess the amount of variability due to residual artefacts, we tested the scan-rescan reliability of our data using a jackknife analysis as described in Mohammadi et al. (2013) (Mohammadi, Freund, *et al.*, 2013)(data analyses not shown). We found that the intra-subject variability (averaged across subjects) was about Δ-FA = 0.02, which is 3% when compared to the reported averaged FA values in the spinal cord (0.02/0.66*100 = 3%). This is smaller than the reported inter-subject variability of Δ-FA = 0.05 (reported in the Results section), which corresponds to 8% variability (0.05/0.66*100% = 8%). Thus, we expect that the scan-rescan variability will not strongly alter the reported effects observed between controls and patients. However, we cannot exclude that the reported high inter-subject variability might be due to the fact that data quality varies between subjects, e.g. variation in motion artefacts between subjects.

To further improve the reproducibility of spinal cord DTI, optimizations at the level of the sequence (e.g. navigators that help discarding poor-quality scans as used in segmented EPI (Porter and Heidemann, 2009) and post-processing techniques (e.g. denoising) as used in brain DTI (Tabelow *et al.*, 2015) should be considered.

Conclusion

Atrophy and tract-specific degeneration of the cervical cord can be detected by means of high-resolution MRI and expands far beyond focal cord damage as assessed by conventional MRI (e.g. MCC, MSCC, and signal change ratio). Importantly, these remote tract-specific changes are related to the clinical presentation and may be applicable as surrogate markers to assess treatment effects (in surgical and drug based interventions) complimentary to clinical outcome measures. Thus, MRI findings above and potentially below the site of stenosis could disclose subclinical sensory and motor impairments of upper and lower limb impairment and

complement the routine clinical and electrophysiological assessment (Ulrich *et al.*, 2013) in individuals with CSM.

Acknowledgments

We would like to thank all participants for spending their valuable time, the staff of the Department of Radiology and Neurology at the University Hospital Balgrist, Janosch Rienert for analysis of conventional MRI measures, and all other colleagues involved in this study.

Funding

This study was funded by the Clinical Research Priority Program "NeuroRehab" of the University of Zurich and the International Foundation for Research in Paraplegia. The Wellcome Trust Centre for Neuroimaging is supported by core funding from the Wellcome Trust 091593/Z/10/Z.

Author contributions

The study was designed by SM, RS, NW, AJT, AC, and PF. The data were acquired by PG, AT, SF, RS, AC, and PF. The analysis was performed by PG, SM, GD, NW, and PF. PG, SM, NW, AJT, AC, and PF wrote the manuscript. All authors reviewed the paper. PF had full access to all the data in the study and takes responsibility for the integrity of the data and the accuracy of the data analysis.

Competing financial interests

Yes, there is potential competing financial interest. PG, SM, AT, SF, GD, RS, AC, and PF report no competing financial interests. Prof. Nikolaus Weiskopf reports that the Wellcome Trust Centre for Neuroimaging has an institutional research agreement with and receives support from Siemens Healthcare. Prof. Alan J. Thompson has received honoraria and support for travel for consultancy from Biogen Idec, MedDay, Eisai, and Novartis, and for teaching from Teva, Novartis, and EXCEMED. He receives an honorarium as editor-in-chief of Multiple Sclerosis Journal.

Chapter 6:

General discussion

The objective of this thesis was to assess the temporal pattern and spatial extent of above lesion neurodegeneration in the spinal cord **(chapter 2 & 5)**, the brainstem **(chapter 3)**, and brain **(chapter 2)** in spinal cord disorders. A further goal was to investigate the effects of virtual reality-augmented lower limb neurorehabilitation on the central nervous system (i.e. plasticity) next to functional improvements **(chapter 4)**.

Progressive diaschisis in spinal cord disorders

Concept of diaschisis

We were able to demonstrate progressive diaschisis far above the level of injury that was evident in the spinal cord, the brainstem, and the brain **(chapter 2, 3, 4, & 5)**. The term 'diaschisis' was introduced by Constantin von Monakow in 1914 and is defined as remote neurophysiological alterations that are caused by focal lesions (Carrera and Tononi, 2014). This concept was developed and used to describe symptoms that could not be fully explained by the focal lesion, but also served as an explanation for functional recovery. In spinal cord disorders, this concept enables us to better understand the disease and to find explanations for the clinical representation that may not be obviously linked to the lesion itself. Thus, it may help us to gain insights into the remote disease mechanisms (Felix *et al.*, 2012; Freund *et al.*, 2013), the evolvement of long-term consequences such as neuropathic pain (Siddall and Loeser, 2001; Siddall *et al.*, 2003; Wrigley, Press, *et al.*, 2009; Gustin *et al.*, 2010, 2012, 2014; Mole *et al.*, 2014; Jutzeler *et al.*, 2015, 2016), the effects of neurorehabilitation (Colombo *et al.*, 2001b; Villiger *et al.*, 2015), and help us to improve clinical trial designs (e.g. anti-Nogo-A) (Steeves *et al.*, 2007; Tanadini *et al.*, 2015). State-of-the-art computational neuroanatomy offers the great opportunity to investigate these dynamic effects of injury in-vivo along the whole neuroaxis (Weiskopf *et al.*, 2015).

Diaschisis in traumatic spinal cord injury

In acute traumatic SCI, the sensory system showed progressive decline in volume and reduced myelin content one year after injury (**chapter 2**). The dynamic and spatial extent of neurodegeneration in the sensory system resembles those observed in the motor system (Freund *et al.*, 2013). Both motor and sensory systems are thus susceptible to atrophy remote to the lesion due to retro- and anterograde degeneration. Atrophy is accompanied by reduction in myelin content and thus related to changes in the underlying myeloarchitecture.

In chronic SCI, enduring trauma-induced neurodegenerative processes were observed in the brainstem **(chapter 3 & 4)** and brain **(chapter 4)**. These macroscopic and ultra-structural changes were revealed in major brainstem pathways and nuclei across the brainstem, and within the cerebellum and primary motor cortex. Interestingly, myelin loss was found in parallel to measures of atrophy and beyond and therefore indicating the greater sensitivity of quantitative MRI readouts. Moreover, the extent of neurodegeneration was related to neurological and functional impairment and thus may complement clinical assessments. Sensory and motor impairment as measured by the International Standards for Neurological Classification of Spinal Cord Injury depends on the level and extent of the spinal lesion. The magnitude of degeneration and reorganization therefore is expected to be multidimensional and influenced by the lesion level and severity, both defining the clinical impairment, and time since injury (Fehlings and Tator, 1995; Cohen-Adad *et al.*, 2011; Freund *et al.*, 2011, 2013; Lundell *et al.*, 2011; Yang *et al.*, 2014; Grabher *et al.*, 2015; Jutzeler *et al.*, 2016).

Diaschisis in cervical spondylotic myelopathy

In cervical spondylotic myelopathy, above-stenosis degeneration in the spinal cord was evident by measures of morphology and microstructure **(chapter 5)**. This is of great interest, as our findings demonstrate that CSM is not solely a focal spinal cord disorder, but also causes remote degenerative effects. Gray matter and white matter atrophy above the level of stenosis was paralleled by tract-specific microstructural changes. This is the result of different pathophysiological mechanisms including remodeling of microvasculature and dysfunction of blood spinal cord barrier (Karadimas *et al.*, 2013), disturbance in blood distribution (Kurokawa *et al.*, 2011; Karadimas *et al.*, 2015), and inflammation (Yu *et al.*, 2011; Karadimas *et al.*, 2013) which are triggered by the chronic and progressive cord compression and the dynamic stress caused by repetitive spinal cord movement (Fehlings and Skaf, 1998; Kalsi-Ryan, Karadimas, *et al.*, 2013; Toledano and Bartleson, 2013). It is likely that remodeling of microvasculature, ischemia, and inflammation, all spread over larger areas, cause impairment in remote spinal segments. Advanced imaging technology offers now the possibility to reveal above-stenosis neuronal degeneration remote to the compression site in CSM (Grabher *et al.*, 2016). In our study, the integrity of the corticospinal tracts and posterior columns was reduced. Furthermore, the magnitude of spinal cord degeneration was related to impairment of sensory and motor function. Crucially, signs of structural dysfunction within the CST were

prominent in our patient cohort that showed only mild or no symptoms of motor impairment, thus these structural changes suggest a risk for future functional decline and may serve as sensitive marker for disease progression.

Analogy of both spinal cord disorders

Clinical representation of CSM can resemble those of traumatic SCI (Moore and Blumhardt, 1997) with signs and symptoms of motor dysfunction with tetraparesis, sensory impairment, and autonomic dysfunction. Thus, the Graded Redefined Assessment of Strength, Sensibility and Prehension (i.e. GRASSP) tool, developed to profile arm and hand function in tetraplegia (Kalsi-Ryan *et al.*, 2012, 2014), was suggested to complement clinical assessments in CSM (Kalsi-Ryan, Singh, *et al.*, 2013). Cervical spondylotic myelopathy is also a risk factor for development of a traumatic central cord syndrome, a common form of cervical SCI (van Middendorp *et al.*, 2010). The underlying pathophysiological mechanisms behind the clinical representation in both disorders include mechanical stress, ischemia, inflammation, and cell death and thus show some overlap; nevertheless the main discrepancy entails disease causation, onset and progression (Fehlings and Skaf, 1998; Kwon, 2004). Traumatic SCI is caused by an immediate damage to the spinal cord neuronal and nonneuronal tissue by disruption of nerve fiber tracts, hemorrhage, and necrosis, causing the primary lesion. These mechanisms of direct and immediate damage are absent in CSM, except in those patients which develop a traumatic central cord syndrome at the level of stenosis (van Middendorp *et al.*, 2010).

In our study cohort, most patients suffered from mild (n=10) and moderate (n=9) CSM, whereas only one patient showed a severe clinical representation. The patients suffered mainly from sensory impairment and pain. Interestingly, the magnitude of neurodegeneration above the stenosis at the vertebral level C2/C3 as revealed by macroscopic and microstructural MRI readouts resembled those seen in traumatic SCI. In our cohort of patients with CSM, cervical cord area was reduced by 12.8%. We unraveled the more specific patterns of atrophy in cervical cord segments by measuring atrophy within the GM (7.2%) and WM (13.9%). The greatest atrophy was observed within the posterior column (16.1%); the magnitude relating to more sensory impairment. Macroscopic decline went in parallel with changes in microstructure as revealed by reduced FA in the posterior columns (12%) and

corticospinal tracts (13%). In acute traumatic SCI, cord atrophy of around 6% was observed within the first year after injury (Freund *et al.*, 2013). This structural decline is levelling off over time (Freund *et al.*, 2015) and reveals cord atrophy of up to 30% in chronic SCI (>10 post-injury) (Freund *et al.*, 2011; Lundell *et al.*, 2011; Jutzeler *et al.*, 2016). However, the extent of GM and WM atrophy within the cervical cord in acute and chronic traumatic SCI remains unknown. At the ultra-structural level, we could show alterations in the cervical cord by reductions in myelin-sensitive MT (15%) and R1 (12%) one year after injury (Grabher *et al.*, 2015). Cohen-Adad and colleagues (2011) did show changes in microstructure in cervical cord WM in chronic SCI by reductions of around 16% in FA and changes in the ultra-structure by reductions in MTR of around 19%. In summary, there is converging evidence that both CSM and SCI show a similar extent of pathological changes above the site of lesion despite their etiological differences.

Despite the different etiologies of both disorders, the (late) clinical and remote macroscopic and microstructural consequences are comparable. The similarities in structural changes above the level of lesion site illustrate diaschisis of both spinal cord disorders and the vulnerability of the central nervous system. It is promising and needs to be emphasized that synergies can be generated by translation and knowledge transfer of neuroimaging protocols and methods that may provide sensitive biomarkers for diagnostic purposes or surrogate markers for treatment response, as well as available (e.g. riluzole) or future treatment possibilities. In a next step, these exciting possibilities will be elaborated in a multi-center study (INSPIRED trial, in preparation) using the same qMRI protocol and including patients with SCI and CSM.

Reorganization and recovery

Most clinical recovery occurs within the first year after traumatic SCI and can be enhanced by intensive neurorehabilitation (Curt *et al.*, 2008). Rehabilitation may induce activity-dependent plasticity and promote cortical (Ghosh *et al.*, 2010; Rosenzweig *et al.*, 2010) and spinal reorganization (Bareyre *et al.*, 2004; Courtine *et al.*, 2008) as delineated by experimental animal models. Activity-based plasticity during neurorehabilitation can be boosted by VR-augmented training that is a powerful tool by providing high amount of repetitions, immediate feedback of performance, and maintain high motivation to endure training (Holden, 2005). We provide evidence that volumetric brain changes relate to training-induced improvements in motor function after intensive VR-augmented lower limb training in chronic iSCI patients **(chapter 4)**. Improvements during intensive neurorehabilitation are reflected by volumetric changes in the brain (i.e. plasticity), thus revealing that the training protocol was engaging the central nervous system and that improvements in motor function were not only the results of improving muscle function and coordination, but also of structural brain plasticity (i.e. reorganization). In summary, we conclude that performance improvement-related plasticity can be induced in the brain next to areas of atrophy and thus either revealing mechanisms of recovery from neurodegeneration or plasticity in the healthy neuronal networks. Interestingly, a recent study could demonstrate partial neurological recovery in chronic motor complete patients after intensive virtual-reality training protocols using brain-machine interfaces (Donati *et al.*, 2016). Donati and colleagues (2016) hypothesized that the observed recovery is a direct results of both spinal and supraspinal plasticity. So far, this promising phenomenon was investigated in healthy subjects (Draganski *et al.*, 2004; Boyke *et al.*, 2008; Taubert *et al.*, 2010), but only in few neurological disorders (Burciu *et al.*, 2013; Sehm *et al.*, 2014). However, the underlying cellular mechanisms of training-induced macrostructural alterations, which are revealed by MRI, are not well established. Candidate mechanism include axonal sprouting, changes in axonal diameter and density, dendritic branching, synaptogenesis, changes in number and size of glial cells, myelin formation, angiogenesis, and neurogenesis (Zatorre *et al.*, 2012). While macrostructural changes are rather unspecific, a future challenge is to determine to the underlying cellular mechanisms (Draganski and May, 2008; Zatorre *et al.*, 2012). This problem will be approached by further development of hMRI (Weiskopf *et al.*, 2015) and by the application of these quantitative MRI readouts that are closer related to histology in large and well-designed training studies (see *Future directions*).

Are neuroimaging biomarkers changing clinical trials in spinal cord disorders?

In the last decade, MRI-based neuroanatomical measures of atrophy (Draganski *et al.*, 2006; Jurkiewicz *et al.*, 2006) and plasticity (Maguire *et al.*, 2000; Gaser and Schlaug, 2003a; Draganski *et al.*, 2004) investigated volumetric changes within the central nervous system that are rather insensitive and unspecific to the underlying cellular mechanisms (Draganski and May, 2008). Recent advances in quantitative MRI and biophysical modelling facilitate the transition from purely structural to more meaningful measures of underlying cellular mechanisms of neurodegeneration and -plasticity (Weiskopf *et al.*, 2015).

Advanced neuroimaging has therefore the potential to expand our knowledge in understanding neurological disorders and to improve translation from bench to bedside (Filli and Schwab, 2015). Integrative frameworks (i.e. embodied neurology) are possible avenues that aim to better understand neurologic disorders and to minimize impairment and maximize outcome in patients as proposed by Freund and colleagues (Freund *et al.*, 2016). The three pillars in this framework include preclinical research, quantitative readouts with an emphasis on neuroimaging, and biophysical models. Nevertheless, quantitative readouts are not exclusive to neuroimaging and may additionally include ancillary quantitative outcome measures such as electrophysiology (Ulrich *et al.*, 2013) and activity measurements (Popp *et al.*, 2016). The challenges of clinical translation from bench to bedside can further be addressed by application of advanced MRI technology that directs to improvements in preclinical research and patient stratification in clinical trial designs, and may serve as outcome measures that are sensitive to detect even subclinical changes.

In our studies, we used myelin- and iron-sensitive quantitative readouts to assess trauma-induced demyelination and iron accumulation (Rooney *et al.*, 2007; Langkammer *et al.*, 2010; Stüber *et al.*, 2014; Callaghan *et al.*, 2015; Harkins *et al.*, 2015). These quantitative readouts demonstrated myelin loss in areas of atrophy and beyond and are thus more sensitive to pathophysiological processes. Therefore, quantitative readouts of myelin and iron allow the investigation of the underlying ultra-structure and are more relevant to pathology than macroscopic measures of atrophy. They provide targetable biomarkers for clinical trials (e.g. anti-Nogo-A) (Steeves *et al.*, 2007) and enable to assess subclinical changes when used as surrogate markers of treatment effects (Katz, 2004). In addition, quantitative readouts may complement clinical assessments with potential for early outcome prediction and patient

stratification. The combination of both advanced imaging techniques and clinical assessments seem to be a very promising approach to overcome some of the obstacles in translational research. Furthermore, quantitative imaging biomarkers can be used for in-vivo measurement of myelin in preclinical research (Turati *et al.*, 2015) and thus enables more efficient study designs by in-vivo longitudinal assessments and by reducing the total number of animals.

In conclusion, the application of surrogate markers has high potentials and is encouraged by the FDA, but the pitfalls need also to be considered (Katz, 2004). Surrogate markers have the capability to enhance translation from preclinical to clinical research, improve clinical trials efficacy and thus offer the potential to facilitate development and approval of effective treatments, and to guide early decision making for interventional procedures.

Limitations and considerations

Specificity of computational neuroanatomy

Computational anatomy can be divided into computational morphometry that reveals volume changes (i.e. atrophy) and quantitative MRI that reveals changes in the underlying microstructure (i.e. axonal integrity, demyelination, iron accumulation). Nevertheless, all these markers measure indirect effects and are related to underlying tissue properties and microstructure, but are not specific to one component only. Computational morphometry is sensitive to disease-specific changes in the central nervous system and thus raises the opportunity to reveal remote structural alterations (like diaschisis). However, morphometric changes are not specific to one single biological process. Volumetric contraction (i.e. atrophy) in the central nervous system can be seen as the sum of different pathophysiological mechanisms including cell atrophy, neuronal and glial cell loss, and demyelination that may all contribute to some extent. The interpretation of these measures becomes even more complex during inflammation, as local swelling may interfere with measures of atrophy and conceal the effective extent of atrophy. Quantitative MRI techniques, sensitive to micro- and ultra-structure that parallel morphometric changes, help us to disentangle the underlying substrate of atrophy (e.g. axonal degeneration, demyelination, iron accumulation, and water deposition). Postmortem validation studies have shown the correspondence between magnetization transfer based measures and myelin content and axonal density (Mottershead *et al.*, 2003; Schmierer *et al.*, 2004; Turati *et al.*, 2015) and between iron content and R2* (Langkammer *et al.*, 2010; Stüber *et al.*, 2014). Multiple factors contribute to R1, including water and iron content, but the contribution from macromolecular content dominates (Rooney *et al.*, 2007; Stüber *et al.*, 2014; Callaghan *et al.*, 2015; Harkins *et al.*, 2015). DTI provides information about fiber orientation and tissue microstructure. FA is related to axonal count (Gouw *et al.*, 2008) and myelin content (Schmierer, Wheeler-Kingshott, *et al.*, 2007), whereas RD and AD are related to demyelination (Klawiter *et al.*, 2011) and axonal degeneration (Zhang *et al.*, 2009), respectively.

Variability of morphometric and microstructural readouts

Inter-subject variability is partly due to normal neuroanatomical differences between subjects and may be influenced by factors such as age, gender, and head size. Therefore, these nuisance variables may be taken into the statistical models (Barnes *et al.*, 2010). In addition,

many factors increase variability in patients that trigger disease-related pathophysiological processes (e.g. diaschisis). In spinal cord disorders, these factors may include lesion level, severity, and time since injury. The level and extent of injury determines the total amount of damaged nerve fibers and it was related to the cross-sectional cord area (Lundell *et al.*, 2011; Jutzeler *et al.*, 2016). However, the relationship was not found in the studies of this thesis and may be concealed by the relatively small sample size and the time needed for these effects to become prominent. It becomes even more challenging as these factors may not depend linearly on the observed diaschisis (e.g. neurodegeneration is levelling off). Nevertheless, clinical impairment that is related with lesion level and extent of damage is associated with measures of atrophy and myelin loss. Using longitudinal cohort studies that are more sensitive to detect small neuroanatomical changes compared to cross-sectional study designs (Ashburner and Ridgway, 2013) and larger sample size may elaborate the interaction of factors in greater detail. Intra-subject variability may be due to acquisition and measurement variability and can be evaluated by measures of repeatability (i.e. measurement within the exactly same set-up) and reproducibility (i.e. measurement in a real-world setting). These are important issues that need to be properly addressed to specify the robustness of the readout and assess the viability as quantitative imaging biomarker (Raunig *et al.*, 2015). Measures of robustness were not specifically addressed in this thesis due to clinical feasibility, but quantitative MRI protocols showed to be robust in terms of repeatability (Deoni *et al.*, 2008) and reproducibility (Weiskopf *et al.*, 2013).

Concluding remarks

Atrophy and micro- and ultra-structural decline expand to remote spinal and supraspinal levels far beyond local cord damage and can be detected by means of advanced high-resolution MRI. Crucially, these remote changes were related to clinical presentation and may thus be applicable as surrogate markers (1) to complement clinical assessments, (2) to assess subclinical treatment effects in clinical trials (e.g. drug treatment, surgery, rehabilitation) and to identify early treatment responses in clinics, and (3) to guide early interventional decision making (e.g. surgery in asymptomatic CSM). Therefore, quantitative imaging surrogate markers may complement clinical assessments and improve clinical trial efficiency.

In conclusion, multimodal imaging approaches will help us to better disentangle specific pathophysiological processes and increase the applicability, sensitivity, and specificity of MRI biomarkers. The information from multimodal imaging may be incorporated and used in integrative frameworks of structure and function that aim to better understand neurological disorders and to minimize the impairment and maximize the recovery in patients (Freund *et al.*, 2016).

Future directions

Towards in-vivo histology

Recent advances in imaging technology including g-ratio mapping (Mohammadi, Carey, *et al.*, 2015) and neurite orientation dispersion and density imaging (NODDI) (Zhang *et al.*, 2012) are pushing the field forward into the direction of in-vivo histology (Weiskopf *et al.*, 2015). They open the avenue for promising research, aiming to characterize disease-specific mechanisms at the micro- and ultra-structural level, and to develop sensitive quantitative neuroimaging biomarkers.

Integrative frameworks

The complex mechanisms of diaschisis may be further investigated in SCI using graph theory to assess structural and functional networks of motor and sensory systems. Graph theory offers the opportunity to study the spreading of structural and functional decline from the lesion site into more remote areas (Bullmore *et al.*, 2009). Incorporating multimodal information of supraspinal, spinal, and peripheral regions and including advanced functional and structural MRI, electrophysiology, activity measures, and clinical representation into integrative networks will boost our understanding of spinal cord disorders and improve the patient's outcome (Freund *et al.*, 2016). Thus, it allows us to get further insights into pathology, disentangle the order, extent, and temporal pattern of remote effects, and may reveal mechanisms causing clinical impairment that may not be explained by the lesion itself.

Longitudinal assessment of above-stenosis degeneration in CSM

The evolution of the spatial and temporal pattern of structural decline above the level of stenosis remains unknown in CSM. A prospective longitudinal study in asymptomatic and mild patients with cervical stenosis would provide more detailed insights into the pathology and evolution of macroscopic and microstructural decline. This would support the development of MRI-based surrogate markers and offer the opportunity to improve treatment guidelines and decision making for surgical interventions. In asymptomatic and mild CSM patients, surgical interventions are controversially discussed. There is a need to do surgery as early as possible when disease progression is expected to be severe, whereas conservative treatment is preferred when disease progression is expected to be low or non-existent.

Comprehensive training study

Our longitudinal pilot study of intensive lower limb training showed promising improvements in clinical and functional outcome that was related to brainstem and brain plasticity. This study revealed that the training paradigm was sufficient enough to engage the central nervous system and that gained improvements were not solely achieved due to compensatory strategies. These highly interesting and promising results were decisive to develop a comprehensive training study that aims to investigate training-induced neuroplasticity in SCI. Upper- and lower extremity training will be performed in SCI and healthy controls. The training paradigm (Figure 17) is intensive (four 30-minute sessions per week over one month) and ensures a high repetition rate of targeted movement patterns. To further increase training effects, the task is challenging (difficulty levels adapted to personal capabilities), provides on-line feedback on performance, and is rich in sensory stimuli (i.e. auditory, visual, haptic). Thus, the training ensures high engagement during all training session and fulfils the relevant key concepts of motor learning (i.e. repetition, feedback, motivation) (Holden, 2005). Advanced qMRI will assess neuroplasticity at the macroscopic and ultra-structural level and probe the relationship to training-induced performance improvements. Thus, some of the limitations from previous training studies (i.e. volumetric changes that are rather unspecific) (Maguire *et al.*, 2000; Gaser and Schlaug, 2003b; Draganski *et al.*, 2004; Sehm *et al.*, 2014) can be addressed.

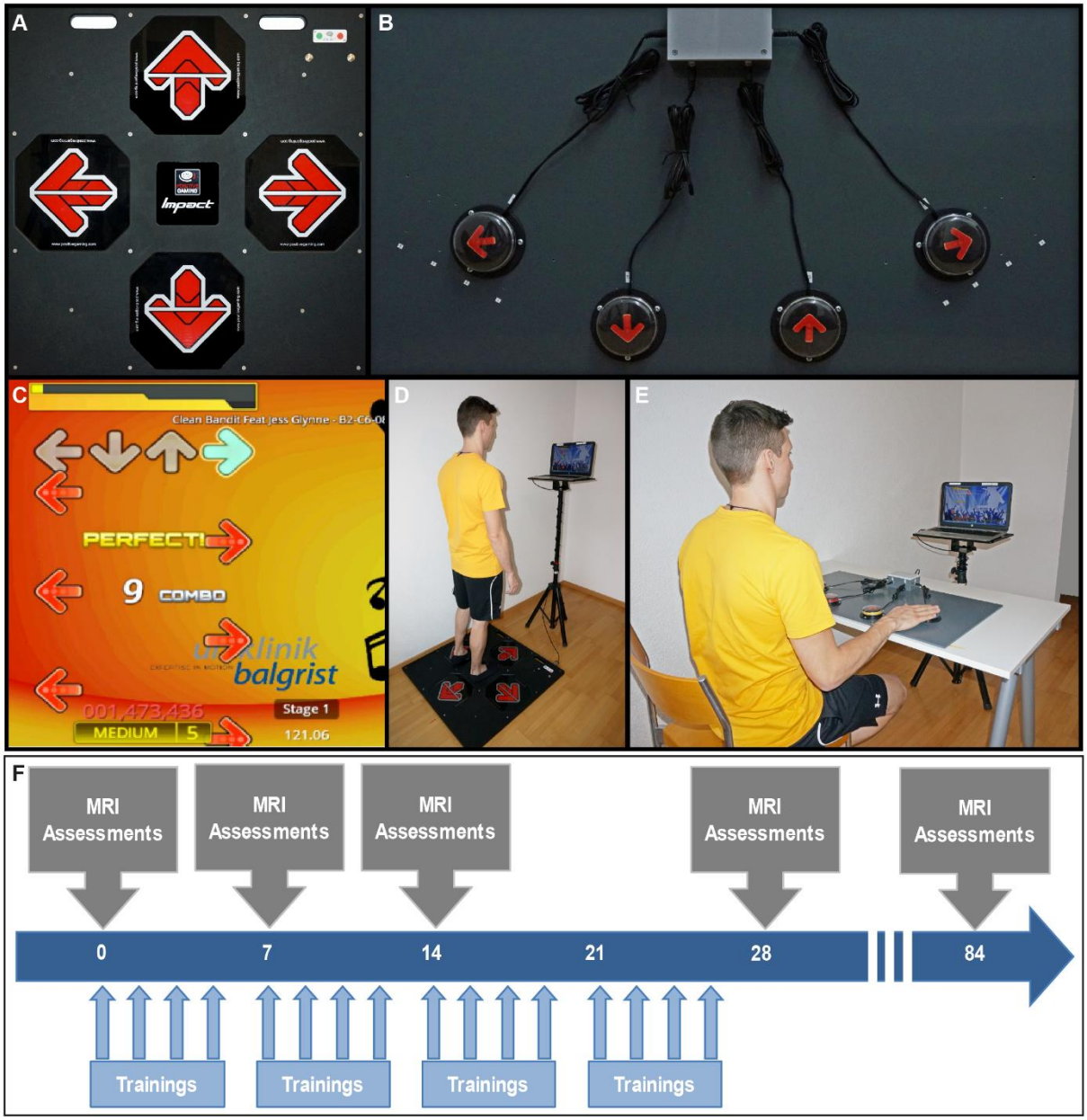

Figure 17: Comprehensive training study in patients with SCI and healthy controls. (A) Dance pad for lower extremities. (B) Customized input device for upper extremities. (C) Open-source dance game with auditory and visual stimuli and online feedback. (D) Lower limb training. (E) Upper limb training. (F) Training paradigm with 16 training sessions and 5 assessments and MRI scans.

References

Adamovich S V, Fluet GG, Tunik E, Merians AS. Sensorimotor training in virtual reality: a review. NeuroRehabilitation 2009; 25: 29–44.

Aguilar J, Humanes-Valera D, Alonso-Calviño E, Yague JG, Moxon K a, Oliviero A, et al. Spinal cord injury immediately changes the state of the brain. J. Neurosci. 2010; 30: 7528–37.

Albouy G, Sterpenich V, Balteau E, Vandewalle G, Desseilles M, Dang-Vu T, et al. Both the hippocampus and striatum are involved in consolidation of motor sequence memory. Neuron 2008; 58: 261–72.

Anderson K, Aito S, Atkins M, Biering-sørensen F, Charlifue S, Curt A, et al. Functional Recovery Measures for Spinal Cord Injury: An Evedence-Based Review for Clinical Practice and Research. J. Spinal Cord Med. 2008; 31: 133–144.

Anderson KD. Targeting Recovery: Priorities of the Spinal Cord-Injured Population. J. Neurotrauma 2004; 21: 1371–1383.

Angeli C a, Edgerton VR, Gerasimenko YP, Harkema SJ. Altering spinal cord excitability enables voluntary movements after chronic complete paralysis in humans. Brain 2014: 1394–1409.

Apps R, Garwicz M. Anatomical and physiological foundations of cerebellar information processing. Nat. Rev. Neurosci. 2005; 6: 297–311.

Arvin B, Kalsi-Ryan S, Karpova A, Mercier D, Furlan JC, Massicotte EM, et al. Postoperative magnetic resonance imaging can predict neurological recovery after surgery for cervical spondylotic myelopathy: A prospective study with blinded assessments. Neurosurgery 2011; 69: 362–368.

Arvin B, Kalsi-Ryan S, Mercier D, Furlan JC, Massicotte EM, Fehlings MG. Preoperative magnetic resonance imaging is associated with baseline neurological status and can predict postoperative recovery in patients with cervical spondylotic myelopathy. Spine (Phila. Pa. 1976). 2013; 38: 1170–1176.

Ashburner J. A fast diffeomorphic image registration algorithm. Neuroimage 2007; 38: 95–113.

Ashburner J, Friston KJ. Voxel-based morphometry--the methods. Neuroimage 2000; 11: 805–21.

Ashburner J, Friston KJ. Morphometry. In: Human Brain Function. Elsevier; 2004. p. 707–722.

Ashburner J, Friston KJ. Unified segmentation. Neuroimage 2005; 26: 839–51.

Ashburner J, Friston KJ. Diffeomorphic registration using geodesic shooting and Gauss-Newton optimisation. Neuroimage 2011; 55: 954–67.

Ashburner J, Ridgway GR. Symmetric diffeomorphic modeling of longitudinal structural MRI. Front. Neurosci. 2013; 6: 1–19.

Bareyre FM, Kerschensteiner M, Raineteau O, Mettenleiter TC, Weinmann O, Schwab ME. The injured spinal cord spontaneously forms a new intraspinal circuit in adult rats. Nat. Neurosci. 2004; 7: 269–77.

Barkhof F, Calabresi PA, Miller DH, Reingold SC. Imaging outcomes for neuroprotection and repair in multiple sclerosis trials. Nat. Rev. Neurol. 2009; 5: 256–266.

Barnes J, Ridgway GR, Bartlett J, Henley SMD, Lehmann M, Hobbs N, et al. Head size, age and gender adjustment in MRI studies: a necessary nuisance? Neuroimage 2010; 53: 1244–1255.

Basbaum a I, Fields HL. The origin of descending pathways in the dorsolateral funiculus of the spinal cord of the cat and rat: further studies on the anatomy of pain modulation. J. Comp. Neurol. 1979; 187: 513–31.

Beaud M, Schmidlin E, Wannier T, Freund P, Bloch J, Mir A, et al. Anti-Nogo-A antibody treatment does not prevent cell body shrinkage in the motor cortex in adult monkeys subjected to unilateral cervical cord lesion. BMC Neurosci. 2008; 9: 5.

Belhaj-saïf A, Cheney PD. Plasticity in the Distribution of the Red Nucleus Output to Forearm Muscles After Unilateral Lesions of the Pyramidal Tract. J. Neurophysiol. 2000; 83: 3147–3153.

Benarroch EE. Periaqueductal gray: An interface for behavioral control. Neurology 2012; 78: 210–217.

Benarroch EE. Pedunculopontine nucleus: functional organization and clinical implications. Neurology 2013; 80: 1148–55.

Benzel EC, Lancon J, Kesterson L, Hadden T. Cervical laminectomy and dentate ligament section for cervical spondylotic myelopathy. J. Spinal Disord. 1991; 4: 286–295.

Berg K, Wood-Dauphinee S, Williams JI. The Balance Scale: reliability assessment with elderly residents and patients with an acute stroke. Scand. J. Rehabil. Med. 1995; 27: 27–36.

Bohil CJ, Alicea B, Biocca FA. Virtual reality in neuroscience research and therapy. Nat. Rev. Neurosci. 2011; 12: 752–62.

Boyke J, Driemeyer J, Gaser C, Büchel C, May A. Training-induced brain structure changes in the elderly. J. Neurosci. 2008; 28: 7031–5.

Bradbury EJ, Moon LDF, Popat RJ, King VR, Bennett GS, Patel PN, et al. Chondroitinase ABC promotes functional recovery after spinal cord injury. Nature 2002; 416: 636–40.

Bryce TN, Biering-Sørensen F, Finnerup NB, Cardenas DD, Defrin R, Lundeberg T, et al. International spinal cord injury pain classification: part I. Background and description. March 6-7, 2009. Spinal Cord 2012; 50: 413–7.

Budde MD, Xie M, Cross AH, Song S-K. Axial diffusivity is the primary correlate of axonal injury

in the experimental autoimmune encephalomyelitis spinal cord: a quantitative pixelwise analysis. J. Neurosci. 2009; 29: 2805–2813.

Bullmore ET, Sporns O, Solla S a. Complex brain networks: graph theoretical analysis of structural and functional systems. Nat. Rev. Neurosci. 2009; 10: 186–98.

Burciu RG, Fritsche N, Granert O, Schmitz L, Sponemann N, Konczak J, et al. Brain Changes Associated with Postural Training in Patients with Cerebellar Degeneration: A Voxel-Based Morphometry Study. J. Neurosci. 2013; 33: 4594–4604.

Buss A, Brook G a, Kakulas B, Martin D, Franzen R, Schoenen J, et al. Gradual loss of myelin and formation of an astrocytic scar during Wallerian degeneration in the human spinal cord. Brain 2004; 127: 34–44.

Buss A, Pech K, Merkler D, Kakulas BA, Martin D, Schoenen J, et al. Sequential loss of myelin proteins during Wallerian degeneration in the human spinal cord. Brain 2005; 128: 356–364.

Buss A, Schwab M. Sequential loss of myelin proteins during Wallerian degeneration in the rat spinal cord. Glia 2003; 42: 424–32.

Cadotte DW, Bosma R, Mikulis D, Nugaeva N, Smith K, Pokrupa R, et al. Plasticity of the injured human spinal cord: insights revealed by spinal cord functional MRI. PLoS One 2012; 7: e45560.

Cadotte DW, Fehlings MG. Will imaging biomarkers transform spinal cord injury trials? Lancet. Neurol. 2013; 12: 843–4.

Callaghan MF, Freund P, Draganski B, Anderson E, Cappelletti M, Chowdhury R, et al. Widespread age-related differences in the human brain microstructure revealed by quantitative magnetic resonance imaging. Neurobiol. Aging 2014; 35: 1862–72.

Callaghan MF, Helms G, Lutti A, Mohammadi S, Weiskopf N. A general linear relaxometry model of R 1 using imaging data. Magn. Reson. Med. 2015; 73: 1309–1314.

Carrera E, Tononi G. Diaschisis: past, present, future. Brain 2014; 137: 2408–22.

Carter LM, McMahon SB, Bradbury EJ. Delayed treatment with Chondroitinase ABC reverses chronic atrophy of rubrospinal neurons following spinal cord injury. Exp. Neurol. 2011; 228: 149–156.

Casha S, Zygun D, McGowan MD, Bains I, Yong VW, Hurlbert RJ. Results of a phase II placebo-controlled randomized trial of minocycline in acute spinal cord injury. Brain 2012; 135: 1224–36.

Catz A, Itzkovich M, Tesio L, Biering-Sorensen F, Weeks C, Laramee MT, et al. A multicenter international study on the Spinal Cord Independence Measure, version III: Rasch psychometric validation. Spinal Cord 2007; 45: 275–91.

Cerminara NL, Koutsikou S, Lumb BM, Apps R. The periaqueductal grey modulates sensory input to the cerebellum: A role in coping behaviour? Eur. J. Neurosci. 2009; 29: 2197–2206.

Chen LM, Qi H-X, Kaas JH. Dynamic reorganization of digit representations in somatosensory cortex of nonhuman primates after spinal cord injury. J. Neurosci. 2012; 32: 14649–63.

Classen J, Liepert J, Wise SP, Hallett M, Cohen LG. Rapid plasticity of human cortical movement representation induced by practice. J. Neurophysiol. 1998; 79: 1117–1123.

Cohen-Adad J, De Leener B, Benhamou M, Lévy S, Touati J, Cadotte D, et al. Spinal Cord Toolbox: an open-source framework for processing spinal cord MRI data. In: Proceedings of the 20th Annual Meeting of OHBM, Hamburg, Germany,. 2014. p. 3633.

Cohen-Adad J, El Mendili M-M, Lehéricy S, Pradat P-F, Blancho S, Rossignol S, et al. Demyelination and degeneration in the injured human spinal cord detected with diffusion and magnetization transfer MRI. Neuroimage 2011; 55: 1024–1033.

Colombo G, Wirz M, Dietz V. Driven gait orthosis for improvement of locomotor training in paraplegic patients. Spinal Cord 2001a; 39: 252–5.

Colombo G, Wirz M, Dietz V. Driven gait orthosis for improvement of locomotor training in paraplegic patients. Spinal Cord 2001b; 39: 252–5.

Courtine G, Van Den Brand R, Musienko P. Spinal cord injury: Time to move. Lancet 2011; 377: 1896–1898.

Courtine G, Song B, Roy RR, Zhong H, Herrmann JE, Ao Y, et al. Recovery of supraspinal control of stepping via indirect propriospinal relay connections after spinal cord injury. Nat. Med. 2008; 14: 69–74.

Crowe MJ, Bresnahan JC, Shuman SL, Masters JN, Crowe MS. Apoptosis and delayed degeneration after spinal cord injury in rats and monkeys. Nat. Med. 1997; 3: 73–76.

Cui J-L, Li X, Chan T-Y, Mak K-C, Luk KD-K, Hu Y. Quantitative assessment of column-specific degeneration in cervical spondylotic myelopathy based on diffusion tensor tractography. Eur. Spine J. 2014; 24: 41–47.

Curt A. Human neural stem cells in chronic spinal cord injury. Expert Opin. Biol. Ther. 2012; 12: 271–3.

Curt A, Van Hedel HJA, Klaus D, Dietz V. Recovery from a spinal cord injury: significance of compensation, neural plasticity, and repair. J. Neurotrauma 2008; 25: 677–85.

Deliagina TG, Beloozerova IN, Zelenin P V., Orlovsky GN. Spinal and supraspinal postural networks. Brain Res. Rev. 2008; 57: 212–21.

Deoni SCL, Williams SCR, Jezzard P, Suckling J, Murphy DGM, Jones DK. Standardized structural magnetic resonance imaging in multicentre studies using quantitative T1 and T2 imaging at 1.5 T. Neuroimage 2008; 40: 662–71.

DeVivo MJ. Causes and costs of spinal cord injury in the United States. Spinal cord Off. J. Int. Med. Soc. Paraplegia 1997; 35: 809–813.

Diedrichsen J. A spatially unbiased atlas template of the human cerebellum. Neuroimage 2006; 33: 127–38.

Dietz V. Proprioception and locomotor disorders. Nat. Rev. Neurosci. 2002; 3: 781–790.

Dietz V, Curt A. Neurological aspects of spinal-cord repair: promises and challenges. Lancet. Neurol. 2006; 5: 688–94.

Dietz V, Fouad K. Restoration of sensorimotor functions after spinal cord injury. Brain 2014; 137: 654–667.

Donati ARC, Shokur S, Morya E, Campos DSF, Moioli RC, Gitti CM, et al. Long-Term Training with a Brain-Machine Interface-Based Gait Protocol Induces Partial Neurological Recovery in Paraplegic Patients. Sci. Rep. 2016; 6: 30383.

Draganski B, Ashburner J, Hutton C, Kherif F, Frackowiak RSJ, Helms G, et al. Regional specificity of MRI contrast parameter changes in normal ageing revealed by voxel-based quantification (VBQ). Neuroimage 2011; 55: 1423–34.

Draganski B, Gaser C, Busch V, Schuierer G, Bogdahn U, May A. Neuroplasticity: changes in grey matter induced by training. Nature 2004; 427: 311–2.

Draganski B, May a. Training-induced structural changes in the adult human brain. Behav. Brain Res. 2008; 192: 137–42.

Draganski B, Moser T, Lummel N, Gänssbauer S, Bogdahn U, Haas F, et al. Decrease of thalamic gray matter following limb amputation. Neuroimage 2006; 31: 951–7.

Driemeyer J, Boyke J, Gaser C, Büchel C, May A. Changes in gray matter induced by learning--revisited. PLoS One 2008; 3: e2669.

Eickhoff SB, Stephan KE, Mohlberg H, Grefkes C, Fink GR, Amunts K, et al. A new SPM toolbox for combining probabilistic cytoarchitectonic maps and functional imaging data. Neuroimage 2005; 25: 1325–35.

Eippert F, Bingel U, Schoell ED, Yacubian J, Klinger R, Lorenz J, et al. Activation of the opioidergic descending pain control system underlies placebo analgesia. Neuron 2009; 63: 533–43.

Eklund A, Nichols TE, Knutsson H. Cluster failure: Why fMRI inferences for spatial extent have inflated false-positive rates. Proc. Natl. Acad. Sci. 2016; 113: 7900–7905.

Ellaway PH, Kuppuswamy A, Balasubramaniam a V, Maksimovic R, Gall A, Craggs MD, et al. Development of quantitative and sensitive assessments of physiological and functional outcome during recovery from spinal cord injury: a clinical initiative. Brain Res. Bull. 2011; 84: 343–57.

Ellingson BM, Kurpad SN, Li S-J, Schmit BD. In vivo diffusion tensor imaging of the rat spinal cord at 9.4T. J. Magn. Reson. Imaging 2008; 27: 634–642.

Ellingson BM, Salamon N, Grinstead JW, Holly LT. Diffusion tensor imaging predicts functional impairment in mild-to-moderate cervical spondylotic myelopathy. Spine J. 2014; 14: 2589–97.

Ellingson BM, Salamon N, Woodworth DC, Holly LT. Correlation between degree of subvoxel spinal cord compression measured with super-resolution tract density imaging and neurological impairment in cervical spondylotic myelopathy. J. Neurosurg. Spine 2015; 22: 631–638.

Faden AI, Wu J, Stoica B a., Loane DJ. Progressive inflammatory-mediated neurodegeneration after traumatic brain or spinal cord injury. Br. J. Pharmacol. 2015; 13601: n/a-n/a.

Fawcett JW, Curt A, Steeves JD, Coleman WP, Tuszynski MH, Lammertse D, et al. Guidelines for the conduct of clinical trials for spinal cord injury as developed by the ICCP panel: spontaneous recovery after spinal cord injury and statistical power needed for therapeutic clinical trials. Spinal Cord 2007; 45: 190–205.

Fehlings MG, Kopjar B, Grossman RG. 329 Efficacy and Safety of Riluzole in Acute Spinal Cord Injury: Rationale and Design of AOSpine Phase III Multicenter Double-Blinded Randomized Controlled Trial (RISCIS). Neurosurgery 2016; 63 Suppl 1: 196.

Fehlings MG, Rao SC, Tator CH, Skaf G, Arnold P, Benzel E, et al. The optimal radiologic method for assessing spinal canal compromise and cord compression in patients with cervical spinal cord injury. Part II: Results of a multicenter study. Spine (Phila. Pa. 1976). 1999; 24: 605–613.

Fehlings MG, Skaf G. A review of the pathophysiology of cervical spondylotic myelopathy with insights for potential novel mechanisms drawn from traumatic spinal cord injury. Spine (Phila. Pa. 1976). 1998; 23: 2730–2737.

Fehlings MG, Tator CH. The relationships among the severity of spinal cord injury, residual neurological function, axon counts, and counts of retrogradely labeled neurons after experimental spinal cord injury. Exp. Neurol. 1995; 132: 220–228.

Fehlings MG, Wilson JR, Karadimas SK, Arnold PM, Kopjar B. Clinical Evaluation of a Neuroprotective Drug in Patients With Cervical Spondylotic Myelopathy Undergoing Surgical Treatment. Spine (Phila. Pa. 1976). 2013; 38: S68–S75.

Fehlings MG, Wilson JR, Kopjar B, Yoon ST, Arnold PM, Massicotte EM, et al. Efficacy and Safety of Surgical Decompression in Patients with Cervical Spondylotic Myelopathy. J. Bone Jt. Surg. 2013; 95: 1651–1658.

Felix M-S, Popa N, Djelloul M, Boucraut J, Gauthier P, Bauer S, et al. Alteration of forebrain neurogenesis after cervical spinal cord injury in the adult rat. Front. Neurosci. 2012; 6: 45.

Filli L, Schwab ME. Structural and functional reorganization of propriospinal connections promotes functional recovery after spinal cord injury. Neural Regen. Res. 2015; 10: 509–13.

Finger S, Koehler PJ, Jagella C. The Monakow Concept of Diaschisis: Origins and Perspectives. Arch. Neurol. 2004; 61: 283–288.

Fonov VS, Le Troter A, Taso M, De Leener B, Lévêque G, Benhamou M, et al. Framework for

integrated MRI average of the spinal cord white and gray matter: The MNI-Poly-AMU template. Neuroimage 2014; 102 Pt 2: 817–827.

Freund P, Friston K, Thompson AJ, Stephan KE, Ashburner J, Bach DR, et al. Embodied neurology : an integrative framework for neurological disorders. Brain 2016: 1–7.

Freund P, Grabher P, Hupp M, J A, Friston K, Weiskopf N, et al. Progressive atrophy, prediction and potential endpoints for trials in acute spinal cord injury. Organ. Hum. Brain Mapp. Conf. 2015

Freund P, Schneider T, Nagy Z, Hutton C, Weiskopf N, Friston K, et al. Degeneration of the injured cervical cord is associated with remote changes in corticospinal tract integrity and upper limb impairment. PLoS One 2012; 7: e51729.

Freund P, Wannier T, Schmidlin E, Bloch J, Mir A, Schwab ME, et al. Anti-Nogo-A antibody treatment enhances sprouting of corticospinal axons rostral to a unilateral cervical spinal cord lesion in adult macaque monkey. J. Comp. Neurol. 2007; 502: 644–59.

Freund P, Weiskopf N, Ashburner J, Wolf K, Sutter R, Altmann DR, et al. MRI investigation of the sensorimotor cortex and the corticospinal tract after acute spinal cord injury: a prospective longitudinal study. Lancet Neurol. 2013; 12: 873–881.

Freund P, Weiskopf N, Ward NS, Hutton C, Gall A, Ciccarelli O, et al. Disability, atrophy and cortical reorganization following spinal cord injury. Brain 2011; 134: 1610–1622.

Freund P, Wheeler-Kingshott C, Nagy Z, Gorgoraptis N, Weiskopf N, Friston K, et al. Axonal integrity predicts cortical reorganisation following cervical injury. J. Neurol. Neurosurg. Psychiatry 2012; 83: 629–637.

Frisoni GB, Fox NC, Jack CR, Scheltens P, Thompson PM. The clinical use of structural MRI in Alzheimer disease. Nat. Rev. Neurol. 2010; 6: 67–77.

Friston KJ, Worsley KJ, Frackowiak RS, Mazziotta JC, Evans a C. Assessing the significance of focal activations using their spatial extent. Hum. Brain Mapp. 1994; 1: 210–20.

Furlan JC, Bracken MB, Fehlings MG. Is age a key determinant of mortality and neurological outcome after acute traumatic spinal cord injury? Neurobiol. Aging 2010; 31: 434–46.

Furlan JC, Noonan V, Singh A, Fehlings MG. Assessment of impairment in patients with acute traumatic spinal cord injury: a systematic review of the literature. J. Neurotrauma 2011; 28: 1445–77.

Garcia-Larrea L, Peyron R. Pain matrices and neuropathic pain matrices : A review. Pain 2013; 154: S29–S43.

Gaser C, Schlaug G. Brain structures differ between musicians and non-musicians. J. Neurosci. 2003a; 23: 9240–5.

Gaser C, Schlaug G. Gray Matter Differences between Musicians and Nonmusicians. Ann. N. Y. Acad. Sci. 2003b; 999: 514–517.

George R, Griffin JW. Delayed macrophage responses and myelin clearance during Wallerian degeneration in the central nervous system: the dorsal radiculotomy model. Exp. Neurol. 1994; 129: 225–36.

Ghosh A, Haiss F, Sydekum E, Schneider R, Gullo M, Wyss MT, et al. Rewiring of hindlimb corticospinal neurons after spinal cord injury. Nat. Neurosci. 2010; 13: 97–104.

Ghosh A, Peduzzi S, Snyder M, Schneider R, Starkey M, Schwab ME. Heterogeneous spine loss in layer 5 cortical neurons after spinal cord injury. Cereb. Cortex 2012; 22: 1309–17.

Ghosh A, Sydekum E, Haiss F, Peduzzi S, Zörner B, Schneider R, et al. Functional and anatomical reorganization of the sensory-motor cortex after incomplete spinal cord injury in adult rats. J. Neurosci. 2009; 29: 12210–9.

Gouw AA, Seewann A, Vrenken H, van der Flier WM, Rozemuller JM, Barkhof F, et al. Heterogeneity of white matter hyperintensities in Alzheimer's disease: post-mortem quantitative MRI and neuropathology. Brain 2008; 131: 3286–3298.

Grabher P, Callaghan MF, Ashburner J, Weiskopf N, Thompson AJ, Curt A, et al. Tracking sensory system atrophy and outcome prediction in spinal cord injury. Ann. Neurol. 2015; 78: 751–761.

Grabher P, Mohammadi S, Trachsler A, Friedl S, David G, Sutter R, et al. Voxel-based analysis of grey and white matter degeneration in cervical spondylotic myelopathy. Sci. Rep. 2016; 6: 24636.

Guest JD, Hiester ED, Bunge RP. Demyelination and Schwann cell responses adjacent to injury epicenter cavities following chronic human spinal cord injury. Exp. Neurol. 2005; 192: 384–93.

Gustin S, Wrigley P, Siddall P, Henderson L. Brain anatomy changes associated with persistent neuropathic pain following spinal cord injury. Cereb. Cortex 2010; 20: 1409–19.

Gustin SM, Peck CC, Cheney LB, Macey PM, Murray GM, Henderson L a. Pain and plasticity: is chronic pain always associated with somatosensory cortex activity and reorganization? J. Neurosci. 2012; 32: 14874–84.

Gustin SM, Wrigley PJ, Youssef a M, McIndoe L, Wilcox SL, Rae CD, et al. Thalamic activity and biochemical changes in individuals with neuropathic pain after spinal cord injury. Pain 2014; 155: 1027–36.

Haefeli J, Kramer JLK, Blum J, Curt A. Assessment of Spinothalamic Tract Function Beyond Pinprick in Spinal Cord Lesions: A Contact Heat Evoked Potential Study. Neurorehabil. Neural Repair 2013; 28: 494–503.

Hains BC, Black J a, Waxman SG. Primary cortical motor neurons undergo apoptosis after axotomizing spinal cord injury. J. Comp. Neurol. 2003; 462: 328–341.

Hametner S, Wimmer I, Haider L, Pfeifenbring S, Brück W, Lassmann H. Iron and neurodegeneration in the multiple sclerosis brain. Ann. Neurol. 2013; 74: 848–861.

Harkins KD, Xu J, Dula AN, Li K, Valentine WM, Gochberg DF, et al. The microstructural correlates of t 1 in white matter. Magn. Reson. Med. 2015; 0: n/a-n/a.

Hassanpour K, Hotz-Boendermaker S, Dokladal P, European Multicenter Study for Human Spinal Cord Injury Study group, Curt A. Low depressive symptoms in acute spinal cord injury compared to other neurological disorders. J. Neurol. 2012; 259: 1142–50.

Hasselblad V. Estimation of Parameters for a Mixture of Normal Distributions. Technometrics 1966; 8: 431–444.

van Hedel HJ, Wirz M, Curt A. Improving walking assessment in subjects with an incomplete spinal cord injury: responsiveness. Spinal Cord 2006; 44: 352–6.

van Hedel HJ, Wirz M, Dietz V. Assessing walking ability in subjects with spinal cord injury: validity and reliability of 3 walking tests. Arch. Phys. Med. Rehabil. 2005; 86: 190–6.

Heidemann RM, Feiweier T, Anwander A, Fasano F, Pfeuffer J, Turner R. High resolution single-shot diffusion-weighted imaging with a combination of zoomed EPI and parallel imaging. In: Proceedings of the 17th Annual Meeting of ISMRM, Honolulu, USA,. 2009. p. 2736.

Helms G, Dathe H, Kallenberg K, Dechent P. High-resolution maps of magnetization transfer with inherent correction for RF inhomogeneity and T1 relaxation obtained from 3D FLASH MRI. Magn. Reson. Med. 2008; 60: 1396–407.

Helms G, Draganski B, Frackowiak R, Ashburner J, Weiskopf N. Improved segmentation of deep brain grey matter structures using magnetization transfer (MT) parameter maps. Neuroimage 2009; 47: 194–8.

Hicks TP, Onodera S. The mammalian red nucleus and its role in motor systems, including the emergence of bipedalism and language. Prog. Neurobiol. 2012; 96: 165–175.

Ho Y-C, Cheng J-K, Chiou L-C. Hypofunction of glutamatergic neurotransmission in the periaqueductal gray contributes to nerve-injury-induced neuropathic pain. J. Neurosci. 2013; 33: 7825–36.

Holden MK. Virtual Environments for Motor Rehabilitation: Review. CyberPsychology Behav. 2005; 8: 187–211.

Holly LT, Freitas B, McArthur DL, Salamon N. Proton magnetic resonance spectroscopy to evaluate spinal cord axonal injury in cervical spondylotic myelopathy. J. Neurosurg. Spine 2009; 10: 194–200.

Holly LT, Moftakhar P, Khoo LT, Shamie a. N, Wang JC. Surgical outcomes of elderly patients with cervical spondylotic myelopathy. Surg. Neurol. 2008; 69: 233–240.

Horsfield M a, Sala S, Neema M, Absinta M, Bakshi A, Sormani MP, et al. Rapid semi-automatic segmentation of the spinal cord from magnetic resonance images: application in multiple sclerosis. Neuroimage 2010; 50: 446–455.

Houk JC, Buckingham JT, Barto AG. Models of the cerebellum and motor learning. Behav. Brain

Sci. 1996; 19: 368–383.

Hua X, Hibar DP, Ching CRK, Boyle CP, Rajagopalan P, Gutman B a, et al. Unbiased tensor-based morphometry: improved robustness and sample size estimates for Alzheimer's disease clinical trials. Neuroimage 2013; 66: 648–61.

Huber E, Curt A, Freund P. Tracking trauma-induced structural and functional changes above the level of spinal cord injury. Curr. Opin. Neurol. 2015; 28: 365–72.

Hutton C, Draganski B, Ashburner J, Weiskopf N. A comparison between voxel-based cortical thickness and voxel-based morphometry in normal aging. Neuroimage 2009; 48: 371–380.

Hutton C, De Vita E, Ashburner J, Deichmann R, Turner R. Voxel-based cortical thickness measurements in MRI. Neuroimage 2008; 40: 1701–1710.

Iles JF, Ali AS, Savic G. Vestibular-evoked muscle responses in patients with spinal cord injury. Brain 2004; 127: 1584–1592.

Jahn K, Deutschländer A, Stephan T, Kalla R, Wiesmann M, Strupp M, et al. Imaging human supraspinal locomotor centers in brainstem and cerebellum. Neuroimage 2008; 39: 786–92.

Jain N, Florence SL, Qi HX, Kaas JH. Growth of new brainstem connections in adult monkeys with massive sensory loss. Proc. Natl. Acad. Sci. U. S. A. 2000; 97: 5546–50.

Jirjis MB, Vedantam A, Budde MD, Kalinosky B, Kurpad SN, Schmit BD. Severity of spinal cord injury influences diffusion tensor imaging of the brain. J. Magn. Reson. Imaging 2015: n/a-n/a.

Jones EG, Pons TP. Thalamic and brainstem contributions to large-scale plasticity of primate somatosensory cortex. Science (80-.). 1998; 282: 1121–1125.

Jurkiewicz MT, Crawley AP, Verrier MC, Fehlings MG, Mikulis DJ. Somatosensory cortical atrophy after spinal cord injury: A voxel-based morphometry study. Neurology 2006; 66: 762–764.

Jutzeler CR, Freund P, Huber E, Curt A, Kramer JLK. Neuropathic Pain and Functional Reorganization in the Primary Sensorimotor Cortex After Spinal Cord Injury. J. Pain 2015; 16: 1256–1267.

Jutzeler CR, Huber E, Callaghan MF, Luechinger R, Curt A, Kramer JLK, et al. Association of pain and CNS structural changes after spinal cord injury. Sci. Rep. 2016; 6: 18534.

Kaas JH, Florence SL, Jain N. Subcortical contributions to massive cortical reorganizations. Neuron 1999; 22: 657–60.

Kaas JH, Qi H-X, Burish MJ, Gharbawie OA, Onifer SM, Massey JM. Cortical and subcortical plasticity in the brains of humans, primates, and rats after damage to sensory afferents in the dorsal columns of the spinal cord. Exp. Neurol. 2008; 209: 407–16.

Kaas JH, Qi H, Burish MJ, Gharbawie OA, Onifer SM, Massey JM. Cortical and subcortical plasticity in the brains of humans, primates, and rats after damage to sensory afferents in the

dorsal columns of the spinal cord. Exp. Neurol. 2008; 209: 407–16.

Kalsi-Ryan S, Beaton D, Curt A, Popovic MR, Verrier MC, Fehlings MG. Outcome of the upper limb in cervical spinal cord injury: Profiles of recovery and insights for clinical studies. J. Spinal Cord Med. 2014; 37: 503–10.

Kalsi-Ryan S, Curt A, Verrier MC, Fehlings MG. Development of the Graded Redefined Assessment of Strength, Sensibility and Prehension (GRASSP): reviewing measurement specific to the upper limb in tetraplegia. J. Neurosurg. Spine 2012; 17: 65–76.

Kalsi-Ryan S, Karadimas SK, Fehlings MG. Cervical spondylotic myelopathy: the clinical phenomenon and the current pathobiology of an increasingly prevalent and devastating disorder. Neuroscientist 2013; 19: 409–421.

Kalsi-Ryan S, Singh A, Massicotte EM, Arnold PM, Brodke DS, Norvell DC, et al. Ancillary outcome measures for assessment of individuals with cervical spondylotic myelopathy. Spine (Phila. Pa. 1976). 2013; 38: S111–S122.

Kantak SS, Jones-Lush LM, Narayanan P, Judkins TN, Wittenberg GF. Rapid plasticity of motor corticospinal system with robotic reach training. Neuroscience 2013; 247: 55–64.

Karadimas SK, Gatzounis G, Fehlings MG. Pathobiology of cervical spondylotic myelopathy. Eur. Spine J. 2014; 24: 132–138.

Karadimas SK, Laliberte AM, Tetreault L, Chung YS, Arnold P, Foltz WD, et al. Riluzole blocks perioperative ischemia-reperfusion injury and enhances postdecompression outcomes in cervical spondylotic myelopathy. Sci. Transl. Med. 2015; 7: 316ra194.

Karadimas SK, Moon ES, Yu W-R, Satkunendrarajah K, Kallitsis JK, Gatzounis G, et al. A novel experimental model of cervical spondylotic myelopathy (CSM) to facilitate translational research. Neurobiol. Dis. 2013; 54: 43–58.

Karpova A, Arun R, Kalsi-Ryan S, Massicotte EM, Kopjar B, Fehlings MG. Do quantitative magnetic resonance imaging parameters correlate with the clinical presentation and functional outcomes after surgery in cervical spondylotic myelopathy? A prospective multicenter study. Spine (Phila. Pa. 1976). 2014; 39: 1488–97.

Katz R. Biomarkers and surrogate markers: an FDA perspective. NeuroRx 2004; 1: 189–95.

Kerschensteiner M, Schwab ME, Lichtman JW, Misgeld T. In vivo imaging of axonal degeneration and regeneration in the injured spinal cord. Nat. Med. 2005; 11: 572–577.

Kessler LG, Barnhart HX, Buckler AJ, Choudhury KR, Kondratovich M V, Toledano A, et al. Statistical Methods in Medical Research scientific studies and regulatory submissions. Stat Methods Med Re 2015; 24: 9–26.

Kirshblum SC, Waring W, Biering-Sorensen F, Burns SP, Johansen M, Schmidt-Read M, et al. Reference for the 2011 revision of the International Standards for Neurological Classification of Spinal Cord Injury. J. Spinal Cord Med. 2011; 34: 547–554.

Klawiter EC, Schmidt RE, Trinkaus K, Liang H-F, Budde MD, Naismith RT, et al. Radial diffusivity predicts demyelination in ex vivo multiple sclerosis spinal cords. Neuroimage 2011; 55: 1454–1460.

Knerlich-Lukoschus F, Noack M, Von Der Ropp-Brenner B, Lucius R, Mehdorn MH, Held-Feindt J. Spinal Cord Injuries Induce Changes in CB 1 Cannabinoid Receptor and C-C Chemokine Expression in Brain Areas Underlying Circuitry of Chronic Pain Conditions. J. Neurotrauma 2011; 634: 619–634.

Koeneke S, Lutz K, Herwig U, Ziemann U, Jäncke L. Extensive training of elementary finger tapping movements changes the pattern of motor cortex excitability. Exp. brain Res. 2006; 174: 199–209.

Koutsikou S, Watson TC, Crook JJ, Leith JL, Lawrenson CL, Apps R, et al. The Periaqueductal Gray Orchestrates Sensory and Motor Circuits at Multiple Levels of the Neuraxis. J. Neurosci. 2015; 35: 14132–47.

Kroner A, Greenhalgh AD, Zarruk JG, PassosdosSantos R, Gaestel M, David S. TNF and Increased Intracellular Iron Alter Macrophage Polarization to a Detrimental M1 Phenotype in the Injured Spinal Cord. Neuron 2014; 83: 1098–1116.

Kuhn F, Halder P, Spiess MR, Schubert M. One-year evolution of ulnar somatosensory potentials after trauma in 365 tetraplegic patients: early prediction of potential upper limb function. J. Neurotrauma 2012; 29: 1829–37.

Kurokawa R, Murata H, Ogino M, Ueki K, Kim P. Altered blood flow distribution in the rat spinal cord under chronic compression. Spine (Phila. Pa. 1976). 2011; 36: 1006–1009.

Kwon B. Pathophysiology and pharmacologic treatment of acute spinal cord injury*1. Spine J. 2004; 4: 451–464.

Kwon BK, Liu J, Messerer C, Kobayashi NR, McGraw J, Oschipok L, et al. Survival and regeneration of rubrospinal neurons 1 year after spinal cord injury. Proc. Natl. Acad. Sci. U. S. A. 2002; 99: 3246–51.

Lambert C, Chowdhury R, Fitzgerald THB, Fleming SM, Lutti A, Hutton C, et al. Characterizing aging in the human brainstem using quantitative multimodal MRI analysis. Front. Hum. Neurosci. 2013; 7: 462.

Lambert C, Lutti A, Helms G, Frackowiak R, Ashburner J. Multiparametric brainstem segmentation using a modified multivariate mixture of Gaussians. NeuroImage. Clin. 2013; 2: 684–94.

Landi SM, Baguear F, Della-Maggiore V. One week of motor adaptation induces structural changes in primary motor cortex that predict long-term memory one year later. J. Neurosci. 2011; 31: 11808–13.

Langkammer C, Krebs N, Goessler W, Scheurer E, Ebner F, Yen K, et al. Quantitative MR Imaging of Brain Iron: A Postmortem Validation Study 1. Radiology 2010; 257: 455–462.

Lawrence DG, Kuypers HG. The functional organization of the motor system in the monkey. I. The effects of bilateral pyramidal lesions. Brain 1968a; 91: 1–14.

Lawrence DG, Kuypers HG. The functional organization of the motor system in the monkey. II. The effects of lesions of the descending brain-stem pathways. Brain 1968b; 91: 15–36.

Lemon RN. Descending Pathways in Motor Control. Annu. Rev. Neurosci. 2008; 31: 195–218.

Liao CC, Dicarlo GE, Gharbawie O a., Qi HX, Kaas JH. Spinal cord neuron inputs to the cuneate nucleus that partially survive dorsal column lesions: A pathway that could contribute to recovery after spinal cord injury. J. Comp. Neurol. 2015; 523: 2138–2160.

Liechti M, Müller R, Lam T, Curt A. Vestibulospinal responses in motor incomplete spinal cord injury. Clin. Neurophysiol. 2008; 119: 2804–2812.

Losseff N a, Webb SL, O'Riordan JI, Page R, Wang L, Barker GJ, et al. Spinal cord atrophy and disability in multiple sclerosis. A new reproducible and sensitive MRI method with potential to monitor disease progression. Brain 1996; 119 (Pt 3: 701–8.

Lundell H, Barthelemy D, Skimminge A, Dyrby TB, Biering-Sørensen F, Nielsen JB. Independent spinal cord atrophy measures correlate to motor and sensory deficits in individuals with spinal cord injury. Spinal Cord 2011; 49: 70–75.

Maguire E a, Gadian DG, Johnsrude IS, Good CD, Ashburner J, Frackowiak RS, et al. Navigation-related structural change in the hippocampi of taxi drivers. Proc. Natl. Acad. Sci. U. S. A. 2000; 97: 4398–403.

Makin TR, Scholz J, Filippini N, Henderson Slater D, Tracey I, Johansen-Berg H. Phantom pain is associated with preserved structure and function in the former hand area. Nat. Commun. 2013; 4: 1570.

Marino RJ, Barros T, Biering-Sorensen F, Burns SP, Donovan WH, Graves DE, et al. International standards for neurological classification of spinal cord injury. J. Spinal Cord Med. 2003; 26 Suppl 1: S50-6.

Markham CH. Vestibular control of muscular tone and posture. Can. J. Neurol. Sci. 1987; 14: 493–496.

Markham J a, Greenough WT. Experience-driven brain plasticity: beyond the synapse. Neuron Glia Biol. 2004; 1: 351–63.

Martin AR, Aleksanderek I, Cohen-Adad J, Tarmohamed Z, Tetreault L, Smith N, et al. Translating state-of-the-art spinal cord MRI techniques to clinical use: A systematic review of clinical studies utilizing DTI, MT, MWF, MRS, and fMRI. NeuroImage Clin. 2016; 10: 192–238.

McCrea D a., Rybak I a. Organization of mammalian locomotor rhythm and pattern generation. Brain Res. Rev. 2008; 57: 134–146.

van Middendorp JJ, Pouw MH, Hayes KC, Williams R, Chhabra HS, Putz C, et al. Diagnostic criteria of traumatic central cord syndrome. Part 2: a questionnaire survey among spine

specialists. Spinal cord Off. J. Int. Med. Soc. Paraplegia 2010; 48: 657–663.

Miyanji F, Furlan JC, Aarabi B, Arnold PM, Fehlings MG. Acute cervical traumatic spinal cord injury: MR imaging findings correlated with neurologic outcome--prospective study with 100 consecutive patients. Radiology 2007; 243: 820–7.

Mohammadi S, Carey D, Dick F, Diedrichsen J, Sereno MI, Reisert M, et al. Whole-Brain In-vivo Measurements of the Axonal G-Ratio in a Group of 37 Healthy Volunteers. Front. Neurosci. 2015; 9: 4413389–441.

Mohammadi S, Freund P, Feiweier T, Curt A, Weiskopf N. The impact of post-processing on spinal cord diffusion tensor imaging. Neuroimage 2013; 70: 377–385.

Mohammadi S, Hutton C, Nagy Z, Josephs O, Weiskopf N. Retrospective correction of physiological noise in DTI using an extended tensor model and peripheral measurements. Magn. Reson. Med. 2013; 70: 358–369.

Mohammadi S, Keller SS, Glauche V, Kugel H, Jansen A, Hutton C, et al. The influence of spatial registration on detection of cerebral asymmetries using voxel-based statistics of fractional anisotropy images and TBSS. PLoS One 2012; 7: e36851.

Mohammadi S, Möller HE, Kugel H, Müller DK, Deppe M. Correcting eddy current and motion effects by affine whole-brain registrations: evaluation of three-dimensional distortions and comparison with slicewise correction. Magn. Reson. Med. 2010; 64: 1047–1056.

Mohammadi S, Tabelow K, Ruthotto L, Feiweier TT, Polzehl JJ, Weiskopf N. High-resolution diffusion kurtosis imaging at 3T enabled by advanced post-processing. Front. Neurosci. 2015; 8: 1–14.

Mole TB, MacIver K, Sluming V, Ridgway GR, Nurmikko TJ. Specific brain morphometric changes in spinal cord injury with and without neuropathic pain. NeuroImage. Clin. 2014; 5: 28–35.

Moon ES, Karadimas SK, Yu WR, Austin JW, Fehlings MG. Riluzole attenuates neuropathic pain and enhances functional recovery in a rodent model of cervical spondylotic myelopathy. Neurobiol. Dis. 2014; 62: 394–406.

Moon TK. The expectation-maximization algorithm. IEEE Signal Process. Mag. 1996; 13: 47–60.

Moore AP, Blumhardt LD. A prospective survey of the causes of non-traumatic spastic paraparesis and tetraparesis in 585 patients. Spinal Cord 1997; 35: 361–367.

Morelli JN, Runge VM, Feiweier T, Kirsch JE, Williams KW, Attenberger UI. Evaluation of a modified Stejskal-Tanner diffusion encoding scheme, permitting a marked reduction in TE, in diffusion-weighted imaging of stroke patients at 3 T. Invest. Radiol. 2010; 45: 29–35.

Moseley GL. Using visual illusion to reduce at-level neuropathic pain in paraplegia. Pain 2007; 130: 294–298.

Mottershead JP, Schmierer K, Clemence M, Thornton JS, Scaravilli F, Barker GJ, et al. High field MRI correlates of myelin content and axonal density in multiple sclerosis: A post-mortem study of the spinal cord. J. Neurol. 2003; 250: 1293–1301.

Moulton E a., Schmahmann JD, Becerra L, Borsook D. The cerebellum and pain: Passive integrator or active participator? Brain Res. Rev. 2010; 65: 14–27.

Moxon KA, Oliviero A, Aguilar J, Foffani G. Cortical reorganization after spinal cord injury: Always for good? Neuroscience 2014

Murray EA, Mishkin M. Relative contributions of SII and area 5 to tactile discrimination in monkeys. Behav. Brain Res. 1984; 11: 67–83.

Naidich TP, Duvernoy HM, Delman BN, Sorensen a. G, Kollias SS, Haacke EM. Duvernoy's Atlas of the Human Brain Stem and Cerebellum: High-Field MRI, Surface Anatomy, Internal Structure, Vascularization and 3 D Sectional Anatomy. 2009.

Naismith RT, Xu J, Klawiter EC, Lancia S, Tutlam NT, Wagner JM, et al. Spinal cord tract diffusion tensor imaging reveals disability substrate in demyelinating disease. Neurology 2013; 80: 2201–2209.

Naismith RT, Xu J, Tutlam NT, Snyder a., Benzinger T, Shimony J, et al. Disability in optic neuritis correlates with diffusion tensor-derived directional diffusivities. Neurology 2009; 72: 589–594.

Nathan PW, Smith MC. The rubrospinal and central tegmental tracts in man. Brain 1982; 105: 223–269.

New PW, Farry A, Baxter D, Noonan VK. Prevalence of non-traumatic spinal cord injury in Victoria, Australia. Spinal Cord 2013; 51: 99–102.

Northover JR, Wild JB, Braybrooke J, Blanco J. The epidemiology of cervical spondylotic myelopathy. Skeletal Radiol. 2012; 41: 1543–6.

Nouri A, Tetreault L, Zamorano JJ, Dalzell K, Davis AM, Mikulis D, et al. Role of Magnetic Resonance Imaging in Predicting Surgical Outcome in Patients With Cervical Spondylotic Myelopathy. Spine (Phila. Pa. 1976). 2015; 40: 171–178.

Ogino Y, Nemoto H, Inui K, Saito S, Kakigi R, Goto F. Inner experience of pain: imagination of pain while viewing images showing painful events forms subjective pain representation in human brain. Cereb. Cortex 2007; 17: 1139–46.

Pascual-Leone A, Nguyet D, Cohen LG, Brasil-Neto JP, Cammarota A, Hallett M. Modulation of muscle responses evoked by transcranial magnetic stimulation during the acquisition of new fine motor skills. J. Neurophysiol. 1995; 74: 1037–45.

Perez MA, Lungholt BKS, Nyborg K, Nielsen JB. Motor skill training induces changes in the excitability of the leg cortical area in healthy humans. Exp. brain Res. 2004; 159: 197–205.

Pierpaoli C, Basser PJ. Toward a quantitative assessment of diffusion anisotropy. Magn. Reson.

Med. 1996; 36: 893–906.

Polman CH, Reingold SC, Banwell B, Clanet M, Cohen J a., Filippi M, et al. Diagnostic criteria for multiple sclerosis: 2010 Revisions to the McDonald criteria. Ann. Neurol. 2011; 69: 292–302.

Popp WL, Brogioli M, Leuenberger K, Albisser U, Frotzler A, Curt A, et al. A novel algorithm for detecting active propulsion in wheelchair users following spinal cord injury. Med. Eng. Phys. 2016; 38: 267–74.

Porter DA, Heidemann RM. High resolution diffusion-weighted imaging using readout-segmented echo-planar imaging, parallel imaging and a two-dimensional navigator-based reacquisition. Magn. Reson. Med. 2009; 62: 468–475.

Post MWM, van Leeuwen CMC. Psychosocial issues in spinal cord injury: a review. Spinal Cord 2012; 50: 382–389.

Powers BE, Lasiene J, Plemel JR, Shupe L, Perlmutter SI, Tetzlaff W, et al. Axonal Thinning and Extensive Remyelination without Chronic Demyelination in Spinal Injured Rats. J. Neurosci. 2012; 32: 5120–5125.

Powers BE, Sellers DL, Lovelett E a, Cheung W, Aalami SP, Zapertov N, et al. Remyelination reporter reveals prolonged refinement of spontaneously regenerated myelin. Proc. Natl. Acad. Sci. U. S. A. 2013; 110: 4075–80.

Quallo MM, Price CJ, Ueno K, Asamizuya T, Cheng K, Lemon RN, et al. Gray and white matter changes associated with tool-use learning in macaque monkeys. Proc. Natl. Acad. Sci. U. S. A. 2009; 106: 18379–84.

Rabe K, Livne O, Gizewski ER, Aurich V, Beck A, Timmann D, et al. Adaptation to visuomotor rotation and force field perturbation is correlated to different brain areas in patients with cerebellar degeneration. J. Neurophysiol. 2009; 101: 1961–71.

Raineteau O, Fouad K, Bareyre FM, Schwab ME. Reorganization of descending motor tracts in the rat spinal cord. Eur. J. Neurosci. 2002; 16: 1761–1771.

Raineteau O, Schwab ME. Plasticity of motor systems after incomplete spinal cord injury. Nat. Rev. Neurosci. 2001; 2: 263–273.

Rajasekaran S, Yerramshetty JS, Chittode VS, Kanna RM, Balamurali G, Shetty AP. The Assessment of Neuronal Status in Normal and Cervical Spondylotic Myelopathy Using Diffusion Tensor Imaging. Spine (Phila. Pa. 1976). 2014; 39: 1183–1189.

Raunig DL, McShane LM, Pennello G, Gatsonis C, Carson PL, Voyvodic JT, et al. Quantitative imaging biomarkers: A review of statistical methods for technical performance assessment. Stat Methods Med Re 2015; 24: 27–67.

Ray S, Hsiao SS, Crone NE, Franaszczuk PJ, Niebur E. Effect of stimulus intensity on the spike-local field potential relationship in the secondary somatosensory cortex. J. Neurosci. 2008; 28: 7334–43.

Rooney WD, Johnson G, Li X, Cohen ER, Kim S-G, Ugurbil K, et al. Magnetic field and tissue dependencies of human brain longitudinal1H2O relaxation in vivo. Magn. Reson. Med. 2007; 57: 308–318.

Rosenzweig ES, Courtine G, Jindrich DL, Brock JH, Ferguson AR, Strand SC, et al. Extensive spontaneous plasticity of corticospinal projections after primate spinal cord injury. Nat. Neurosci. 2010; 13: 1505–1510.

Sagi Y, Tavor I, Hofstetter S, Tzur-Moryosef S, Blumenfeld-Katzir T, Assaf Y. Learning in the fast lane: new insights into neuroplasticity. Neuron 2012; 73: 1195–203.

Sampaio-Baptista C, Filippini N, Stagg CJ, Near J, Scholz J, Johansen-Berg H. Changes in functional connectivity and GABA levels with long-term motor learning. Neuroimage 2014; 106C: 15–20.

Sauerbeck A, Schonberg DL, Laws JL, McTigue DM. Systemic iron chelation results in limited functional and histological recovery after traumatic spinal cord injury in rats. Exp. Neurol. 2013; 248: 53–61.

Schendan HE, Searl MM, Melrose RJ, Stern CE. An FMRI study of the role of the medial temporal lobe in implicit and explicit sequence learning. Neuron 2003; 37: 1013–25.

Schmid MR, Pfirrmann CW, Koch P, Zanetti M, Kuehn B, Hodler J. Imaging of patellar cartilage with a 2D multiple-echo data image combination sequence. AJR Am J Roentgenol 2005; 184: 1744–1748.

Schmierer K, Scaravilli F, Altmann DR, Barker GJ, Miller DH. Magnetization transfer ratio and myelin in postmortem multiple sclerosis brain. Ann. Neurol. 2004; 56: 407–15.

Schmierer K, Tozer DJ, Scaravilli F, Altmann DR, Barker GJ, Tofts PS, et al. Quantitative magnetization transfer imaging in postmortem multiple sclerosis brain. J. Magn. Reson. Imaging 2007; 26: 41–51.

Schmierer K, Wheeler-Kingshott C a M, Boulby P a, Scaravilli F, Altmann DR, Barker GJ, et al. Diffusion tensor imaging of post mortem multiple sclerosis brain. Neuroimage 2007; 35: 467–477.

Sehm B, Taubert M, Conde V, Weise D, Classen J, Dukart J, et al. Structural brain plasticity in Parkinson's disease induced by balance training. Neurobiol. Aging 2014; 35: 232–9.

Siddall PJ, Loeser JD. Pain following spinal cord injury. Spinal Cord 2001; 39: 63–73.

Siddall PJ, McClelland JM, Rutkowski SB, Cousins MJ. A longitudinal study of the prevalence and characteristics of pain in the first 5 years following spinal cord injury. Pain 2003; 103: 249–257.

Singh A, Tetreault L, Kalsi-Ryan S, Nouri A, Fehlings MG. Global prevalence and incidence of traumatic spinal cord injury. Clin. Epidemiol. 2014; 6: 309–31.

Steeves JD. Bench to bedside: Challenges of clinical translation. Prog. Brain Res. 2015; 218:

227–239.

Steeves JD, Lammertse D, Curt A, Fawcett JW, Tuszynski MH, Ditunno JF, et al. Guidelines for the conduct of clinical trials for spinal cord injury (SCI) as developed by the ICCP panel: clinical trial outcome measures. Spinal Cord 2007; 45: 206–221.

Stroman PW, Tomanek B, Krause V, Frankenstein UN, Malisza KL. Mapping of neuronal function in the healthy and injured human spinal cord with spinal fMRI. Neuroimage 2002; 17: 1854–60.

Stroman PW, Wheeler-Kingshott C, Bacon M, Schwab JM, Bosma R, Brooks J, et al. The current state-of-the-art of spinal cord imaging: methods. Neuroimage 2014; 84: 1070–81.

Stüber C, Morawski M, Schäfer A, Labadie C, Wähnert M, Leuze C, et al. Myelin and iron concentration in the human brain: A quantitative study of MRI contrast. Neuroimage 2014; 93: 95–106.

Tabelow K, Mohammadi S, Weiskopf N, Polzehl J. POAS4SPM: a toolbox for SPM to denoise diffusion MRI data. Neuroinformatics 2015; 13: 19–29.

Tanadini LG, Hothorn T, Jones LAT, Lammertse DP, Abel R, Maier D, et al. Toward Inclusive Trial Protocols in Heterogeneous Neurological Disorders: Prediction-Based Stratification of Participants With Incomplete Cervical Spinal Cord Injury. Neurorehabil. Neural Repair 2015; 29: 867–77.

Tanadini LG, Steeves JD, Hothorn T, Abel R, Maier D, Schubert M, et al. Identifying Homogeneous Subgroups in Neurological Disorders: Unbiased Recursive Partitioning in Cervical Complete Spinal Cord Injury. Neurorehabil. Neural Repair 2014; 28: 507–15.

Tao G, Datta S, He R, Nelson F, Wolinsky JS, Narayana P a. Deep gray matter atrophy in multiple sclerosis: a tensor based morphometry. J. Neurol. Sci. 2009; 282: 39–46.

Tardif CL, Collins DL, Pike GB. Sensitivity of voxel-based morphometry analysis to choice of imaging protocol at 3 T. Neuroimage 2009; 44: 827–38.

Tattersall TL, Stratton PG, Coyne TJ, Cook R, Silberstein P, Silburn PA, et al. Imagined gait modulates neuronal network dynamics in the human pedunculopontine nucleus. Nat. Neurosci. 2014; 17: 449–54.

Taubert M, Draganski B, Anwander A, Müller K, Horstmann A, Villringer A, et al. Dynamic properties of human brain structure: learning-related changes in cortical areas and associated fiber connections. J. Neurosci. 2010; 30: 11670–7.

Taubert M, Lohmann G, Margulies DS, Villringer A, Ragert P. Long-term effects of motor training on resting-state networks and underlying brain structure. Neuroimage 2011; 57: 1492–8.

Tessa C, Lucetti C, Giannelli M, Diciotti S, Poletti M, Danti S, et al. Progression of brain atrophy in the early stages of Parkinson's disease: A longitudinal tensor-based morphometry study in de novo patients without cognitive impairment. Hum. Brain Mapp. 2014; 0

Tetreault L, Kopjar B, Nouri A, Arnold P, Barbagallo G, Bartels R, et al. The modified Japanese Orthopaedic Association scale: establishing criteria for mild, moderate and severe impairment in patients with degenerative cervical myelopathy. Eur. Spine J. 2016

Toledano M, Bartleson JD. Cervical Spondylotic Myelopathy. Neurol. Clin. 2013; 31: 287–305.

Toosy AT, Kou N, Altmann D, Wheeler-Kingshott CAM, Thompson AJ, Ciccarelli O. Voxel-based cervical spinal cord mapping of diffusion abnormalities in MS-related myelitis. Neurology 2014; 83: 1321–1325.

Totoiu MO, Keirstead HS. Spinal cord injury is accompanied by chronic progressive demyelination. J. Comp. Neurol. 2005; 486: 373–83.

Turati L, Moscatelli M, Mastropietro A, Dowell NG, Zucca I, Erbetta A, et al. In vivo quantitative magnetization transfer imaging correlates with histology during de- and remyelination in cuprizone-treated mice. NMR Biomed. 2015

Ulrich A, Haefeli J, Blum J, Min K, Curt A. Improved diagnosis of spinal cord disorders with contact heat evoked potentials. Neurology 2013; 80: 1393–1399.

Vallery H, Lutz P, von Zitzewitz J, Rauter G, Fritschi M, Everarts C, et al. Multidirectional transparent support for overground gait training. In: 2013 IEEE 13th International Conference on Rehabilitation Robotics (ICORR). IEEE; 2013. p. 1–7.

Villiger M, Bohli D, Kiper D, Pyk P, Spillmann J, Meilick B, et al. Virtual Reality-Augmented Neurorehabilitation Improves Motor Function and Reduces Neuropathic Pain in Patients With Incomplete Spinal Cord Injury. Neurorehabil. Neural Repair 2013; 27: 675–683.

Villiger M, Grabher P, Hepp-Reymond M-C, Kiper D, Curt A, Bolliger M, et al. Relationship between structural brainstem and brain plasticity and lower-limb training in spinal cord injury: a longitudinal pilot study. Front. Hum. Neurosci. 2015; 9: 1–10.

Villiger M, Hepp-Reymond M-C, Pyk P, Kiper D, Eng K, Spillman J, et al. Virtual reality rehabilitation system for neuropathic pain and motor dysfunction in spinal cord injury patients. In: nternational Conference on Virtual Rehabilitation. Zurich: 2011. p. 1–4.

Walz AD, Doppl K, Kaza E, Roschka S, Platz T, Lotze M. Changes in cortical, cerebellar and basal ganglia representation after comprehensive long term unilateral hand motor training. Behav. Brain Res. 2014; 278C: 393–403.

Wannier-Morino P, Schmidlin E, Freund P, Belhaj-Saif A, Bloch J, Mir A, et al. Fate of rubrospinal neurons after unilateral section of the cervical spinal cord in adult macaque monkeys: effects of an antibody treatment neutralizing Nogo-A. Brain Res. 2008; 1217: 96–109.

Ward RE, Huang W, Kostusiak M, Pallier PN, Michael-Titus a T, Priestley J V. A characterization of white matter pathology following spinal cord compression injury in the rat. Neuroscience 2014; 260: 227–39.

Weiskopf N, Lutti A, Helms G, Novak M, Ashburner J, Hutton C. Unified segmentation based

correction of R1 brain maps for RF transmit field inhomogeneities (UNICORT). Neuroimage 2011; 54: 2116–24.

Weiskopf N, Mohammadi S, Lutti A, Callaghan MF. Advances in MRI-based computational neuroanatomy: from morphometry to in-vivo histology. Curr. Opin. Neurol. 2015; 28: 313–22.

Weiskopf N, Suckling J, Williams G, Correia MM, Inkster B, Tait R, et al. Quantitative multi-parameter mapping of R1, PD(*), MT, and R2(*) at 3T: a multi-center validation. Front. Neurosci. 2013; 7: 95.

Wen CY, Cui JL, Liu HS, Mak KC, Cheung WY, Luk KDK, et al. Is diffusion anisotropy a biomarker for disease severity and surgical prognosis of cervical spondylotic myelopathy? Radiology 2014; 270: 197–204.

Wen CY, Cui JL, Mak KC, Luk KDK, Hu Y. Diffusion tensor imaging of somatosensory tract in cervical spondylotic myelopathy and its link with electrophysiological evaluation. Spine J. 2014; 14: 1493–1500.

Wheeler-Kingshott CA, Stroman PW, Schwab JM, Bacon M, Bosma R, Brooks J, et al. The current state-of-the-art of spinal cord imaging: applications. Neuroimage 2014; 84: 1082–93.

Whishaw IQ, Gorny B, Sarna J. Paw and limb use in skilled and spontaneous reaching after pyramidal tract, red nucleus and combined lesions in the rat: Behavioral and anatomical dissociations. Behav. Brain Res. 1998; 93: 167–183.

Widerström-Noga E, Biering-Sørensen F, Bryce TN, Cardenas DD, Finnerup NB, Jensen MP, et al. The International Spinal Cord Injury Pain Basic Data Set (version 2.0). Spinal Cord 2014; 52: 282–6.

Widerström-Noga E, Pattany PM, Cruz-almeida Y, Felix ER, Perez S, Cardenas DD, et al. Metabolite concentrations in the anterior cingulate cortex predict high neuropathic pain impact after spinal cord injury. Pain 2013; 154: 204–212.

Woods TM, Cusick CG, Pons TP, Taub E, Jones EG. Progressive transneuronal changes in the brainstem and thalamus after long-term dorsal rhizotomies in adult macaque monkeys. J. Neurosci. 1999; 20: 3884–3899.

World Health Organization & International Spinal Cord Society. International perspectives on spinal cord injury. Geneva, Switzerland: World Health Organization; 2013.

Worsley KJ, Evans AC, Marrett S, Neelin P. A three-dimensional statistical analysis for CBF activation studies in human brain. J. Cereb. Blood Flow Metab. 1992; 12: 900–18.

Wrigley PJ, Gustin SM, Macey PM, Nash PG, Gandevia SC, Macefield VG, et al. Anatomical changes in human motor cortex and motor pathways following complete thoracic spinal cord injury. Cereb. Cortex 2009; 19: 224–32.

Wrigley PJ, Press SR, Gustin SM, Macefield VG, Gandevia SC, Cousins MJ, et al. Neuropathic pain and primary somatosensory cortex reorganization following spinal cord injury. Pain 2009; 141: 52–9.

Wu J, Stoica B a, Luo T, Sabirzhanov B, Zhao Z, Guanciale K, et al. Isolated spinal cord contusion in rats induces chronic brain neuroinflammation, neurodegeneration, and cognitive impairment: Involvement of cell cycle activation. Cell cycle 2014; 13: 2446–2458.

Wu J, Zhao Z, Sabirzhanov B, Stoica XB a, Kumar A, Luo T, et al. Spinal Cord Injury Causes Brain Inflammation Associated with Cognitive and Affective Changes : Role of Cell Cycle Pathways. J. Neurosci. 2014; 34: 10989–11006.

Wyndaele M, Wyndaele J-J. Incidence, prevalence and epidemiology of spinal cord injury: what learns a worldwide literature survey? Spinal Cord 2006; 44: 523–529.

Yague JG, Foffani G, Aguilar J. Cortical hyperexcitability in response to preserved spinothalamic inputs immediately after spinal cord hemisection. Exp. Neurol. 2011; 227: 252–63.

Yang P-F, Qi H-X, Kaas JH, Chen LM. Parallel functional reorganizations of somatosensory areas 3b and 1, and S2 following spinal cord injury in squirrel monkeys. J. Neurosci. 2014; 34: 9351–63.

Yiannakas MC, Kearney H, Samson RS, Chard DT, Ciccarelli O, Miller DH, et al. Feasibility of grey matter and white matter segmentation of the upper cervical cord in vivo: a pilot study with application to magnetisation transfer measurements. Neuroimage 2012; 63: 1054–1059.

Young a E, Murphy GC. Employment status after spinal cord injury (1992-2005): a review with implications for interpretation, evaluation, further research, and clinical practice. Int. J. Rehabil. Res. 2009; 32: 1–11 10.1097/MRR.0b013e32831c8b19.

Yu WR, Baptiste DC, Liu T, Odrobina E, Stanisz GJ, Fehlings MG. Molecular mechanisms of spinal cord dysfunction and cell death in the spinal hyperostotic mouse: Implications for the pathophysiology of human cervical spondylotic myelopathy. Neurobiol. Dis. 2009; 33: 149–163.

Yu WR, Liu T, Kiehl T-R, Fehlings MG. Human neuropathological and animal model evidence supporting a role for Fas-mediated apoptosis and inflammation in cervical spondylotic myelopathy. Brain 2011; 134: 1277–1292.

Zaaimi B, Edgley S a., Soteropoulos DS, Baker SN. Changes in descending motor pathway connectivity after corticospinal tract lesion in macaque monkey. Brain 2012; 135: 2277–2289.

Zariffa J, Kramer JLK, Fawcett JW, Lammertse DP, Blight a R, Guest J, et al. Characterization of neurological recovery following traumatic sensorimotor complete thoracic spinal cord injury. Spinal Cord 2011; 49: 463–71.

Zatorre RJ, Fields RD, Johansen-Berg H. Plasticity in gray and white: neuroimaging changes in brain structure during learning. Nat. Neurosci. 2012; 15: 528–36.

Zhang H, Schneider T, Wheeler-Kingshott CA, Alexander DC. NODDI: Practical in vivo neurite orientation dispersion and density imaging of the human brain. Neuroimage 2012; 61: 1000–1016.

Zhang J, Jones M, DeBoy CA, Reich DS, Farrell JAD, Hoffman PN, et al. Diffusion tensor

magnetic resonance imaging of Wallerian degeneration in rat spinal cord after dorsal root axotomy. J. Neurosci. 2009; 29: 3160–3171.

Zhou FQ, Tan YM, Wu L, Zhuang Y, He LC, Gong HH. Intrinsic Functional Plasticity of the Sensory-Motor Network in Patients with Cervical Spondylotic Myelopathy. Sci. Rep. 2015; 5: 9975.

Zörner B, Bachmann LC, Filli L, Kapitza S, Gullo M, Bolliger M, et al. Chasing central nervous system plasticity: the brainstem's contribution to locomotor recovery in rats with spinal cord injury. Brain 2014; 137: 1716–32.

Zörner B, Schwab ME. Anti-Nogo on the go: from animal models to a clinical trial. Ann. N. Y. Acad. Sci. 2010; 1198 Suppl: E22-34.

Abbreviations

10MWT	10 meter walking test
α	Flip angle
ACC	Anterior cingulate cortex
AD	Axial diffusivity
ANCOVA	Analysis of covariance
APW	Anterior-posterior width
AIS	ASIA impairment scale
ASIA	American spinal injury association
BBS	Berg balance scale
CI	Confidence interval
CNS	Central nervous system
CSF	Cerebrospinal fluid
CSM	Cervical spondylotic myelopathy
CST	Corticospinal tract
DARTEL	Diffeomorphic anatomical registration through exponentiated lie algebra
DTI	Diffusion tensor imaging
EMSCI	European multicenter study about spinal cord injury
FA	Fractional anisotropy
FDA	Food and drug administration
FLASH	Fast low-angle shot
fMRI	Functional magnetic resonance imaging
FOV	Field of view
FWE	Family-wise error
FWHM	Full width at half maximum
GLM	General linear model
GM	Gray matter
GRAPPA	Generalized auto calibrating partial parallel acquisition
GRASSP	Graded redefined assessment of strength, sensibility and prehension

hMRI	Histological magnetic resonance imaging
iSCI	Incomplete spinal cord injury
ISCNSCI	International standards for neurological classification of spinal cord injury
LEMS	Lower extremity motor score
LRW	Left-right width
LT	Light touch
M1	Primary motor cortex
MCC	Maximal canal compromise
MD	Mean diffusivity
MEDIC	Multiple echo data image combination
mJOA	Modified Japanese Orthopedic Association
ML	Medial lemniscus
MNI	Montreal Neurological Institute
MPRAGE	Magnetization prepared rapid acquisition gradient-echo
MPM	Multi-parameter mapping
MRI	Magnetic resonance imaging
MSCC	Maximal spinal cord compression
MT	Magnetization transfer saturation
MTR	Magnetization transfer ratio
MTw	Magnetization transfer weighted
MVA	Motor vehicle accident
PAG	Periaqueductal gray
PC	Posterior column
PDw	Proton density weighted
PET	Positron emission tomography
PP	Pinprick
QIBA	Quantitative imaging biomarker alliance
qMRI	Quantitative magnetic resonance imaging
R1	Longitudinal relaxation rate
R2*	Effective transverse relaxation rate
RD	Radial diffusivity

RF	Radio frequency
RN	Red nucleus
ROI	Region of interest
S1	Primary somatosensory cortex
S2	Secondary somatosensory cortex
SCI	Spinal cord injury
SCIM	Spinal cord independence measure
SD	Standard deviation
SNR	Signal to noise ratio
SPM	Statistical parametric mapping
T1w	T1 weighted
TE	Time of echo
TI	Time of inversion
TIV	Total intracranial volume
TMS	Transcranial magnetic stimulation
TPM	Tissue probability maps
TR	Time of repetition
TBM	Tensor-based morphometry
UEMS	Upper extremity motor score
VBCT	Voxel-based cortical thickness
VBM	Voxel-based morphometry
VBQ	Voxel-based quantification
VBS	Voxel-based statistics
VR	Virtual-reality
WM	White matter

Curriculum Vitae

First Name	**Patrick**
Last Name	**Grabher**
Date of Birth	November 13th 1987
Home town	Sursee LU
Citizenship	Swiss

Education

2013 - 2016	**PhD in Neuroscience** University of Zurich, Zurich, Switzerland *Thesis title: "Neurodegeneration and Reorganization in Spinal Cord Disorders"* Supervisors: Prof. M. Rudin, Prof. A. Curt, Prof. D. Bach, Dr. P. Freund
2013 - 2016	**International PhD Program in Neuroscience** University of Zurich and ETH Zurich, Zurich, Switzerland
2011	**Swiss Federal Diploma in Pharmacy** Federal Department of Home Affairs, Bern, Switzerland
2009 – 2011	**Master of Science in Pharmacy** University of Basel, Basel, Switzerland
2006 – 2009	**Bachelor of Science in Pharmaceutical Sciences** University of Basel, Basel, Switzerland

Research Experience

2013 - 2016	**Research Assistant at the Spinal Cord Injury Center** University Hospital Balgrist, Zurich, Switzerland
03.2015 – 06.2015	**Visiting Student at the Wellcome Trust Centre for Neuroimaging** University College London, London, United Kingdom Supervisor: Prof. J. Ashburner

2010	**Master's Thesis at the Division of Pharmaceutical Biology** University of Basel, Basel, Switzerland Thesis title: "Isolation and characterization of DYRK1A and CLK1 inhibitors from plant extracts" Supervisors: PD Dr. O. Potterat, Prof. M. Hamburger

Working Experience

03.2013 – 06.2013	**TopPharm Apotheke Meyer, Sursee, Switzerland** Pharmacist
01.2013 – 03.2013	**Department of Obstetrics, University Hospital Zurich, Zurich, Switzerland** Intern in Clinical Pharmacy
10.2011 – 10.2012	**TopPharm Apoteca Piz Ot, Samedan, Switzerland** Pharmacist
09.2010 – 07.2011	**TopPharm Apotheke Meyer, Sursee, Switzerland** Pharmacy Practice Residency

Teaching Experience

2014 – 2015	**Supervision of Master's Thesis in** Human Movement Science, ETH Zurich (1 student)
2014 – 2015	**Supervision of Internships in** Human Movement Science, ETH Zurich (3 students)
2013 -	**Block course** entitled "Functional Assessment of Human Spinal Cord Injury" to undergraduate students in biology of the University of Zurich and ETH Zurich.
2013 -	**Research Seminar in Paraplegia**. Biannual lecture of the Neuroscience Center Zurich of the University of Zurich and ETH Zurich.

Awards

2016	**International Society for Magnetic Resonance in Medicine** Annual Meeting Educational Stipend
2015, 2016	**Neuroscience Center Zurich** Travel Grant

2013	**International Neurorehabilitation Symposium** Poster prize, 3rd Place
2010	**Amedis Award - Best Master's Thesis in Pharm. Sciences** 3rd Place, University of Basel and ETH Zurich, Switzerland

Reviewer for Peer-reviewed Scientific Journals

Journal of Neurotrauma
Neurorehabilitation & Neural Repair

Conference Proceedings

Grabher P, Blaiotta C, Curt A, Ashburner J, Freund P (2016). Myelin changes and atrophy in the brainstem in patients with spinal cord injury relate to clinical impairment. Organization for Human Brain Mapping Conference 2016, Geneva, Switzerland.

Grabher P, Blaiotta C, Curt A, Ashburner J, Freund P (2016). Subcortical brainstem changes in the motor system in patients with chronic spinal cord injury revealed by quantitative MRI protocols. ISMRM 2016, Singapore.

Callaghan MF, Dick F, **Grabher P**, Keller T, Freund P, Weiskopf N (2016). Post-processing Correction of Transmit Field Inhomogeneity in R1 Maps. ISMRM 2016, Singapore.

Grabher P, Mohammadi S, Trachsler A, Friedl S, Sutter R, Weiskopf N, Thompson A, Curt A, Freund P (2015). Cervical spondylotic myelopathy induces structural changes of spinal pathways remote from stenosis. Organization for Human Brain Mapping Conference 2015, Honolulu, Hawaii, USA.

Freund P, **Grabher P**, Hupp M, Ashburner J, Friston K, Weiskopf N, Thompson A, Ziegler G (2015). Progressive atrophy, prediction and potential endpoints for trials in acute spinal cord injury. Organization for Human Brain Mapping Conference 2015, Honolulu, Hawaii, USA.

Huber E, **Grabher P**, Killeen T, Trachsler A, Kubin T, Lachappelle P, Bolliger M, Draganski B, Weiskopf N, Thompson A, Curt A, Freund P (2015). Tracking structural MRI changes in the spinal cord and brain as surrogate markers for interventions in SCI rehabilitation. ZNZ Neuroscience Symposium 2015, Zurich, Switzerland.

Huber E, **Grabher P**, Killeen T, Trachsler A, Kubin T, Bolliger M, Draganski B, Weiskopf N, Thompson A, Curt A, Freund (2015). Plasticity of grey and white matter in response to motor skill training in healthy individuals and those with spinal cord injury. Swiss Society for Neuroscience Annual Meeting, 2015, Fribourg, Switzerland.

Grabher P, Curt A, Weiskopf N, Callaghan MF, Ashburner J, Friston K, Thompson AJ, Freund P (2014). Tracking structural changes following traumatic spinal cord injury: a prospective longitudinal study. ZNZ Neuroscience Symposium 2014, Zurich, Switzerland.

Grabher P, Curt A, Weiskopf N, Callaghan MF, Ashburner J, Friston K, Thompson AJ, Freund P (2014). Tracking structural changes following traumatic spinal cord injury: a prospective longitudinal study. UCL Neuroscience Symposium 2013, London, United Kingdom.

Grabher P, Callaghan MF, Jutzeler CR, Fries S, Wolf K, Thompson AJ, Curt A, Weiskopf N and, Freund P (2013). Tract-specific changes of the microstructure in the injured human spinal cord revealed by quantitative MRI. International Neurorehabilitation Symposium INRS 2013, Zurich, Switzerland.

Publications

Published and Peer-reviewed

Grabher P, Mohammadi S, Trachsler A, Friedl S, David G, Sutter R, Weiskopf N, Thompson AJ, Curt A, Freund P. Voxel-based analysis of grey and white matter degeneration in cervical spondylotic myelopathy. Sci. Rep. 2016; 6: 24636.

Grabher P, Callaghan MF, Ashburner J, Weiskopf N, Thompson AJ, Curt A, Freund P. Tracking sensory system atrophy and outcome prediction in spinal cord injury. Ann. Neurol. 2015; 78: 751-761.

Villiger M*, **Grabher P***, Hepp-Reymond M-C, Kiper D, Curt A, Bolliger M, Hotz-Boendermaker S, Kollias S, Eng K, Freund, P. Relationship between structural brainstem and brain plasticity and lower-limb training in spinal cord injury: a longitudinal pilot study. Front. Hum. Neurosci. 2015; 9: 1–10.

Grabher P, Durieu E, Kouloura E, Halabalaki M, Skaltsounis LA, Meijer L, Hamburger M, Potterat O. Library-based discovery Library-based discovery of DYRK1A/CLK1 inhibitors from natural product extracts. Planta Med. 2012; 78: 951–6.

*Shared first authorship

Under Revision

Ziegler G*, **Grabher P***, Altmann D, Hupp M, Ashburner J, Friston K, Weiskopf N, Thompson A, Curt A, Freund P. Progressive diaschisis following spinal cord injury: implications for clinical trials (submitted to Lancet Neurology).

*Shared first authorship

In Preparation

Grabher P, Blaiotta C, Curt A, Ashburner J, Freund P. Relationship between structural brainstem neurodegeneration and clinical impairment in traumatic spinal cord injury (Target Journal: Neuroimage: Clinical).

Published and Not Peer-reviewed

Villiger M & **Grabher P.** http://www.paraplegie-balgrist.ch/blog/verbesserte-motorik-durch-virtuell-verstaerktes-gangtraining-fuehrt-zu-veraenderungen-im-hirn-bei-menschen-mit-einer-querschnittslaehmung/. Post on Balgrist Paraplegia Research Blog. May 12, 2015.

Acknowledgements

First of all, I would like to thank my committee members, Prof. Markus Rudin, Prof. Armin Curt, Prof. Dominik Bach, and Dr. Patrick Freund for all their insightful comments and their invaluable support. I want to sincerely thank my supervisors and mentors Armin and Patrick for giving me the opportunity to perform my PhD thesis in the Spinal Cord Injury Center at the Balgrist University Hospital, their constant help and guidance, and all the opportunities they provided me throughout all these years.

Furthermore, I would like to thank the Clinical Research Priority Program "NeuroRehab" of the University of Zurich for the financial support.

I am grateful to all the people with whom I collaborated with and for all their help and efforts: Prof. John Ashburner, Prof. Alan Thompson and Dr. Martina Callaghan from University College London, Prof. Nikolaus Weiskopf from the Max Planck Institute in Leipzig, and Dr. Siawoosh Mohammadi from the Medical Center Hamburg-Eppendorf. Thank you very much for all the technical assistance and your intellectual inputs.

Great thank you goes to all colleagues of the Paralab for the fruitful discussions and the moments we shared. I also would like to thank the staff of the Department of Radiology and Neurology. It was a great pleasure to work with you. Special thanks to Catherine, Chris, Eve, Gergely, Janosch, Luca, Miriam, Mike, Maryam, Mathi, Matze, and Tim for their support and the amazing time we shared during coffee breaks, all running/hiking/climbing activities and other social events.

I also would like to say thank you to all volunteers that participated in my studies and spent their valuable time in the scanner. That cannot be taken for granted. Thank you very much.

Finally, I would like to acknowledge my family and friends. My heartfelt thank you goes to my parents, Karin and Markus Grabher, and my sisters, Iris and Sandra. I am very grateful to them and without their support I would not be there where I am right now. Last but not least, my special thanks to Selina for her patience and unconditional support during pursuing my studies and for being my partner in crime.